PONTIFICIA UNIVERSIDAD CATOLICA DE CHILE

ESCUELA DE INGENIERIA

CO-SEISMIC LANDSLIDES: AN APPROACH USING SYNTHETIC SEISMOGRAMS AND NEWMARK ANALYSIS. CASE STUDY: COASTAL RANGE OF VALPARAÍSO, CHILE

DOMINIQUE D. VALDIVIA LARENAS

Thesis submitted to the Office of Research and Graduate Studies in partial fulfillment of the requirements for the Degree of Master of Science in Engineering

Advisor:

CARLOS MARQUARDT ROMÁN

Santiago de Chile, (December, 2020)

PONTIFICIA UNIVERSIDAD CATOLICA DE CHILE

ESCUELA DE INGENIERIA

CO-SEISMIC LANDSLIDES: AN APPROACH USING SYNTHETIC SEISMOGRAMS AND NEWMARK ANALYSIS. CASE STUDY: COASTAL RANGE OF VALPARAÍSO, CHILE

DOMINIQUE DE LOURDES VALDIVIA LARENAS

Members of the Committee:

CARLOS MARQUARDT

JORGE CREMPIEN

SARA ELGUETA

SERGIO SEPÚLVEDA

LEONARDO VANZI

Thesis submitted to the Office of Research and Graduate Studies in partial fulfillment of the requirements for the Degree of Master of Science in Engineering

Santiago de Chile, (December, 2020)

A María Ignacia y Emma, mis pequeñas sobrinas, cuyo futuro sea sustentable, resiliente y en igualdad

ACKNOWLEDGEMENTS

Quisiera agradecer a mis padres, Blanca y Carlos, por su apoyo constante e incondicional, sin ellos absolutamente nada de este trabajo sería posible. A mis abuelas, Emma y Herminda, a quienes admiro infinitamente, de ellas he aprendido y continúo aprendiendo. A mis hermanos Valeska y Carlos, y a sus respectivos compañeros de vida Roland y Carolina a quienes considero hermanos también, gracias por todos sus consejos y orientación a lo largo de mi camino universitario y del magíster.

En especial quisiera agradecer a la Escuela de Ingeniería UC, donde conocí a grandes docentes que me confirmaron que la investigación y la docencia es mi camino por seguir. A Sara Elgueta, que por tantos años me transmitió su conocimiento, me permitió trabajar codo a codo y me brindó tantas oportunidades. A Carlos Marquardt que me acogió desde el primer día como su alumna, me permitió explorar y contribuir con ideas nuevas en este trabajo y me motivó constantemente. A Jorge Crempien, quien con paciencia y motivación me guio en gran parte de este trabajo. A Gonzalo Yáñez y Esteban Sáez, por permitirme ser parte del proyecto FONDEF +Andes 2.0, donde se gestó este trabajo. A José Cembrano, Gonzalo Yáñez y Gloria Arancibia por mostrarme lo bello de la geología y su apoyo constante durante el pregrado y postgrado.

A Felipe, Javi y Ronny, por el apañe en terreno, a todo el grupo de Geociencias UC por el apañe en San Joaquín. A Rorro, gracias a este postgrado gané un gran amigo. A Laura, Cototo, Fran, Toti, por hacer siempre más ameno el trabajo diario en la salita de postgrado del DIM. A Claudio, Pato, Valeria, Marco y Daniel, por estar siempre dispuestos retroalimentar mis avances. A mis amigos de la vida Katherine y Chris, que me escucharon y soportaron mis locuras. A Lucho que apareció en la última etapa a apañar.

A los funcionarios del DIM, quienes me acogieron desde el primer día, en especial a Cecilia Meza, quien siempre me orientó cuando lo necesité. Al DIEG, donde siempre estuvieron disponibles a ayudarme. A Danisa Herrera, quien siempre supo resolver mis dudas en la Dirección de Postgrado.

A Andrew Hodgkin por ayudarme incondicionalmente en terreno, en gabinete y en la realización de esta tesis.

A Kate Allstadt, Randy Jibson y Bill Murphy, que siempre estuvieron dispuestos a resolver mis dudas. A los profesores y asistentes de iRALL School 2019, que me brindaron la oportunidad de mirar de otra forma el estado del arte y me brindaron sugerencias que mejoraron mi trabajo.

A los miembros de mi comisión, Leonardo Vanzi, Sergio Sepúlveda, Jorge Crempien, Carlos Marquardt y Sara Elgueta que me entregaron la retroalimentación y las sugerencias necesarias para mejorar aún más este trabajo.

GENERAL INDEX

Pág.

INDEX OF TABLES

Pag.

INDEX OF FIGURES

Pag.

RESUMEN

Las remociones en masa co-sísmicas son parte de una cadena de geo-peligros asociadas al evento desencadenante, las cuales son parte del inicio de varios procesos superficiales. En áreas urbanas costeras densamente pobladas con potenciales fallas sismogénicas, como el caso del área costera entre Valparaíso y Maitencillo, Chile, es necesario pronosticar potenciales terremotos y remociones en masa causadas por ellos. El objetivo de este trabajo fue estudiar las posibles remociones en masa causadas por terremotos corticales de cinemática Normal o Sinistral, bajo condiciones de suelo saturado y seco. Los potenciales escenarios sísmicos están asociados a las fallas Marga-Marga y Aconcagua, miembros del Sistema de Falla Valparaíso-Melipilla (VMFS). Primero, analicé las pendientes y la geología superficial para categorizar cualitativamente el peligro de remociones en masa. Segundo, elegí áreas de acercamiento en ambos bloques de cada falla, en cada una seleccioné puntos representativos de laderas críticas, donde desarrollé un modelo predictivo basado en sismogramas sintéticos y análisis de Newmark. Los desplazamientos son del orden de 10^{-7} a 10^{1} m, están principalmente controlados por la litología, secundariamente por la ruptura sísmica y la directividad. El escenario de un sismo en falla Marga-Marga con cinemática normal, generaría los deslizamientos más grandes. En el escenario de un sismo en falla de Aconcagua con cinemática normal, los deslizamientos son ligeramente menores. Para ambas fallas, en los casos con cinemática normal poseen deslizamientos más grandes que los casos con cinemática Sinistral debido a la directividad sísmica. Aun cuando los deslizamientos calculados no pueden ser interpolados, pueden ser interpretados en terreno como una ladera más grande con las mismas características geológicas, geotécnicas y geomorfológicas, donde es posible extender el potencial comportamiento para la ladera completa bajo cada escenario.

Palabras Claves: Remociones en masa co-sísmicas, terremoto cortical, análisis de Newmark, sismogramas sintéticos, Valparaíso, Chile, Marga-Marga, Aconcagua

ABSTRACT

Co-seismic landslides are a geo-hazard caused by the transient stresses during the ground motion shaking. Predictive-landslide models are useful tools to explore several scenarios for mitigation and risk reduction assessments. The objective is to study potential landslides caused by crustal earthquakes under strike-slip and dip-slip fault kinematics, and under saturated and dry soil conditions. The earthquake scenarios are studied in relation to the Marga-Marga and Aconcagua faults, part of the Valparaíso-Melipilla Fault System in the Coastal Range of Central Chile (32.5–33◦S). First, the slopes and surface geology were analyzed to categorize qualitatively the landslide hazard. Second, several areas were selected on both sides of each fault, ca. 120 representative points of critical slopes were selected for each scenario, where a predictive model was developed using synthetic seismograms and Newmark analysis. The computed displacements are from negligible to 10^1m. The displacements show a stronger lithological control than the seismic rupture and its directivity. The Marga-Marga normal earthquake scenario shows the largest displacements, and they are slightly lower in the Aconcagua normal earthquake scenario. Normal earthquake scenarios have larger displacements than sinistral earthquake scenarios due to the orientation of seismic rupture plane and the seismic directivity. Even though the computed slope displacements cannot be interpolated, they can be interpreted as a larger slope with the same geological, geotechnical, and geomorphological characteristics, where is possible to extend the potential performance for the entire slope under each scenario.

Keywords: Co-seismic landslides, crustal earthquake, Newmark analysis, synthetic seismograms, Valparaíso, Chile, Marga-Marga, Aconcagua

1 INTRODUCTION

A descending mass movement along a slope due to gravitational influence is defined as a landslide. These phenomena can occur on natural slopes of landslides, anthropomorphic slopes and dams. Varnes (1978, 1984) and Cruden & Varnes (1996) established a classification of landslides based on the material and the type of movement involved. The material of the mass wasting phenomena can be rock, debris or earth. The movement is classified as falls, topples, rotational slides, planar slides, wedge slides, lateral spreads, avalanches, flows, slope deformation or a complex of two or more movements. This proposed classification was updated by Hungr et al. (2014), where the material has been classified according to the geotechnical and geological properties to reach consensus on a shared terminology and facilitate its usage. In the resulting classification, shown in Table 1, there are 32 possible types of landslides organized according to the main movement and material. These events usually are conditioned by properties of the material related to:

a) **Geology**: lithology, joint orientation, bedding, faulting planes, weathering, texture, particle sorting, matrix, and cement composition.

b) **Geotechnics**: cohesion, internal fiction angle, granulometry.

c) **Geomorphology**: Slope angle, orientation, sun exposure, slope height.

d) **Hydrology**: water level, ground water circulation, humidity, thickness of the saturated portion

e) **Anthropic activity**: man-made slopes, dams, bench design

Table 1: Landslide Classification proposed by Hungr et al. (2013), after Varnes (1984)

Type of movement	Rock	Soil
Fall	1.Rock/ice fall	2.Boulder/debris/silt fall
Topple	3.Rock block topple	5.Gravel/Sand/Silt topple
	4.Rock flexural topple	
Slide	6.Rock rotational slide	11. Clay/silt rotational slide
	7. Rock planar slide	12. Clay/silt planar slide
	8. Rock wedge slide	13. Gravel/sand/debris slide
	9. Rock compound slide	14. Clay/silt compound slide
	10. Rock irregular slide	
Spread	15.Rock slope spread	16.Sand/silt liquefaction spread
		17. Sensitive clay spread
Flow	18.Rock/ice avalanche	19. Sand/silt/debris dry flow
		20. Sand/silt/debris flow slide
		21. Sensitive clay flow slide
		22. Debris flow
		23. Mud flow
		24. Debris flood
		25. Debris avalanche
		26. Earthflow
		27. Peat flow
Slope Deformation	28.Mountain slope deformation	30.Soil slope deformation
	29.Rock slope deformation	31.Soil creep
		32.Solifluction

Landslides can be triggered by the influence of gravity, rainfall, volcanic activity, and seismic activity when the soliciting stresses are greater than the resistance of the slope. The co-seismic landslides are caused by the transient stresses associated to the ground strong motion (Murphy, 2015).

1.1 Landslides caused by earthquakes: A brief review

Landslides caused by earthquakes are considered as chains of geological hazards that occur over time following the triggering event (Fan et al., 2019). During the earthquake falls, flows, or slides may occur on some slopes and, on others only fracture propagation and weakening may occur (Figure 1). These events can provide debris to create landslide reactivations and flows in the next months and years due to rainfall or new earthquakes (independently of its seismogenic source). In the long term, all the erosion and wasted

debris material form part of the sedimentary infill of the basins (Chen et al., 2020; Nakamura et al., 2014; Okamoto et al., 2013; Hovius et al., 2011; Korup et al., 2010).

The size and distribution are related to the intensity measures (such as PGA, PGV, CAV, IA, duration of shaking) (Jibson 2011). Further, they are controlled by earthquake focal mechanism, location respect epicenter and fault trace location (if landslide location is at the hanging wall or foot wall) and the directivity of the propagation of seismic waves during rupture (Chen et al, 2017; Marc et al., 2016; Meunier et al., 2013; Chigira et al, 2010).

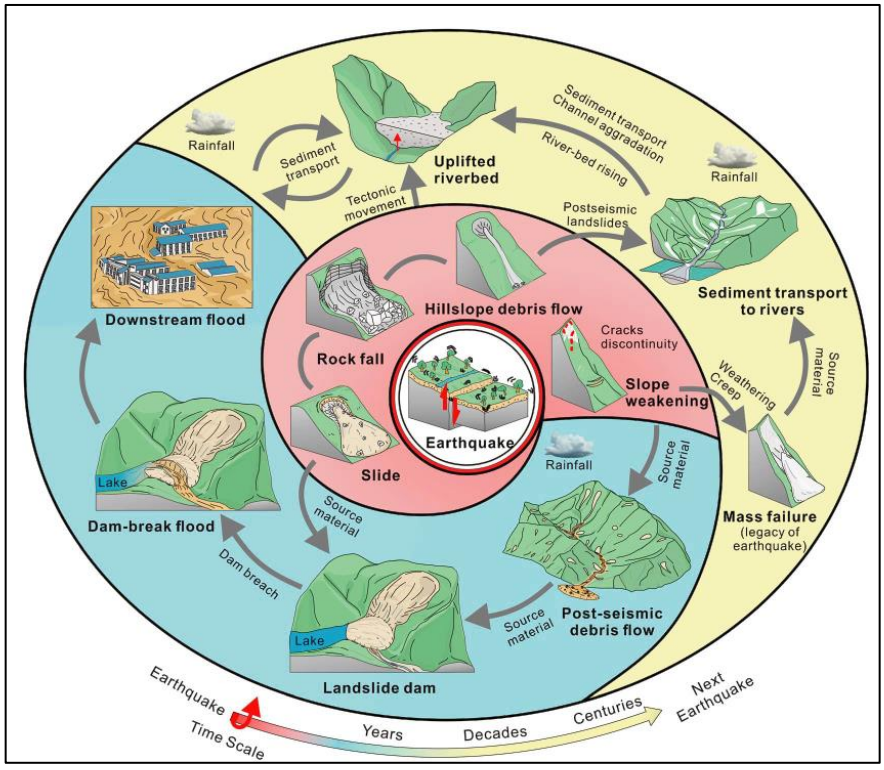

Figure 1: Co-seismic Landslides and their subsequent hazards triggered by crustal earthquakes. (Modified from Fan et al., 2019)

1.2 Case Study: Coastal Range of Central Chile, Valparaíso Region, Chile

The study area is the west slope of the coastal range of the Valparaíso Region, between Maitencillo and Valparaíso cities, between 32.5°S and 33°S (Figure 2). The area extends from the western flanks of the Coastal Cordillera, at their foothills, to the west at the coastal plains, marine terraces and active coastal cliffs.

1.3 Research question and Hypothesis

The research questions are: Which are the major controlling factors on earthquake triggered landslides in this part of the emerged forearc of central Chile? How different could be the spatial distribution and displacements of landslides caused by crustal earthquakes scenarios: an earthquake on Marga-Marga fault or on Aconcagua fault, a normal kinematic or sinistral kinematic, in dry or saturated conditions?

The working hypothesis is, the major controlling factor is lithology, and secondarily the rupture process in the earthquake (Somerville et al., 1997). In the strike-slip scenarios, the potential landslides and their displacements have a symmetrical distribution around the fault. In normal earthquake scenarios, the potential triggered landslides and their displacements are larger and more concentrated at the footwall than in the hanging wall (at the SW-block in Aconcagua case, and at de NW-block on Marga-Marga case). The area between Aconcagua and Marga-Marga faults in normal faulting corresponds to the footwall of both faults, in this area and these cases, the potential landslides would be smaller and sparse than in the hanging walls in both faults.

The aim of this work is to study the potential earthquake-triggered landslide hazard in coastal areas where there is more than one potential fault kinematic. We explored in crustal earthquakes associated to strike-slip and dip-slip kinematic, where its fault traces are in high populated urban areas. A good study case is the coastal area of central Chile, between latitudes 32.5°S and 33°S, among the cities of Maitencillo and Valparaíso.

1.4 Objectives

1.4.1 Main Objective

Explore the magnitude and location of potential shallow landslides caused by crustal earthquakes in different scenarios associated to Marga-Marga and Aconcagua faults.

1.4.2 Specific Objectives

The specific objectives of this study are:

a) Identify the critical areas that could be affected by co-seismic landslide based on the slope angle and lithology.

b) Explore the potential behavior of critical slopes in different seismic scenarios

c) Calculate the potential displacement of critical slopes in wet and dry conditions

d) Know the spatial distribution of potential co-seismic shallow landslides

2 GEOLOGICAL SETTING

2.1 Geomorphological Setting

The area between 32.5°S and 33°S consist of, from E to W, the Coastal Cordillera, coastal plains, and coastal active cliffs. The Coastal Cordillera is composed of Paleozoic – Mesozoic intrusive bodies and Jurassic volcanic sequences of the Ajial Fm. Its maximum height in the study area is 1040 m.a.s.l. The remnant flat relief has been interpreted as uplifted peneplains, whose development was initiated close to the sea level (Farías et al., 2008). The coastal plains are related to marine terraces covered by Neogene and Quaternary marine, transitional and continental units. The foot of the most recent marine terrace is delimited by a continuous active marine cliff from southern Horcon to Maitencillo, which exposes the Neogene Horcon Fm. Their emerged deposits imply an uplift of neritic sandstones at least ca.150 m during the Pliocene and Quaternary (Encinas et al., 2006, 2008; Valdivia et al.,2018).

The Aconcagua River crosses the area in E-W direction, its flood plains and estuary form a narrow flat surface of low elevation. In Concon, there is an active littoral dune field and in Horcon there is an inactive to sub-actual very extensive dune field. Both covers the intrusive basement and Neogene sedimentary units, forming a relative smooth and flat relief. Gorges carved on all type of rocks and sedimentary deposits by streams are frequent, whose steepest slopes are related to very narrow gorges. These stream incisions and the high level peneplains are indicative of continuous uplift of the region, which probably began before 10 Ma. Ago (Farias et al., 2008)

2.2 Stratigraphy

The study area is in the southernmost part of the Chilean-Pampean flat-slab (Figure 2) (Isacks, 1988; Ramos 2009; Charrier et al., 2014). The low angle of subduction and the absence of volcanic activity in the Quaternary in this segment are due to the subduction

of the Juan Fernández Ridge (JFR) since ca. 2 Ma (Yáñez et al., 2001; Le Roux et al., 2006). The stratigraphic units are described below:

2.2.1 Paleozoic Units

These include the **Paleozoic Valparaíso Metamorphic Complex** outcropping at the Valparaíso peninsula (Gana et al., 1996). This complex is intruded by **Cochoa and Mirasol plutonic units**, of Upper Carboniferous and Permian ages respectively (Rivano, 1993; Gana et al, 1994; Creixell et al., 2006).

a) Metamorphic Rocks

Valparaíso Metamorphic Complex

(Gana et al., 1996)

In the southern coastal area, basement rocks belong to the **Paleozoic Valparaíso Metamorphic Complex**. This was described by Gana et al. (1996) as composed of orthogneiss and paragneiss, with subordinated granites, tonalites, migmatites with amphibolitic and chloritic schists intercalations. Further south, outcropping granitic gneisses and amphibolite, were associated to this complex by Webb and Klepeis (2019).

The main foliation is NW-W, dipping to S. Creixell et al. (2006) associate L-S tectonites with NW-W subvertical foliation to this same unit. This complex is intruded by granitoids, tonalites and gabbro units of Paleozoic and Mesozoic ages.

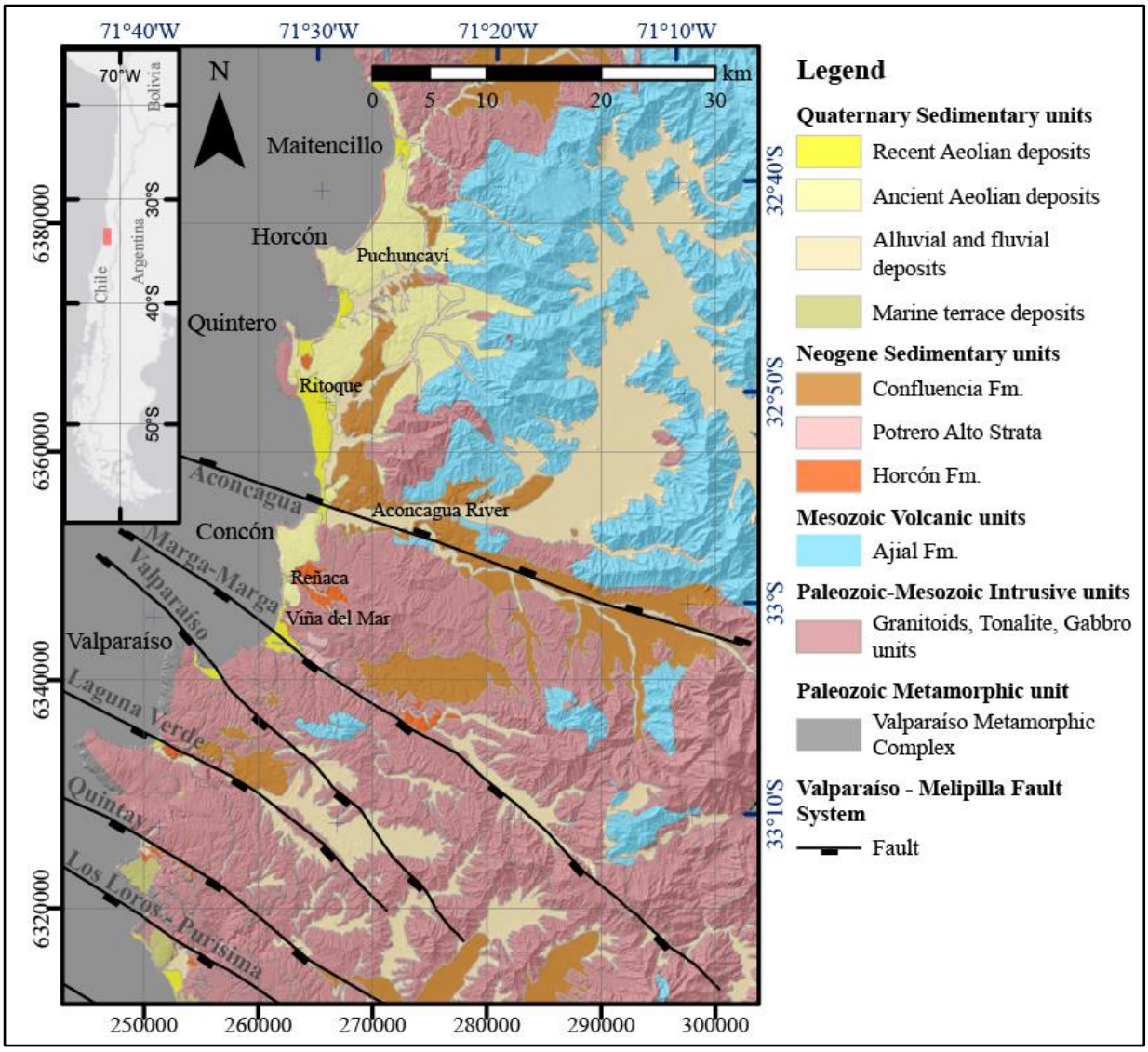

Figure 2: Simplified Geological Map of Coastal Range of Valparaiso Region, Chile. Geological units of Paleozoic and Mesozoic ages are grouped by rock type. Sedimentary units of Neogene and Quaternary are shown in detail. Quaternary units from West to East are: Marine Terraces Deposits, Aeolian Deposits, Aeolian palaeodunes Deposits, Alluvial and Colluvial Deposits and Fluvial Deposits.

b) Intrusive Rocks

Cochoa Unit

Pennsylvanian (Late Carboniferous)

(Rivano, 1993)

The oldest plutonic rocks pertain to the **Cochoa Unit** of Late Carboniferous age that outcrops between Concon and Reñaca towns. This unit is composed by stocks and sills of tonalite, granodiorite, monzogranite, granite, sienogranite, diorite and quartz-diorite (Rivano,1993). Creixell et al. (2006) report tectonic foliation in 315°-360°/72-90° and lineation in 167°-175°/42°-50°, associated to a high temperature deformation. It is intruded by a Middle Jurassic dyke swarm, controlled by NW-SE structures and linked to a NNW-SSE extensional regime (Creixell et al., 2006)

Mirasol Unit

Permian

(Gana et al., 1994)

The **Mirasol plutonic Unit** of Permian age is emplaced on the metamorphic basement; it outcrops at the southern part of the area (Gana et al., 1994). In Gana et al. (1996) it is equivalent to the abbreviature Pzmg.

It is composed by tonalites, granodiorites, monzogranites, sienogranites, granites, with dioritic and quartz-dioritic inclusions. The granitoids have magmatic foliation associated to the orientation of the mafic inclusions and to a heterogeneous mylonitic deformation (Gana et al., 1996; Gana and Tosdal, 1996).

2.2.2 Mesozoic Units

They inclide a plutonic super unit: the Jurassic **Mincha Super Unit** that grouped several minor granitoid bodies, and a sedimentary unit: **Quebrada del Pobre Formation** which is overlain by the volcano-sedimentary **Ajial Formation**, both of Lower Jurassic.

a) Intrusive Rocks

Mincha Super Unit

Jurassic

(Rivano et al., 1993)

Several Mesozoic plutonic stocks units have been identified in the northern part of the area by Rivano (1993) who grouped them into the Mincha Super Unit, composed by the Cavilolén, Tranquila and Puerto Oscuro Units. In the southern part of the area, they were described by Gana et al. (1994, 1996) and Gana and Tosdal (1996) as Sauce, Peñuelas, Lliu-Lliu and Limache Units. This last unit is equivalent to the Puerto Oscuro Unit of Rivano (1993). They constitute N-S plutonic discontinuous belts, whose ages are younger from W to E (Vergara et al., 1995, Gana and Tosdal 1996, Parada et al., 1999, Creixell et al., 2006). In turn, this Super Unit has been grouped with other Paleozoic intrusive units for simplicity in Figure 2.

b) Volcano-Sedimentary Rocks

Quebrada del Pobre Formation

Hettangian? – Sinemurian? (Lower Jurassic)

(Thomas, 1958)

Quebrada del Pobre Formation is a marine sedimentary unit, composed of sandstones and mudstones with intercalations of limestones and pebbly conglomerates (Rivano, 1993). This unit outcrops at the western flanks of the Coastal Cordillera, east of Puchuncaví. This

formation disconformably overlays La Ligua Formation and is conformably covered by the Ajial Formation. Towards the north, out of the study area, this unit has a transgressive relationship with Los Molles Formation (Charrier et al., 2007).

Ajial Formation

Pliensbachian? – Aalenian? (Lower Jurassic)

(Thomas, 1958)

It is a volcano-sedimentary formation composed of ash tuffs, pumicitic lapilli-ash tuffs, volcanic breccias with andesitic and riodacitic fragments and sedimentary clasts in minor abundance. These are intercalated with plagioclase-phyric andesitic to basaltic lavas with a partially devitrified matrix, some ocoitic and porphyric dacitic layers are also present (Rivano, 1993). This formation also includes conglomerates with andesitic, dacitic and rhyolitic clasts, with sandy matrix and calcareous cement, sub arkoses, greywackes with calcareous cement, mudstones, calcilutites and calcarenites. Some syn-sedimentary folding and crossbedding has been reported in some sedimentary strata.

This unit outcrops at the north-eastern part of the area, north of the Aconcagua river and at the west side of the Coastal Cordillera. In the Aconcagua Valley, the rocks had a dynamic metamorphism and some obliteration of the original textures. It has a conformably relationship with both, the underlying La Calera and Quebrada del Pobre Formations.

2.2.3 Cenozoic Units

All Cenozoic units of the study area are sedimentary in origin, deposited in marine, transitional or continental environments, with a time-span from Miocene to the Present. Neogene rocks are represented by the Confluencia, Potrero Alto and Horcon Formations. Quaternary sediments are associated to eolian, alluvial, colluvial and fluvial processes.

a) Neogene Sedimentary Rocks

Confluencia Formation

Miocene – Pliocene

(Rivano and Sepúlveda, 1986)

It is a 100 m thick sub-horizontal sequence of continental origin, composed of medium to weakly lithified, matrix-supported sandy conglomerates interstratified with large cross bedded lithic sandstones and mudstone lenses. Clasts are polymictic well-rounded, sizes up to 15cm, showing imbricated structure. This unit outcrops from South of La Serena to Valparaíso; it corresponds to the basal unit that unconformably overlies on Paleozoic intrusive and metamorphic basement and on and Mesozoic volcano-sedimentary rocks and interpreted as deposited in alluvial and fluvial systems (Rivano and Sepúlveda, 1986; Rivano, 1993); it is covered by younger continental sediments, such as Quaternary dunes, paleodunes, fluvial and alluvial deposits. Coquimbo Formation that outcrops outside the study area in the coastal range of Coquimbo Region is a lateral equivalent ti the Confluencia Formation, both aged Miocene-Pliocene (Rivano and Sepúlveda, 1986)

Outcrops of this formation are observed S of Puchuncaví; in this area, they from part of a continental unit whose Miocene – Pliocene marine equivalents are the top of Navidad Formation and Horcon Formation (Gana et al., 1996; Wall et al, 1996) and Horcon Formation (Rivano, 1993).

Potrero Alto Strata

Miocene – Pleistocene?

(Wall et al., 1996)

They consist of sub horizontal layers of weakly to moderately consolidated conglomerates, with sandstone and mudstone intercalations, some of which locally contain poorly preserved plant remains. They are interpreted as accumulated in alluvial and fluvial domains (channels and flooding plains) domains (FONDEF D10E1027 Project, unpublished report, 2017). Some diatomite beds suggest lacustrine environments. These strata were deposited over Confluencia, Horcon, Coquimbo, and La Cueva Formations. They are covered by Quaternary alluvial and aeolian sediments. Their thickness varies from a few meters up to 50 m.

The age is not well defined, estimates vary from Miocene to Pleistocene, having consensus on a Pliocene age. On one hand, Wall et al (1996) describe an outcrop where conglomerates are deposited over the Pudahuel Ignimbrite (0.4 Ma). On the other hand, Wall and Lara (2001) infer a Pleistocene age because some beds of Potrero Alto Strata were deposited on marine terraces constructed over Lavas Las Pataguas (18.8 to 17.8 Ma). Locally there are some deposits of gravels interbedded with palaeodunes deposits.

These units of conglomerates and sandstones of continental origin were grouped on a newly defined unit named as “Gravel of Central Coast”. It is composed by Confluencia Formation and Potrero Alto Strata, and they overlay to marine Neogene units.

Horcon Formation

Late Pliocene

(Thomas, 1958)

It is described as a marine to transitional sedimentary sequence of Late Pliocene, poorly consolidated, up to 80 m thick, composed of dark brown to light grey, fine to medium, litho–feldspathic sandstones, interbedded with minor conglomerates and mudstones (Tavera, 1960; Thomas,1958; Rivano, 1993). There are some fossiliferous beds with vertebrates, chondrichthyan fossils, bivalves, gastropods, and arthropods. A specimen of *Thalassocnus* (probably *T. littoralis, T. carolomartini* or *T. yaucensis*) was described in

Playa La Luna with an isolated phalanx (De Los Arcos et al.,2017). It would be the youngest Upper Pliocene sample found of the genus in the Neogene marine basins along the Andean coast (Peralta-Prato and Solórzano, 2019). Carrillo–Briceño et al. (2013) describe a diverse chondrichthyan fossil association, such as *Callorhinchus sp., Heterodontus sp., Carcharodon carcharias, Isurus oxyrinchus, Galeorhinus galeus, Carcharhinus brachyurus, Hexanchus griseus, Squatina sp., Pristiophorus sp., Rajidae, Dasyatidae and Myliobatidae*. These taxa suggest shallow marine system with warm waters and high biodiversity.

Micro-conglomeratic coarse sandstones are at the base of the formation, whose clasts come from the erosion of the intrusive basement, exposed north of the Horcon town.

This unit was deposited in shallow marine environments varying from moddle to inner shelf that include shoreface and transitional environments, associated to a low energy protected bay and warm shallow waters. In its type – locality (Horcon area) it lies directly over Paleozoic – Mesozoic intrusive basement rocks in a non-conformity relationship; southwards it conformably overlies the Navidad Formation. It is covered by Quaternary palaeodunes and aeolian deposits. It correlates to La Cueva Formation to the South, out of the study area. Its continental lateral equivalent is the Confluencia Formation. It is fully exposed in a continuous coastal cliff between Maitencillo and Horcon and discontinuously from Horcon to Viña del Mar. Also, it is well exposed on gullies and anthropogenic slopes in Quintero, Los Maitenes, Mantagua and Las Gaviotas localities.

Neogene marine and transitional units such as Horcon Formation are included in the Navidad Group; other formations outside from the study area are also included, e.g.: Capas de Lo Abarca (Brüggen, 1934, 1950; Covacevich and Frassinetti, 1986, 1990), La Cueva (Brüggen 1934, 1950), Navidad (Darwin, 1846), Licancheu and Rapel (Tavera 1968, 1979). These related to the sedimentation and filling of the homonymous basin and its northern depocenter in Horcon.

b) Quaternary Deposits

Deposits of marine terraces

In the study area, there are at least 3 levels of marine terraces, carved on intrusive or metamorphic basement or on Neogene sedimentary rocks. They are covered by marine gravels and sands, and by aeolian deposits. The most recent levels are partially covered by fossiliferous lenses with a maximum thickness of 0.5m; these are slightly indurated coquinas (hardgrounds-like with different grades of lithification). Those lenses are partially or fully covered by aeolian sands.

Palaeodunes and Aeolian deposits

Aeolian inactive to active deposits composed by medium to fine grained well sorted sands, partially weathered, cover the marine terraces; weathering gives them a characteristic reddish-brown color. They are covered by grey to yellow medium grained, well sorted loose sands. There is a vegetational cover with incipient soil development. The deposits preserve part of their original morphology. Total maximum thickness is 30m including inactive, sub-actual and actual dunes. Two depositational events can be recognized in the palaeodunes, however it is difficult to separate from each other. Extension of the aeolian deposits reaches up to 15km inland from the actual coastline. They cover all the underlying units obliterating their presence.

Alluvial, colluvial and fluvial deposits

Alluvial and colluvial deposits of gravel and sand are found at the piedmont of the Cordillera de la Costa, at the foothills and in the upper part of gorges. Fluvial deposits of gravel, sand, and mud are on the actual river streams or on its terraces, floodplains, or their estuaries.

2.3 Seismotectonic Setting

The study area is in the Andean subduction margin, where are several seismogenic sources such as: Thrust, Intraplate of intermediate depth, Outer-rise and Crustal (e.g., Leyton et al, 2010; Perez-Estay et al., 2016; Ruiz and Madariaga, 2018; Santibañez et al., 2019; Yañez and Rivera, 2019).

Lay et al. (2012) have been defined four megathrusts faulting domains based on several records of earthquakes along subduction zones and where rupture nucleates in each case as shown in the W – E depth view in Figure 3. Domain A is the nearest domain to the trench are related to tsunami earthquakes with low short period energy, anelastic deformation and stable sliding. Domain B is central megathrust rupture zone, where large slip earthquakes with low short period energy occur. Domain C is a deeper rupture zone, below the Moho, with modest slip earthquake with high short-period energy. Domain D is a transitional domain of slow slip, of low frequency earthquakes and seismic tremors at intermediate to high deep.

In the historical record of megathrusts in Central Chile of domain A and B (Figure 3), with large rupture areas and magnitude greater than Mw8.0, are the events of 1647, 1730 and 1751 (Ruiz and Madariaga, 2018). The 1906 Mw8.2 Valparaíso, 1928 Mw7.7 Talca, 1985 Mw8.0 Valparaíso, and 2010 Mw8.8 Maule earthquakes initiated the rupture in the domain C (Ruiz and Madariaga, 2018).

The crustal seismicity is commonly related to intra – arc fault systems and to forearc fault systems. The 1958 Mw6.3 Las Melosas was related to a fault system in the volcanic arc of Principal Cordillera. Its hypocenter was at 15km depth, it had surface rupture and possible focal mechanism sinistral in a plane of strike N-S or dextral in a plane of strike E-W (Sepúlveda et al., 2008; Alvarado et al., 2009). The 2004 6.5Mw Teno earthquake was related to an intra-arc fault as well, which hypocenter was located at 4.7 km depth (González, 2008). The focal mechanism indicates a dextral slip in a fault plane

N21°E/61°E, -178°; or a sinistral slip in a fault plane N70°W/88°N, -29° (CMT Global Catalog, Ekström et al., 2012).

Additionally, at the southern extreme of Chile a well-studied case is the 2007 Mw6.2 Aysén earthquake (CMT Global Catalog, Ekström et al., 2012). This event is related to Liquiñe – Ofqui Fault System, a sinistral intra-arc fault system, whose focal mechanism N84E/86E,2 and N06W/88S,176 (CMT Global Catalog, Ekström et al., 2012) with a high angle N-S sinistral slip (Legrand et al., 2011).

At the forearc domain, in Pichilemu fault two earthquakes occurred a few days after Mw8.8 Maule in 2010, their magnitudes were Mw7.0 and Mw6.9 (Farías et al., 2011). Those events were part of a group of crustal seisms that occurred immediately after the megathrust, due an appropriated fault orientation respect to the rupture zone of the Maule earthquake (Vigny et al., 2011; Hayes et al., 2013; Aron et al., 2013). The deformation in the continental lithosphere was related to a Coulomb stress increment and an extensional local regime in the over-riding plate associated to an elliptical energy radiation pattern (Aron et al, 2013). The Pisagua Mw6.7 in 2014 is a cortical post-megathrust event, occurred immediately after Iquique Mw8.3 as well (Santibañez et al., 2019).

In the forearc, between 32°S – 34°S a long-live NW-SE fault system has been recognized from geophysical data, surface structural data and field observations. The Melipilla Anomaly (Yáñez et al, 2001, 1998; Yañez and Rivera, 2019) has been interpreted as tabular and flat igneous body aligned with strike WNW along the Maipo Valley (at 33°30’S), and sub-vertical dip. This zone would be a zone of weakness of the upper crust present since the Mesozoic. Yáñez et al. (1998) associates this fault with a dextral-transpressional kinematic due a N-S compression and an oblique convergence between the Mesozoic Farallon plate and the over-riding South American plate.

From the Melipilla fault to the north there are a set of NW faults, which is called Valparaíso – Melipilla Fault System (VMFS). They are associated to magnetic anomalies just as Melipilla fault and its anomaly (Yáñez et al., 1998). The offshore architecture has

been studied by several authors (such as, Mordojovic et al., 1981; Von Huene et al., 1997: Laursen et al., 2002: Rodrigo et al., 2011), where there are NW to WNW faults with Normal or Strike-slip kinematic, similar to the faults present inland. Thus, the fault traces of the VMFS might be extended to the offshore. Their neotectonic activity is revealed by the uplift of marine terraces in the coastal range. The uplift rates vary between 0.1 to 0.4 mm/year in the Holocene (FONDEF D10E1027 Project, unpublished report, 2017).

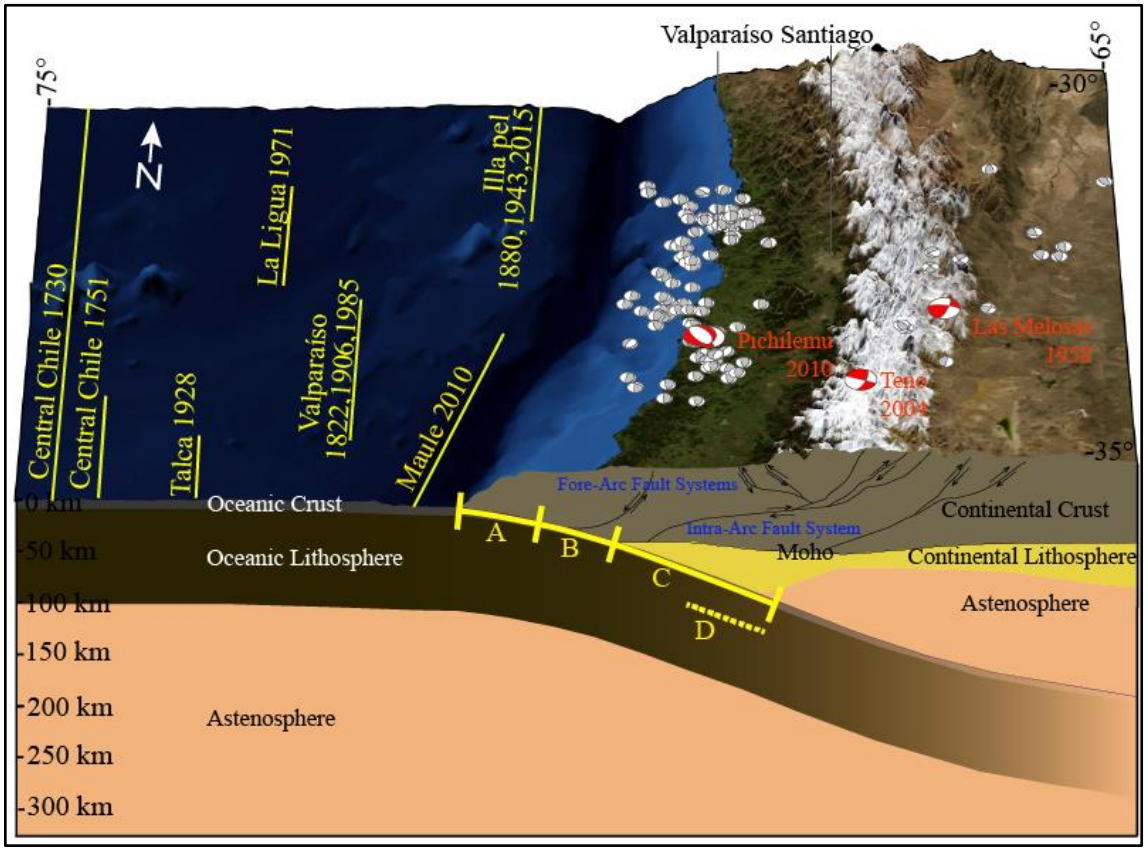

Figure 3: Block Diagram of Seismicity in Andean Subduction zone, between latitudes 30S and 35S. Historical megathrusts are shown with yellow lines of its rupture lengths in the area (Based on Ruiz & Madariaga (2018). Crustal seismicity is exhibited by the focal mechanisms of events between 1976 and 2018 (CMT Global Catalog, Ekström et al., 2012). The focal mechanisms in red corresponds to major events such as: Las Melosas Mw6.3 1958 (Sepúlveda et al, 2008), Mendoza 6.4Mw, Teno Mw6.5 2004, Pichilemu Mw7.0 and Mw6.9 2010 (CMT Global Catalog). Slab geometry based on SLAB1.0 USGS project. Internal structure of Lithosphere and Asthenosphere is based on thermal model of Valdenegro et al., (2019). Megathrusts faulting domains A, B C and D (Lay et al., 2012) are shown as yellow bold segments. Crustal faults architecture is based on Giambiagi et al. (2015)

In this work, the two northernmost faults of the VMFS were analyzed: Aconcagua fault and Marga-Marga fault. The first one, might be coincident with a surface lineament of 53 km, that guides the lower course of the Aconcagua river and its estuary with NW strike and NE high angle dip. The second one, is a set of structures with NW strike and SW high angle dip near Marga-Marga creek, in a 5km damage zone width and 65km of length (Gana et al., 1996; Thorson, 1999; Sabaj, 2008). In Marga-Marga fault has been recognized evidence of strike – slip sinistral and normal (with SW dip) kinematic (Gana et al., 1996; Thorson, 1999). This is the reflect of the cumulative movement in these faults along the time.

The evidence of strike-slip and dip-slip in crustal faults has been linked with the Andean seismic cycle of megathrusts earthquakes by several authors (e.g., Aron et al., 2013, Gonzalez et al., 2015, Del Valle et al, in prep.). In the same way, Pichilemu Mw7.0 and Mw6.9 of 2010 earthquakes have been related to a normal faulting immediately after the megathrust of Maule Mw8.8 2010 (Vigny et al., 2011; Hayes et al., 2013; Aron et al., 2013), due an appropriated fault orientation respect to the rupture zone of the megathrust. So, in the co-seismic of a megathrust, the well oriented structures could be reactivated with normal kinematic. During the inter–seismic with very low occurrence, enough energy could be accumulated in a compressive or transpressive regime, which is related to fragile deformation and strike-slip faulting (FONDEF D10E1027 Project, unpublished report, 2017).

3 METHODOLOGY

3.1 Conditioning factor of landslide hazard analysis

The conditioning factors were analyzed to obtain a spatial model of the landslide hazard. Our input information were a 5-m resolution DEM and a geological geodatabase. This last was made by field mapping campaign and based on previous geological maps (Wall et al.,1996; Gana et al.,1996; Rivano,1993). Two input maps were obtained with 5-meters resolution: one with lithological information, one with a slope map. We have established five categories for the landslide hazard based in a simplified methodology of Lara (2007). In general, a slope steeper than 15° is categorized with high co-seismic landslide hazard according to Keefer (1994). So, we analyzed only the slopes with a dip greater than 15 degrees. The hazard was categorized by lithology and slope angle as shown in Table 2. For simplicity of the analysis, the attitude of local faulting on slopes, topographic amplification, and ground water conditions were not considered.

Table 2: Hazard categorization based on dip and lithology of slope

CATEGORY	DIP [DEG.]	LITHOLOGICAL UNIT OR SEDIMENTARY DEPOSIT
Null	0 – 15	Any rock or sediment cover
Low	15 – 30	Intrusive, extrusive, and metamorphic competent rocks
Moderated	15 – 30	Sedimentary soft rock or sedimentary deposit slowly to moderately competent
High	≥30	Intrusive, extrusive, and metamorphic competent rocks low to moderately competent
Very High	≥30	Sedimentary soft rock or sedimentary deposit low to moderately competent

3.2 GIS based Spatial distribution analysis

Once the analysis of conditioning factors was done, in order to get a sample of spatial points in different lithology, slope angle and sun exposition, multiple ring buffer around the fault traces were created. Due limitations of the broadband ground motion simulation methodology, the distance to the fault trace were increased in steps of 100 m, from 1km up to 30km away. At each buffer ring, points equally spaced at 100 m were created. The points at slopes with dip angle larger than 15° were selected, because co-seismic shallow landslides can be triggered only on slopes steeper than 15° (Keefer, 1994). In order to optimize the subsequent computation of broadband synthetic seismograms and Newmark sliding block analysis, 13 areas of 1km per 1km were chosen. The selection of the areas was taking in account the localization of the first selection of slopes and the localization of areas with medium to high hazard susceptibility. Because most of the large landslides triggered by crustal earthquakes commonly occur in the surrounding area of the fault trace, at distances less than 15km (Sepúlveda et al., 2010; Shinoda and Miyata, 2017; Roback et al., 2018). Nevertheless, some co-seismic landslides can occur at greater distances, where there would be a much lower landslide density.

For all cases, 7 of the zoom-in selected areas were chosen between Aconcagua and Marga-Marga fault trace, in Viña del Mar and Concón cities (shown as blue squares in **Error! Reference source not found.**4). They are at the footwalls of each fault in the dip-s lip scenarios. For the Marga-Marga scenarios, 6 zoom-ins were at the southern area in Valparaíso, at the SW block of the Marga-Marga fault (shown as red squares in **Error! R eference source not found.**4). For the Aconcagua scenarios, 6 zoom-ins were at the northern area in Concón, Quintero and Puchuncaví communes at the NE block of the Aconcagua fault.

At each zoom-in area, were chosen between 4 to 16 points representing critical slopes, whose hazard is categorized as Moderated to Very High (those areas are shown as yellow to red colors, Figure 4). In some cases, there are some extra points that were put in critical

slopes to increase the detail of the analysis. The criteria to choose the points to analyze was:

- The points must be at a minimum distance of 100m and a maximum distance of 500m between each other.
- The points must be at different lithologies, slope dip, slope orientation.

The selected points for compute the analysis for dip-slip and strike-slip scenarios are the same, but they are not the same for the Aconcagua and Marga-Marga scenarios, due the first sampling of points related to the multiple ring buffers around their fault traces. The selection of zoom-in areas for Aconcagua and Marga-Marga scenarios were done independently because they are independent cases.

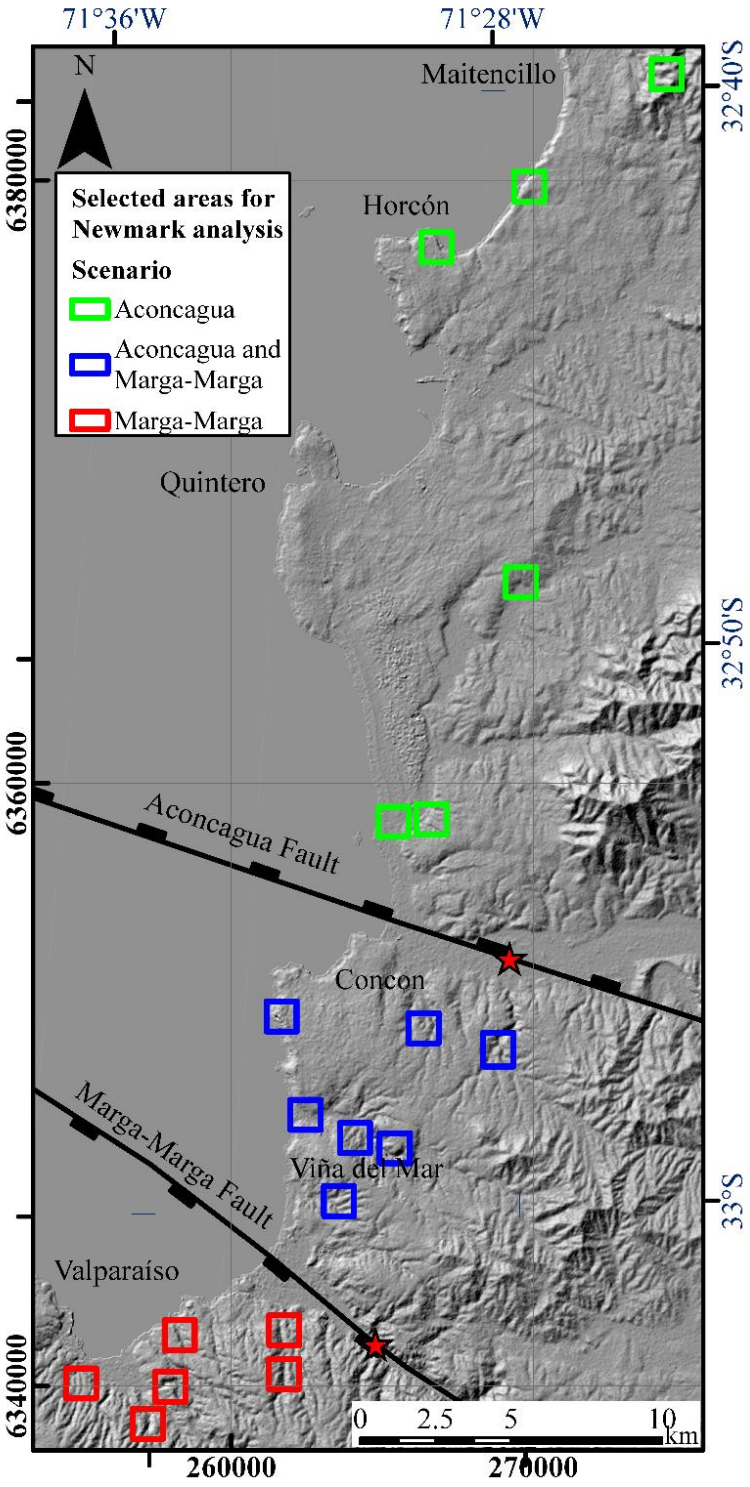

Figure 4: Map of study sub-areas, where the Broadband synthetic seismograms and Newmark analysis where computed. The Marga-Marga and Aconcagua faults are shown. The hypothetic epicenters for strike-slip scenarios are shown as red stars.

3.3 Broadband Synthetic Seismograms

Towards to synthesize seismic signals of the strong motion, we have taking in account the two possible fault kinematics for each fault: as a Normal or Sinistral. Thus, the source parameters as, fault geometry, corner frequency, focal mechanism were parametrized according to Leonard (2010). Because of the stochastic behavior of the rupture in the fault plane, used in Crempien and Archuleta (2015) method, ca. 60 simulations were made for each sub case. The broadband synthetic seismograms were simulated between 0Hz and 20Hz.

The fault geometry was set up according to the maximum inferred length of each fault, strike of the fault trace. To compute the rupture process using Green's functions, the fault area was discretized in 1024 sub faults along strike and 512 sub faults along dip.

For all cases, the source parameters were escalated using Leonard (2010). The maximum magnitude of an earthquake in Marga-Marga or Aconcagua fault is approximately an Mw7.0 or Mo=$4.027 \cdot 10^{+19}$Nm, according to the maximum inferred length of 65.9km and 53.4 km respectively. Moreover, according to Leonard (2010), the input shear wave velocity was β=3.9 km/s, the rupture velocity $v_r = 0.8\beta = 3.12$km/s.

Table 3: Values of input parameters of UCSB Broadband Synthetic seismograms

VARIABLES		MARGAMARGA fault		ACONCAGUA fault	
		Dip – Slip (Normal)	Strike Slip (Sinistral)	Dip – Slip (Normal)	Strike Slip (Sinistral)
Length (km)		65.9251	65.9251	53.3922	53.3922
Width (km) W		20.0	20.0	20.0	20.0
Area (km²)		1318.5	1318.5	1067.8	1067.8
Strike (°) φ		130.0	130.0	290.0	290.0
Dip (°) θ		Random (60,80)	90	Random (60,80)	90
Rake (°)		-90.0	0.0	-90.0	0.0
Distance in strike direction (km)		20	20	35	35
Distance in down-dip direction (km) d_d		Random (0.0, W)			
Depth of top of co-seismic rupture area Z_{TOR} (km)		Random (1.0,20.0)			
Hypocenter depth		$Z_{TOR} + d_d sin(\theta)$	$Z_{TOR} + d_d$	$Z_{TOR} + d_d sin(\theta)$	$Z_{TOR} + d_d$
Epicenter coordinates WGS 84 UTM 19S	Y UTM E (m)	$Y = y_1 + d_d cos(\theta) sin(\psi)$ $\psi = 360° - \varphi y_1 = 264794$	264794	$Y = y_1 + d_d cos(\theta) sin(\psi)$ $\psi = 360° - \varphi y_1 = 269222$	269222
	X UTM N (m)	$X = x_1 + d_d cos(\theta) cos(\psi) \psi = 360° - \varphi x_1 = 6341400$	6341400	$X = x_1 + d_d cos(\theta) cos(\psi) \psi = 360° - \varphi y_1 = 6354190$	6354190

3.4 Newmark Analysis

In the Newmark (1965) method the problem is approximated by a rigid block (Figure 5), which would slide along an infinite surface only when the seismic acceleration exceeds the critical acceleration a_c (e.g., Jibson and Keefer, 1993; Jibson, 2011). The block displacement is accumulated each time critical acceleration is exceeded.

The parameters that control the block behavior are internal friction angle between block and surface (ϕ), surface dip(α). In addition, the critical acceleration (a_c) also depends on bulk density of the material(γ'), bulk density of the water(γ_w), effective cohesion (c) and the thickness of the sliding block (t) (Figure 5).

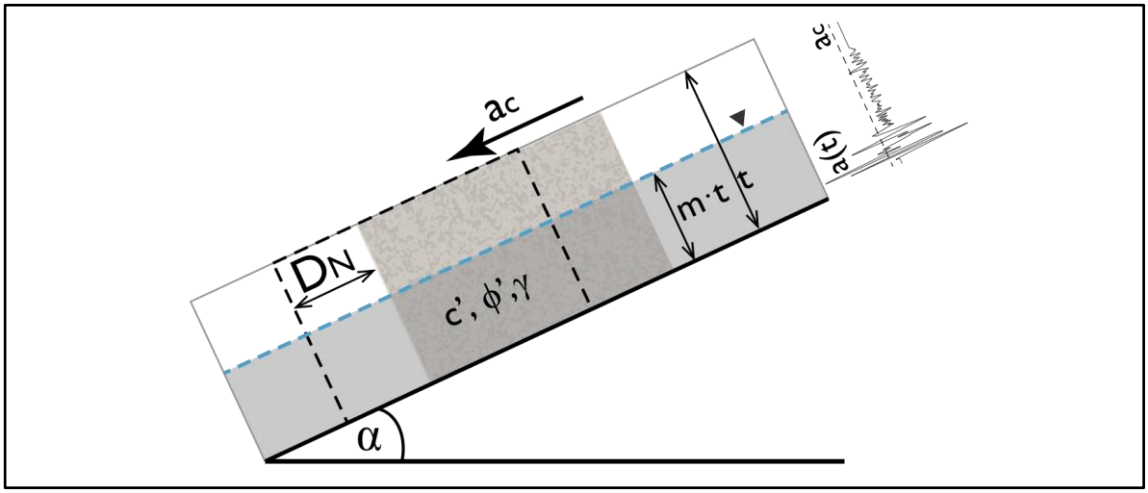

Figure 5: Newmark sliding block scheme. The problem is approximated by rigid sliding block with known cohesion, friction angle, bulk density, thickness, and saturated proportion. The component of acceleration-time history a(t) in dip and dip-direction is used in 1-D Newmark Analysis. This block moves only when the acceleration is greater than the critical acceleration. (After Jibson, 2011; Du, 2018)

The co-seismic displacement in the terrestrial surface is expressed in terms of Newmark Displacement (Dn). Corresponds to the displacement of a block of rock or soil for an oscillation cycle due ground strong motion. In pursuance of estimate the accumulated displacement for co-seismic landslides, is necessary to have the predominant period and the oscillation duration for each point analyzed (Towhata, 2008). In this work, to calculate

the Newmark Displacement we calculated a Safety Factor (FS) for infinite slope previously, then the critical acceleration (a_c) (Jibson, 2011).

The final Dn is the double integration of the difference between the acceleration time-history and the critical acceleration (Figure 6), only in the intervals where:

$$\int a(t) - a_c(t) > 0$$

$$F_S = \frac{c'}{\gamma t sin(\alpha)} + \frac{tan(\phi')}{tan(\alpha)} - \frac{m\gamma_w tan(\phi')}{\gamma tan(\alpha)}$$

$$a_c = (F_S - 1)gsin(\alpha)$$

$$D_N = \int \int \big(a(t) - a_c(t)\big)dt$$

We select two probable seismogenic faults: Marga-Marga fault and Aconcagua fault, which are part of the VMF. The Marga-Marga and Aconcagua faults have two potential kinematic behavior. The first case is a Dip-Slip Normal kinematic due a change in Coulomb stress just after a mega-thrust earthquake. This case would be like Pichilemu 2010 Mw7.0 and Mw6.9 earthquakes, which were related to Maule 2010 Mw.8.8, occurred one month before those events. Both events have shown normal focal mechanisms (Aron et al., 2013). In long term neotectonic deformation in SFVM, in inter-seismic phase those faults would have a Strike-slip behavior. So, the second case is a Strike-Slip Sinistral kinematic, which is consistent with some of the striae rake reported by del Valle (in prep.)

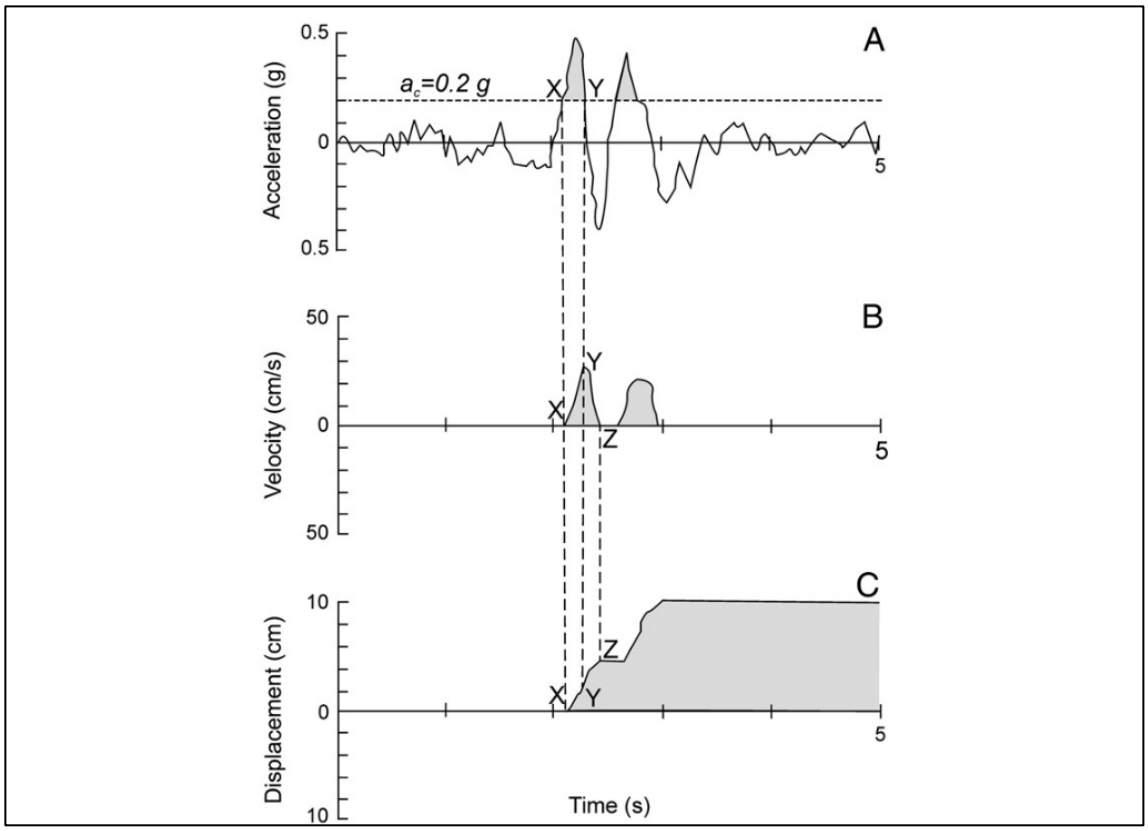

Figure 6: Newmark integration algorithm. A, acceleration time-history in solid line, critical acceleration (dashed line), the area between both curves is integrated to obtain the velocity. B, velocity versus time of the sliding block. C, Accumulated displacement of the sliding block (Jibson, 2011)

4 RESULTS: PAPER SUBMITTED TO ENGINEERING GEOLOGY

Title: **Predicting landslides caused by crustal seismicity: A case study along the Coastal Range, Central Chile**

Dominique Valdivia[a], Carlos Marquardt[a, *], Jorge G. F. Crempien[a, b], Sara Elgueta[a], Gonzalo Yáñez [a], Esteban Sáez [a, b]

[a]Escuela de Ingeniería, Pontificia Universidad Católica de Chile, Vicuña Mackenna 4860, Macul, Santiago, Chile

[b] National Research Center for Integrated Natural Disaster Management (CIGIDEN), CONICYT/FONDAP/15110017, Santiago, Chile

Abstract

Co-seismic landslides are geo-hazards resulting from the triggering event of an earthquake. Predictive landslide models under, likely seismic scenarios, are useful tools for mitigation and reduction risk assessment. Our objective was to explore landslides caused by crustal seismicity in the Andean forearc of Chile and how such kinematics may vary between strike-slip and dip-slip scenarios under dry and saturated conditions and how the conditioning parameters might control the displacements. In the Coastal Range of Central Chile (32.5–33°S), a part of the Valparaíso–Melipilla fault System (VMFS) occurs, a long-lived NW-SE-trending fault system in the Andean forearc. The two northern faults were selected, namely the Aconcagua and Marga–Marga faults, whose traces pass through highly populated coastal cities including Valparaíso, Viña del Mar and Concón. First, the slopes and surface geology were analyzed to obtain a hazard categorization. Then, several areas were chosen to develop a predictive model under different earthquake scenarios using synthetic seismograms and Newmark analysis. The computed displacements are from negligible to 10^1 m. However, under saturated conditions they can be larger by up to one order of magnitude than in dry conditions. The displacements also show a stronger lithological control than the ground motion itself. The largest computed displacements were for the Marga–Marga Normal earthquake scenario and the location of the largest displacements in all scenarios is primarily controlled by the rock/soil competence and secondarily by the directivity of the seismic rupture.

∗Corresponding author.

Email address: cmarquardt@ing.puc.cl (Carlos Marquardt)

Keywords: Valparaíso, Chile, Crustal Earthquake, Co-seismic landslide, Newmark Displacement, Broadband Synthetic Seismograms

1. Introduction

At active tectonic margins across the Earth, in particular, along subduction zones, there are several types of seismic sources, each with different rupture mechanics, hypocenter location, wave propagation and associated seismic hazards. In subduction zones, the main seismic hazard is from megathrust earthquakes (Leyton et al., 2009; Melnick et al.,2009; Vigny et al., 2011; Idini et al., 2017; Ruiz and Madariaga, 2018) and the secondary seismic hazard is from shallow crustal earthquakes (Barrientos et al., 2004; Sepulveda et al., 2008; Alvarado et al.,2009; Ammirati et al., 2019; Santibáñez et al., 2019), outer-rise (Satake and Tanioka, 1999) and intermediate- depth earthquakes (Beck et al., 1998). In subduction zones, co-seismic landslides are not well understood, those caused by crustal earthquakes. (Schulz et al., 2012; Valagussa et al., 2019). In regions such as California, Taiwan, Papua New Guinea, and Japan there have been efforts to estimate the spatial distribution of co-seismic landslides in near-real time (Nowicki et al., 2014), to study the topographic effect on co-seismic landslides ((Meunier et al., 2008) or to study the geological characteristics of co-seismic landslides (Chigira & Yagi, 2006) .In fact, co-seismic landslides can potentially cause damage that is greater than that caused by the triggering earthquake itself.

The Coastal Range of Central Chile is located at the subduction margin between the Nazca oceanic plate and the South American Plate, where the latter subducts beneath the former at a rate of 60–70 mm/yr. The Coastal Range is situated in the southernmost part of the Pampean flat-slab region. It is affected by the NW-SE-trending Valparaíso–Melipilla fault System (VMFS), whose faults are assumed to be seismogenic (Thorson, 1999; Santibáñez et al., 2019). In this work we take the two northern faults of this system, Marga-Marga and Aconcagua faults and adjacent areas between 32.5 and 33°S (Figure 1) to analyze the slope behavior under different seismic scenarios product of the activation of these crustal faults.

One of the greatest challenges in natural hazards and earth surface processes, in populated areas in seismic zones is landslide hazard assessment to save human life and to anticipate future events (National Academies of Sciences, 2003, 2018) , especially using improved physics-based methods (Jibson, 2011; Wasowski et al., 2011, 2014). For this research, it is necessary to determine the potential spatial distribution, size and displacement of co-seismic landslides that might affect the target area. Historically, co-seismic and post-seismic landslides have been responsible for fatalities, damage to infrastructure like dams or embankment and floods (e.g., Keefer, 2000; Bommer and Rodriguez, 2002; Jibson, 2007; Keefer, 2012). Rodríguez et al. (1999) argued that co-seismic and post-seismic landslides are typically related to medium-to-high intensity earthquakes with magnitudes over Mw 5.0, regardless of the seismic source.

Earthquake-triggered landslides are the main hazard in both mountainous regions and steep coastal landscapes (Fan et al., 2019). For instance, specific conditions are required for an earthquake to be tsunamigenic (Satake et al., 2020), however, any earthquake can trigger landslides and rock falling in slopes. There have been many studies of earthquake-triggered landslides. Some authors have implemented qualitative approaches using the categorization of hazards based on susceptibility indexes, while others have used computer-based quantitative mathematical models. The first studies involving the categorization of hazards were based on geotechnical properties, lithology, topography, slope orientation and angle, precipitation and snow coverage, among others (e.g., Lara et al., 2018; Lara, 2007; Farías, 2012; Fuenzalida, 2015; Tanyaş et al., 2017). Quantitative models have been used to classify co-seismic landslides in terms of their geomorphology and types of movement, the geology of the involved material, the distance to rupture and intensity measures (e.g., Chigira et al., 2003; Chigira and Yagi, 2006; Higaki and Abe, 2013; Sugimoto et al., 2013; Chen et al., 2020; Shafique, 2020).

The National Academies of Sciences (2003) and Wasowski et al. (2011) recommend the construction of more complete landslide inventories due to their relevance as an input for further hazard assessments. Some of these inventories are focused on particular

earthquakes (Keefer, 1984, 2000; Gorum et al., 2011; Harp et al., 2011; Wartman et al., 2013; Xu, 2015; Serey et al., 2019), while others are extensive worldwide inventories (Rodríguez et al., 1999; Malamud et al., 2004; Tanyaş et al., 2017). This kind of information is valuable for statistical and spatial analyses of landslide distribution, size, and classification (e.g., Keefer, 2000; Malamud et al., 2004; Meunier et al., 2007; Caccavale et al., 2017; Marc et al., 2017). Other authors have focused on particular landslides or areas to study the mechanics of landslides, the interaction between seismic waves and landslides, or the motion of flows and falls, through numerical modelling (e.g., De Blasio, 2011; Lenti and Martino, 2012; Worni et al., 2013), finite-element modelling for an hypothetical or real landslide (e.g., Griffiths and Lane, 1999; Huang, 2013; Harp et al., 2014; Liu et al., 2014; Podolskiy et al., 2015, García et al., 2018), or spectral-element modeling for a regional-scale case study (e.g., Huang et al., 2020). Physics-based methods for seismic stability analysis has been implemented at small scale and at local to regional scale by several authors (Crespellani et al., 1998; Miles and Ho, 1999; Bray, 2007; Del Gaudio and Wasowski, 2011; Allstadt et al., 2013; Gorum and Carranza, 2015; Lenti and Martino, 2012; Marc et al., 2017; Leshchinsky, 2018). Additionally, various authors have proposed predictive models based on statistics (Romeo, 2000; Stavrou et al., 2011; Sharifi-Mood et al., 2017; Pellicani et al., 2017; Zhang et al., 2017; Jafarian et al., 2019; Han et al., 2019) and some have proposed empirical relationships between landslide size, location, landslide density, or displacement using intensity measures (e.g., Peak Ground Acceleration (PGA), Peak Ground Velocity (PGV), Arias Intensity (I_A), Fundamental Period of soil (T_F) (Rathje and Antonakos, 2011; Du and Wang, 2016; Nowicki et al., 2014; Shao et al., 2020; Vahedifard and Meehan, 2011; Parker et al., 2017).

Some authors have used worldwide datasets to predict and to propose relations between landslides and the seismic moment, the focal mechanism, the hypocenter depth, among others(Marc et al., 2016, 2017; Vahedifard & Meehan, 2011). Re-scaling events for predictive modelling is not an accurate method when seismic datasets from other tectonic regions are used. However, a physics-based method involving synthetic

seismograms offers a more robust approach (Miles and Ho, 1999; Shanmugam and Wang, 2015; Huang et al., 2020). A traditional way to estimate seismic-induced-displacement in slopes is through rigid block analysis of Newmark (1965). There have been many interpretations of the computed displacements of co-seismic landslides with Newmark Analysis, in which they are associated with the potential slope behavior in the field and with hazard categorizations (Wieczorek et al., 1985; Keefer and Wilson, 1989; Jibson and Keefer, 1993; Romeo, 2000; Blake et al., 2002; California Geological Survey and California State Mining and Geology Board, 2008; Jibson and Michael, 2009; Jibson, 2011).

Our research questions are: (1) What are the major controlling factors for crustal-earthquake-triggered landslides in the forearc of subduction settings? (2) What is the spatial distribution and displacement of landslides caused by crustal earthquakes?

The working hypothesis was that the major controlling factor is the lithology, and the secondary controlling factor is the earthquake rupture process. In strike-slip earthquake scenarios, the potential landslides and their displacements have a symmetrical distribution about the fault. Meanwhile, in normal earthquake scenarios, the potential triggered landslides and their displacements are larger and more concentrated the hanging wall than in the footwall (Fan et al., 2019; Gorum et al., 2011). In normal earthquake scenarios, on the footwall, the potential landslides are smaller and have a lower spatial density than at the hanging wall. The aim of this work is to study the hazard from potential earthquake-triggered landslides in coastal areas where there is more than one potential fault kinematic. Crustal earthquakes were studied associated with strike-slip and dip-slip kinematics where fault traces occur close to highly populated urban areas.

In the emerged forearc of Central Chile, potential earthquake scenarios associated with the two northern faults of the VMFS—the Marga–Marga and Aconcagua faults—were analyzed. These faults have potential dual kinematics; they can have sinistral strike-slip

kinematics or normal dip-slip kinematics depending on changes in Coulomb stresses (Rodrigo, 2011; Aron et al., 2013). The occurrence and displacement of co-seismic landslides were analyzed using a first approach based on conditioning factors and a physics-based model for four potential earthquake scenarios. First, a preliminary analysis was performed based on the main conditioning factors of slope failure. A GIS-based technique considering spatial features to represent the geology and a 5m resolution Digital Elevation Model (DEM) was implemented, using a hazard index which does not depend on the seismic source. On the basis of this first analysis several areas of 1 km x 1 km were identified, each containing several slopes where we have developed a susceptibility analysis based on surface lithology and slope angle. For these areas, broadband synthetic seismograms were constructed, and the Newmark displacement was calculated. The final co-seismic displacements were calculated in the dip direction of the slope following the classic Newmark method (Newmark, 1965) under dry and saturated soil conditions.

2. Geological and geomorphological setting

The study area is located in the Coastal Range of the emerged forearc of Chile, between 32.5 and 33° S, at the southernmost part of the Chilean Pampean flat-slab region (Isacks, 1988; Ramos 2009; Charrier et al., 2014). The low angle of subduction and the absence of Quaternary volcanic activity in the flat slab is due to the subduction of the Juan Fernandez Ridge (JFR) since ca. 8-10 Ma (Yáñez et al.,2001; Le Roux et al., 2006), immediately offshore of the study area.

The main morphostructural units from E to W are: The Coastal Cordillera, whose maximum height in the study area is 1040 m.a.s.l.; coastal plains and a narrow beach backed by active coastal cliffs. The flat relief of the summit areas of the Coastal Cordillera here has been interpreted as remnant peneplains that have been rapidly uplifted from the original position close to sea level (Farías et al., 2008; Saillard et al., 2009). The coastal plains are related to Neogene and Quaternary marine, transitional,

and continental sedimentary units covering the basement units and their morphology is that of marine terraces uplifted in the Pleistocene–Holocene (Marquardt et al., 2004; Rodríguez et al., 2013; Sepúlveda et al., 2015; Binnie et al., 2016). The exposure of Pliocene marine units in a continuous cliff in the northern Maitencillo and Horcon – part of the study area- suggests an uplift of at least 100 m during the Pliocene and Quaternary (Encinas et al., 2006, 2008; Valdivia et al., 2018).

Moreover, the marine terraces in this area have an apparent high uplift rate of 0.25 to 0.3 mm/yr. since 0.4 Ma (Melnick, 2016). The uplift of the marine terraces is segmented along the Andean coastal range (Melnick et al., 2009; Martinod et al., 2016). This uplift has been related to the seismic cycle and to the rupture process of megathrust earthquakes, and higher uplift rates have been related to the boundaries of historical megathrust earthquakes areas with low slip (Jara-Muñoz and Melnick,2015; Melnick, 2016).

The basement of the Coastal Cordillera is composed of Paleozoic metamorphic rocks, Paleozoic and Mesozoic intrusive rocks, and Mesozoic volcanic rocks (Gana et al., 1996; Servicio Nacional de Geología y Minería (SERNAGEOMIN), 2003). The Paleozoic Valparaiso Metamorphic Complex outcrops in the southern coastal area of Valparaíso (Figure 1) (Gana et al., 1996). This complex is intruded by granitoids, tonalites, and gabbro units of Paleozoic and Mesozoic ages; these units form N-S-trending discontinuous belts whose ages become younger from west to east (Rivano et al., 1993; Gana and Tosdal, 1996; Gana et al., 1996; Creixell et al., 2006). These intrusive rocks are partially covered by the Ajial Formation (shown in light blue in Figure 1), which was defined by Thomas (1958) as a volcano-sedimentary sequence of Jurassic age (Charrier et al., 2014; Boyce et al., 2020). This formation is composed of andesitic, rhyodacitic, and basaltic lavas, with additional conglomerates, sub arkoses, greywackes, and calcarenites (Rivano et al., 1993). The Ajial Formation is intruded by Upper Jurassic to Cretaceous plutonic rocks (Parada et al., 2005; Boyce et al.,2020).

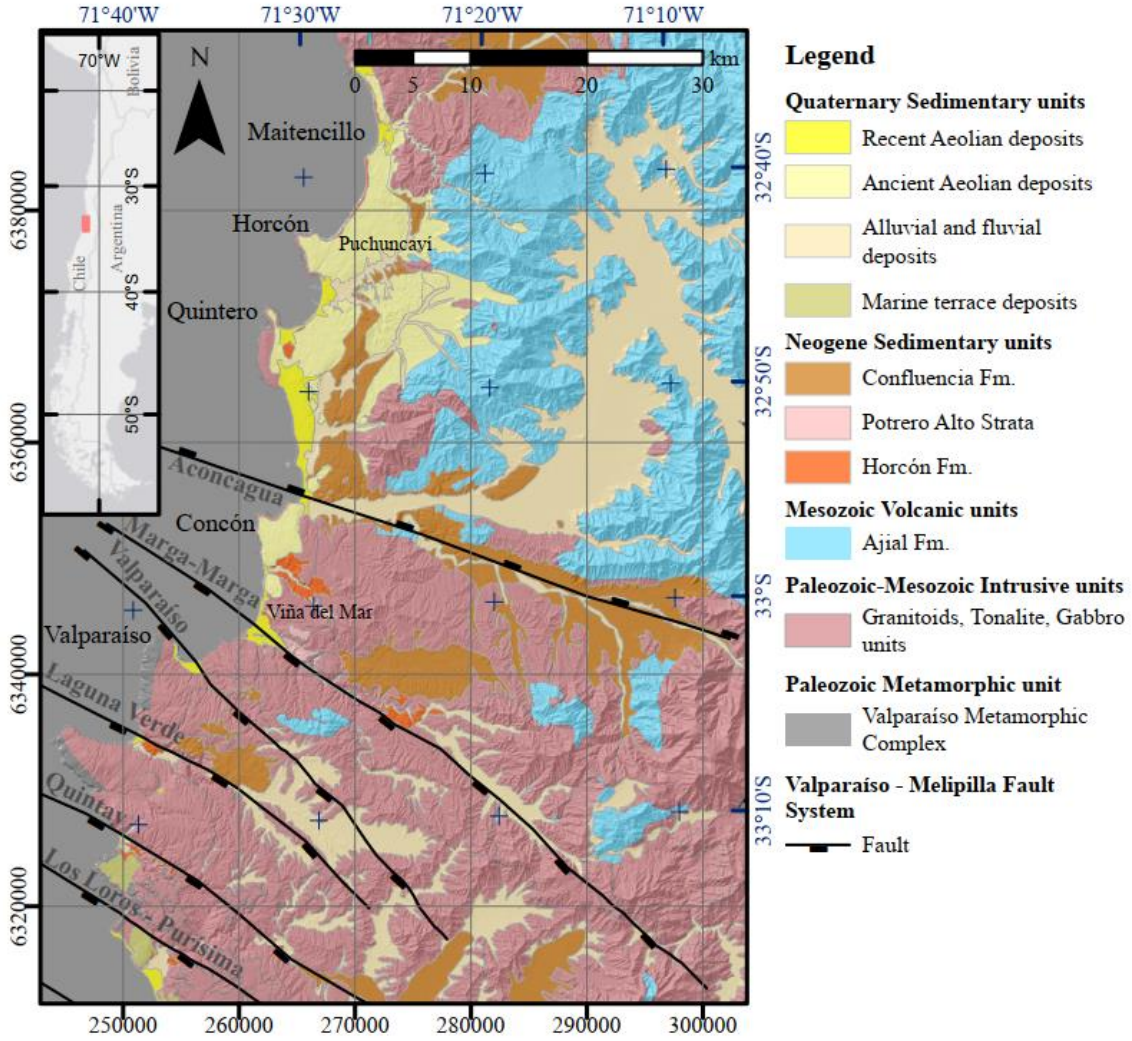

Figure 1: Simplified geological map of the study area. Note the inferred Aconcagua fault dipping to the NE and the inferred Marga–Marga fault dipping to the SW. Modified from Rivano et al. (1993), Gana et al. (1996), SERNAGEOMIN (2003), and Charrier et al. (2014).

The Neogene units overlying the intrusive rocks and the Ajial Formation are part of the Navidad Group, whose members are part of the sedimentary infill of the Navidad Basin (Lavenu and Encinas, 2005; Encinas et al., 2006) and its northern depocenter in Horcon. In the study area, the Pliocene Horcon Formation is the youngest unit (Thomas, 1958; Carrillo-Briceño, 2013; De Los Arcos et al., 2017; Valdivia et al., 2018). The Horcon Formation is constituted by three facies—micro-conglomeratic coarse lithic fossiliferous sandstone; fine-to-medium grained litho-feldspathic fossiliferous

sandstones interbedded with polymictic conglomerates; and fine-to-medium grained potassic feldspar-quartz fossiliferous sandstones—all of them with low-to-medium lithification (Valdivia et al., 2018). In these upper facies, researchers have described bivalves, vertebrates, chondrichthyans, and arthropods (Carrillo-Briceño, 2013; De Los Arcos et al., 2017). This unit was deposited in shallow marine varying to beach transitional sedimentary systems associated with a low-energy protected bay and warm shallow waters. In Figure 1, the Horcon Formation appears in orange; it outcrops in a continuous active coastal cliff between Maitencillo and Quintero and is well exposed in gullies, marine scarps, and anthropogenic slopes in the eastern area of Puchuncaví and Viña del Mar.

The gravels of the Central Coast, whose members include the Confluencia Formation (Rivano and Sepulveda, 1991) (equivalent to the Horcon Formation) and the overlying Potrero Alto strata (Wall et al., 1996), are related to continental sedimentary systems (shown in brown and pink in Figure 1, respectively). Both the Confluencia Formation and the Potrero Alto strata are sedimentary sequences of medium-to-low lithification composed of imbricated conglomerates interbedded with sandstones and mudstones with large-scale crossbedding; they are related to alluvial, fluvial, and eolian systems.

In the study area, there are at least three levels of marine terraces (Rodríguez, 2008; Guerrero, 2020). The associated deposits of marine sands, gravels, and eolian sand deposits are in unconformable contact above intrusive or metamorphic Paleozoic–Mesozoic basement. Most recent levels are partially covered with coquinas (hardgrounds-like with different grades of lithification) that are partially or fully covered by eolian sand deposits, which are related to Quaternary palaeodunes, sub-actual dunes, and actual dunes that can reach up to 15 km from the actual coastline to the east. The composition of the Quaternary eolian deposits is medium-to-fine grained sands with some alteration at the lower levels. The younger levels are well-sorted fine and loose sands; they are related to the palaeodune field of Puchuncaví and Quintero and to the actual dune fields of Ritoque and Concón (this work).

In the foothills of the Coastal Cordillera and along gorges and gullies in this mountain range there are alluvial and colluvial deposits of gravel and sands. Recent fluvial deposits are related to actual river streams, such as the lower course of the Aconcagua River, as well as its terraces, floodplains, and an estuary next to Concón (this work).

1. **Seismotectonic Setting**

The study area is in the Andean subduction margin, where several seismogenic sources are possible, such as: interplate and intraplate (Shearer, 1975). The interplate domain is the more complex domain, where rupture occurs due to a loss of coupling between the overriding continental crust and the under-riding oceanic crust (Brune, 1970,1971; Madariaga, 1976; Aki, 1984; Loveless et al., 2010; Lay et al., 2012; Briggs, 2016). The intraplate domain in the oceanic plate includes intraplate earthquakes of intermediate depth (Beck et al., 1998) and outer-rise earthquakes (Satake and Tanioka, 1999). The intraplate domain in the continental plate is a shallow crustal domain (e.g., Sepulveda et al., 2008; Alvarado et al., 2009 Leyton et al., 2010; Ruiz and Madariaga, 2018; Santibáñez et al., 2019).

Lay et al. (2012) defined four megathrust faulting domains: A, B, C and D; based on several earthquake records along subduction zones and the location where the rupture nucleates, as shown in the E-W depth cross-section in Figure 2. Domain A is the nearest domain to the trench and is related to tsunami earthquakes with low, short-period energy radiation, anelastic deformation, and stable sliding. Domain B is the central megathrust rupture zone and generates large slip earthquakes with low, short-period energy radiation. Domain C is a deeper rupture zone, below the Moho, and produces modest slip earthquakes with high, short-period energy radiation. Domain D is a transitional domain with slow slip, low-frequency earthquakes, and seismic tremors at intermediate to high depth.

The historical record of megathrust earthquakes—that is those with large rupture areas and magnitudes greater than Mw 8.0—in domains A and B of Central Chile, include the

events of 1647, 1730 and 1751 (Ruiz and Madariaga, 2018). The 1906 Mw 8.2 Valparaíso, 1928 Mw 7.7 Talca, 1985 Mw 8.0 Valparaíso, and 2010 Mw 8.8 Maule earthquakes initiated the rupture in Domain C (Ruiz and Madariaga, 2018), and their rupture propagated upward towards the trench.

Crustal seismicity is commonly related to intra-arc and forearc fault systems (Farías et al., 2010; Leyton et al., 2010; Heinze, 2003). The 1958 Mw 6.3 Las Melosas earthquake was related to a fault system in the volcanic arc of the Main Cordillera. Its hypocenter was at 15 km depth, it had a surface rupture, and its focal mechanism was possibly sinistral on a plane striking N-S or dextral on a plane striking E-W (Sepulveda et al., 2008; Alvarado et al., 2009). The 2004 Mw 6.5 Teno earthquake was also related to an intra-arc fault, whose hypocenter was at 4.7 km depth (Gonzalez, 2008). Its focal mechanism indicates dextral slip on a fault plane with strike N21◦E, dip 61◦E, and rake -178◦ or sinistral slip on a fault plane with strike N70◦W, dip 88◦N, and rake -29◦ (Global CMT Catalog, Ekström et al., 2012).

Another well-studied earthquake is the 2007 Mw 6.2 Aysén earthquake (Global CMT Catalog, Ekström et al., 2012), which occurred in the south of Chile. This event was related to the Liquiñe–Ofqui Fault System, which is a sinistral intra-arc fault system, and its focal mechanism had the solution of a fault plane with strike N84°E, dip 86°E, and rake 2°, and a plane with strike N06°W, dip 88°S, and rake 176° (Global CMT Catalog, Ekström et al., 2012) with high-angle N-S sinistral slip (Legrand et al., 2011). Several landslides and a tsunami were triggered by the Aysén earthquake, which have been well studied by Sepúlveda and Serey (2009) and Sepúlveda et al. (2010). These authors found that the main controlling factors for the landslides were the geotechnical and geomorphological characteristics of the rock slopes.

In the forearc domain, there are several fault systems with recent activity such as the Pichilemu fault (Arriagada et al., 2011; Alfaro, 2011; Aron et al., 2013), the El Yolki fault (Melnick et al., 2019), the Atacama Fault System (Niemeyer et al., 1996; Cembrano

et al., 2005; Hoffmann-Rothe et al., 2006; Gonzalez, 2008; Allmendinger and Gonzalez, 2010; Cortés, 2012),the East-West Transversal Fault System (Allmendinger et al., 2005; Gonzalez, 2008; Gonzalez, 2010) and the Andean Transverse Fault System (Sielfeld et al., 2019) or Trans Lithospheric Faults in the definition of Yañez and Rivera (2019). Two earthquakes occurred on the Pichilemu fault on 11 March 2010, a few days after the Mw 8.8 Maule megathrust earthquake on 27 February 2010. These events had magnitudes of Mw 7.0 and Mw 6.9 (Farías et al., 2011) and were part of a group of crustal earthquakes that occurred immediately after the Maule megathrust earthquake due to a favorable fault orientation with respect to the rupture zone of the Maule earthquake (Vigny et al., 2011; Hayes et al., 2013; Ruiz et al., 2014). Aron et al. (2013) found that the deformation in the continental lithosphere caused by the Mw 7.0 and Mw 6.9 events was related to an increase in Coulomb stress and an extensional local regime in the overriding plate associated with an elliptical energy radiation pattern. Similarly, the Pisagua Mw 6.7 earthquake in 2014 was a cortical event which occurred immediately after the Iquique Mw 8.3 earthquake (González et al., 2015; Santibáñez et al., 2019). In the Chilean forearc there are neotectonic strike-slip faults such as Chomache fault, Domeyko fault system, with geomorphological evidence of their displacement and seismic records (Allmendinger & González, 2010; Bloch et al., 2014; Mpodozis & Cornejo, 2012).

In the forearc, between 32◦ S and 35◦ S, a long-lived NW-SE-oriented fault system has been recognized from geophysical data, surface structural data, and field observations. The Melipilla Anomaly (Yáñez et al., 1998; Yáñez et al., 2001) is a magnetic and CMST anomaly interpreted as a flat tabular igneous body striking WNW along the Maipo Valley (at 33◦30’S) with a sub-vertical dip. This anomaly represents a zone of weakness in the upper crust that has been present since the Mesozoic, that is represented at surface by the Melipilla fault (Wall et al., 1996). Yáñez et al. (1998) associated this fault with dextral-transpressional kinematics due to a N-S compression and an oblique convergence between the Mesozoic Farallon Plate and the overriding South American Plate. From the Melipilla fault to the north there is a set of NW to WNW-trending faults

called the Valparaíso–Melipilla Fault System (VMFS). These are associated with magnetic anomalies, as are the Melipilla fault and its anomaly (Yáñez et al., 1998). This system has been studied with field observations (Rodríguez, 2008; Sabaj, 2008) and by the recognition of lineaments in drainage systems (Gana et al., 1996; Castro and Brignardello, 1997). Figure 1 shows, from N to S, the Aconcagua, Marga–Marga, Valparaíso, and Laguna Verde faults of the VMFS.

The offshore architecture of this fault system has been studied by several authors (Mordojovic, 1981; von Huene et al., 1997; Laursen et al., 2002; Rodrigo, 2011), who identified NW to WNW-trending faults with normal or strike-slip kinematics, similar to the faults located inland. Thus, the VMFS, as a fault system, appears to be extended to the offshore area. The neotectonic activity of the VMFS is revealed by the uplift rates of marine terraces in the Coastal Range, which vary between 0.1 and 0.4 mm/year (Sáez et al., FONDEF D10E1027 Project, unpublished report, 2018) and is supported by stratigraphic evidence.

The present study is focused on potential co-seismic landslides associated with different earthquake scenarios related to the Aconcagua and Marga–Marga faults, which are the northernmost faults of the VMFS. Different seismic scenarios on the Marga–Marga and the Aconcagua fault—which have been suggested to have either normal or sinistral kinematics—and under dry and saturated conditions were computed.

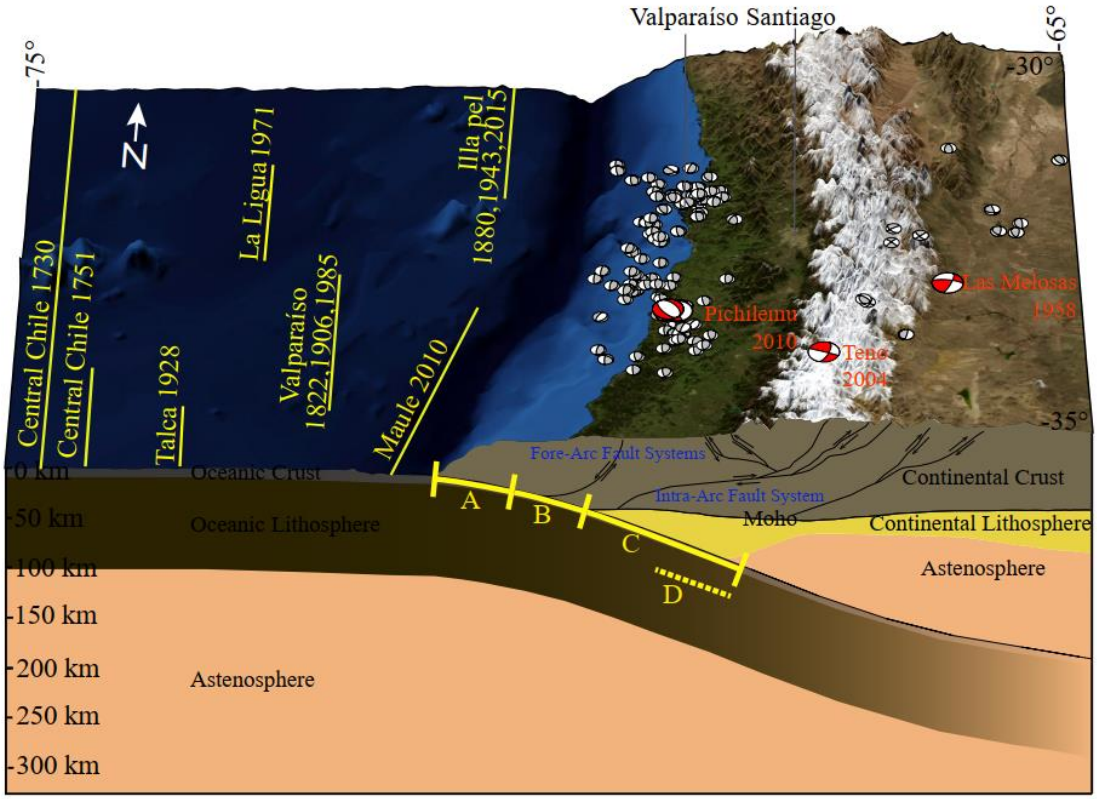

Figure 2: Block diagram of seismicity in the Andean subduction zone between latitudes of 30◦ S and 35◦ S. The rupture lengths of historical megathrust earthquakes are shown with yellow lines (based on Ruiz and Madariaga (2018)). Crustal seismicity is shown by the focal mechanisms of events between 1976 and 2018 (Global CMT Catalog, Ekström et al. (2012)). The focal mechanisms in red correspond to major cortical events, namely: the 1958 Las Melosas Mw 6.3 (Sepulveda et al. (2008)), the 2004 Mendoza 6.4 Mw, the 2004 Teno Mw 6.5, and 2010 Pichilemu Mw 7.0 and Mw 6.9 earthquakes (Global CMT Catalog). Slab geometry is based on the USGS SLAB1.0 project. The internal structures of the lithosphere and asthenosphere are based on the thermal model of Valdenegro et al. (2019). Megathrust faulting domains A, B, C, and D (Lay et al.,2012) are shown by yellow.

4. Co-seismic landslide hazard analysis based on conditioning factors

The conditioning factors of slope failure were analyzed to obtain a spatial model of the landslide hazard. The input information was as follows: a DEM with a 5-m resolution, and a geological geodatabase. The geodatabase was constructed based on a field mapping campaign and previous geological maps (Wall et al., 1996; Gana et al., 1996;

Rivano et al., 1993). Two rasters were obtained with a 5-m resolution, one with lithological information and one with a slope map.

The slope characteristics that are most used in the qualitative assessment of landslides are the slope angle and the regional-scale lithology. For instance, for the 2008 Mw 6.9 Wenchuan earthquake, Liu et al. (2012) produced a slope stability classification based on slope angle and rock competence. The slope angles were classified into four classes of 0–10◦, 11–30◦, 31–40◦, and >40◦, while the lithology and its competence were classified into four classes: high competence (thick layers of limestone, sandstone, and metamorphic rocks), high-to-medium competence (interbedded limestone and sandstone), low-to-medium competence (highly fractured rocks), and low competence (Cenozoic sandstones and unconsolidated sediments).

Five categories for the landslide susceptibility were established based on a simplification of the methodology of Lara (2007) and Liu et al. (2012) (see Table 1). According to Keefer (1994), in general, slopes steeper than 15◦ are categorized as having high co-seismic landslide hazard. Therefore, we analyzed only slopes with a dip greater than 15◦, and these slopes were classified as having null hazard. The hazard was categorized by lithology and slope angle as shown in Table 1. For analytical simplicity, the distance to fault traces and groundwater conditions were not considered to analyze only the main conditioning factors. Landslide susceptibility was classified according to the slope angle in the following three sub-classes: [0◦–15◦], [15◦–30◦], [30◦,90◦]. Additionally, the susceptibility was classified according to the lithological cover in the following two sub-classes: (a) Paleozoic–Mesozoic intrusive, extrusive, and metamorphic rocks; and (b) Cenozoic sedimentary rocks, and unconsolidated sedimentary deposits. Furthermore, landslide hazard was classified according to the competence of the rock in the following two sub-classes: (1) competent rocks; and (2) low to moderate competent rocks. These sub-classes were used to produce a categorization with five categories: Null (Any rock or sedimentary deposit with slope angle lower than 15°), Low (competent Paleozoic–Mesozoic intrusive, extrusive, and metamorphic rocks, with slope angles between 15◦

and 30◦), Moderate (lowly to moderately competent and moderately weathered Cenozoic soft sedimentary rocks and unconsolidated sedimentary deposits, with slope angles between 15◦ and 30◦); Moderate-to-High (lowly to moderately competent or moderately to highly weathered Paleozoic–Mesozoic intrusive, extrusive, and metamorphic rocks, with slope angles larger than 30◦); High (lowly to moderately competent Cenozoic soft sedimentary rocks and unconsolidated sedimentary deposits, with slope angles larger than 30◦).

Table 1: Susceptibility categorization based on dip and lithology of slopes

Category	Dip	Lithological Unit or Sedimentary Deposit
Null	0◦–15◦	Any rock or sediment cover
Low	15◦–30◦	Intrusive, extrusive, and metamorphic competent rocks
Moderated	15◦–30◦	Lowly to moderately competent soft sedimentary rock or sedimentary deposits
High	≥ 30◦	Lowly to moderately competent intrusive, extrusive, and metamorphic rocks
Very High	≥ 30	Lowly to moderately competent soft sedimentary rock or sedimentary deposits

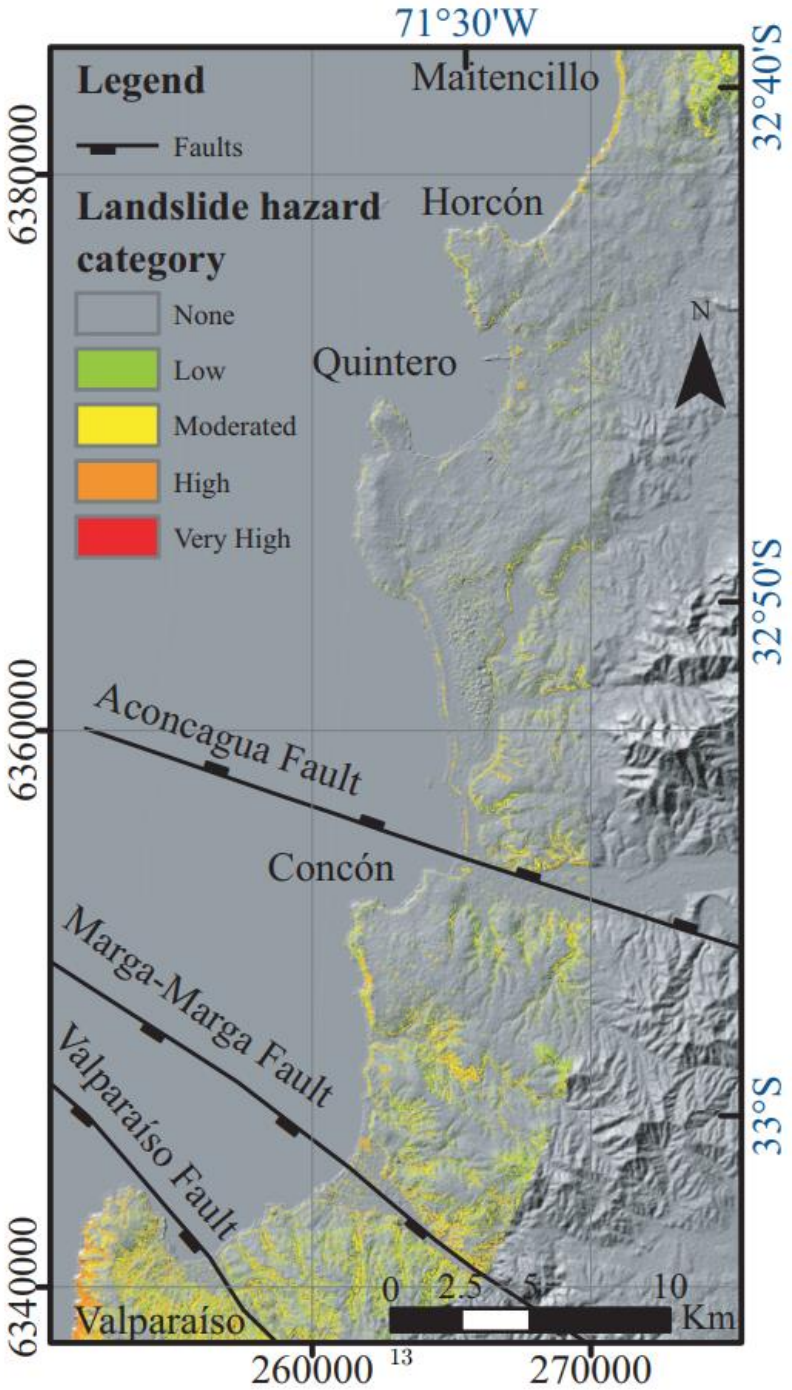

Figure 3: Qualitative categorization of landslide hazard based on lithology and slope.
bold segments. Crustal structures are taken from del Valle et al. (in prep) and Santibáñez et al. (2019).

4.1. Landslide susceptibility

Categories of landslide hazard were defined as shown in Table 1. As shown in Figure 3, most of the steep slopes with high or very high hazard are located in the south of the study area near the cities of Valparaíso and Viña del Mar and in the north of the study area near Puchuncaví. In the former area, most of the high hazard is related to Quaternary sedimentary deposits with low cohesion and steep slopes situated above metamorphic and intrusive basement rocks. In the latter area, the high hazard is associated with a continuous cliff where Neogene sedimentary rocks outcrop. Figure 4 shows some examples of recent landslides in the study area which coincide with areas of high hazard. Along the coastal area in the northern part of the study area, we observed old rotational landslides with horizontal displacements of ca. 5 m (e.g., Figure 4A) whose trigger is unknown; these landslides occurred on medium-competence Neogene marine sandstone of the Horcon Formation, which outcrops in the most recent marine scarp in Horcon city. Figure 4B shows a translational landslide to the south of a road close to Quintero which may have been triggered by heavy rainfall in winter; its displacement is 3–4 meters and it occurred on low-competence Neogene continental coarse sandstone of the Confluencia Formation. Figure 4C shows a complex landslide at Maitencillo; it is an old rotational landslide on very low-competence Quaternary eolian deposits with a displacement of ca. 15 m. This landslide has some reactivation of smaller rotational and translational landslides with displacements of 1–3 m and several debris flows, whose runouts are 10–15 m in length. Figure 4 D shows a toppling on Neogene marine sandstones of the Horcon Formation on the active coastal cliff, with a maximum displacement of ca. 5 m.

Based on this first categorization, areas of 1 km x 1 km were chosen to refine the analysis at a local scale and assess the potential displacements in areas categorized as having medium-to-high landslide hazard.

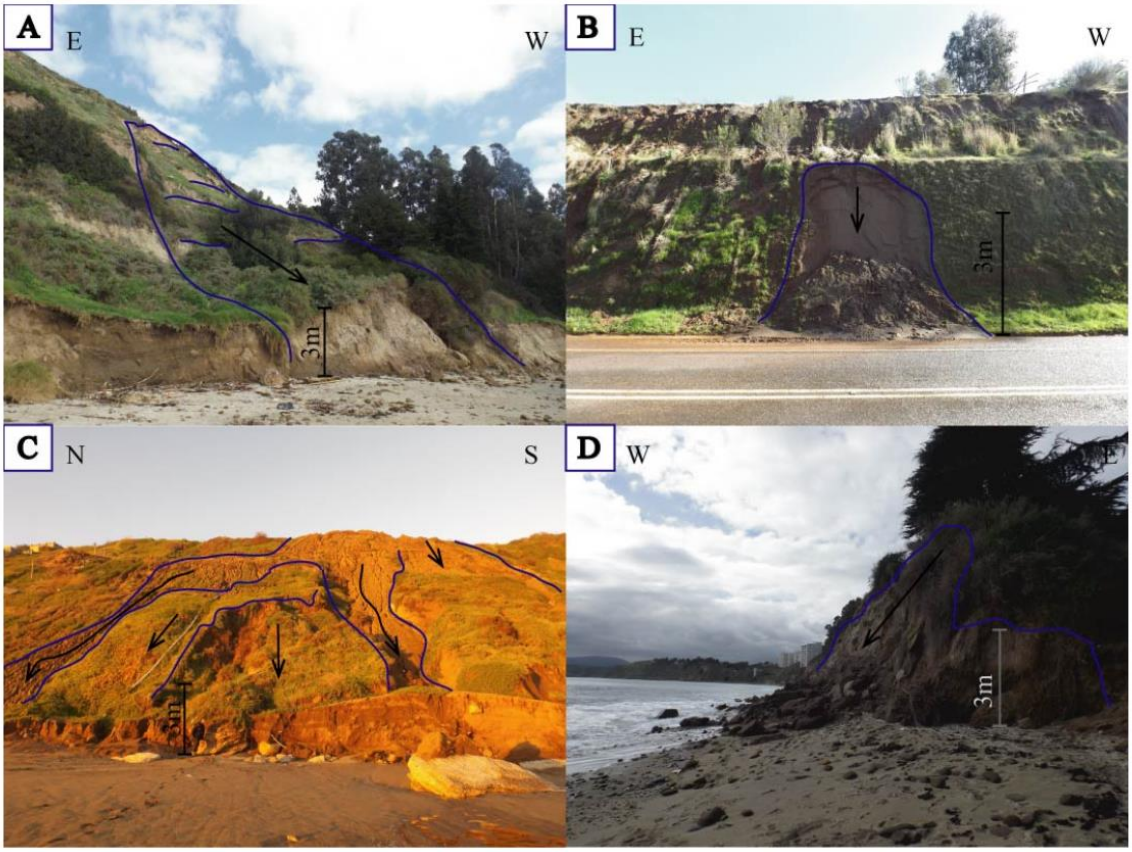

Figure 4: Example of landslides in the field (photographs taken in winter 2017). (A) Rotational landslide on Neogene marine sandstones with medium competence. (B) Translational landslide on Neogene continental sandstones with low competence. (C) A complex landslide, a translational landslide with small debris flows on Quaternary eolian sand deposits with low competence. D) Topping on Neogene marine sandstone with medium-to-low competence in the active coastal cliff.

5. **Ground motion simulation and Newmark analysis**

In the Newmark (1965) method, a shallow translational landslide is approximated by a rigid block which slides along an infinite plane surface only when the seismic acceleration exceeds the critical acceleration a_c, as shown in Figure 5 (e.g., Jibson, 1993; Bray and Travasarou, 2007; Jibson, 2011; Rathje and Antonakos, 2011; Du and Wang, 2016; Kan et al., 2017; Veylon et al., 2017; Yuan et al., 2017). The parameters that control the block behavior are as follows: the effective friction angle between the block and surface ϕ'; the surface dip α; the unit weight of the sliding material γ; the unit weight of the water γ_w; the effective cohesion of the sliding material c'; the thickness of the

sliding block t; and the ratio of the portion of saturated soil m. The safety factor FS is calculated using Equation 1 with these parameters, assuming an infinite slope model. Therefore, a_c is calculated from the safety factor using Equation 2. The procedure for the calculation of the Newmark displacement DN includes a double integration, in the interval where $\int a(t) - a_c(t)dt > 0$ (Eq. 3). The displacement stops when velocity decreases to 0, because the block slows down if a(t) < ac(t) (Towhata, 2008). Physically, the block displacement is accumulated in each cycle in which the critical acceleration is exceed. The co-seismic displacement of the surface is expressed in terms of the Newmark displacement DN. To obtain the Newmark displacement, the safety factor was calculated (Eq. 1), and then the critical acceleration a_c was calculated (Eq. 2, based on Jibson et al., 2000; Niño et al., 2014; Zhang et al., 2017; and Han et al., 2019).

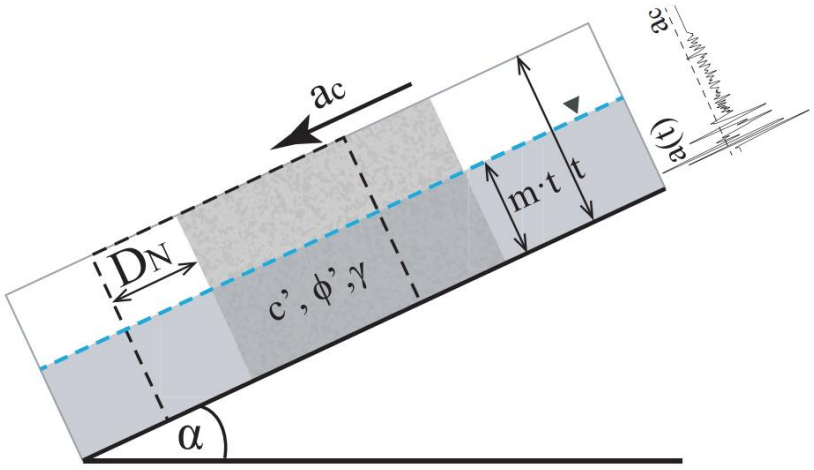

Figure 5: Newmark sliding block scheme. The component of the acceleration–time history a(t) in dip-direction is used in 1-D Newmark Analysis. After Jibson (2011) and Du (2018). ϕ': effective friction angle between the block and surface in degrees; α: surface dip angle in degrees; γ: bulk density of the sliding material in (kg/m^3); γ_w: bulk density of the water in (kg/m^3); c': effective cohesion of the sliding material in (Pa); t: thickness of the sliding block in (m); m is the ratio of saturated soil (adimensional).

$$F_S = \frac{c'}{\gamma t sin(\alpha)} + \frac{tan(\phi')}{tan(\alpha)} - \frac{m\gamma_w tan(\phi')}{\gamma tan(\alpha)} \quad (1)$$

$$a_c = (F_S - 1)gsin(\alpha) \quad (2)$$

$$D_N = \int\int \big(a(t) - a_c(t)\big)dt^2 \text{ , } where \int a(t) - a_c(t)dt > 0 \quad (3)$$

Thus, two crustal faults were parametrized, and synthetic seismograms were generated for different earthquake scenarios in dip-slip and strike-slip kinematics, as explained later in the text. Once the seismic signals were obtained, intensity measures were calculated, namely the Arias Intensity (Arias, 1970), PGA, and PGV. Then, the Newmark displacement DN was calculated as shown in Eq. 3, as a double integral only in the intervals where $\dot{a}(t) > 0$.

5.1. Ground motion synthetic signals

We selected the Marga–Marga fault and the Aconcagua fault, two probably seismogenic faults which are part of the VMFS with two potential kinematic behavior. The first case that was considered was dip-slip normal kinematics due to a change in Coulomb stress immediately after a megathrust earthquake. This case is similar to the 2010 Pichilemu. The second case that was considered was strike-slip sinistral kinematics due to the stresses in the inter-seismic period of the megathrust seismic cycle.

Mw 7.0 and Mw 6.9 earthquakes, which were related to the 2010 Maule Mw 8.8 megathrust earthquake which occurred one month before. Those events have been shown to have normal focal mechanisms (Aron et al., 2013).

In the long-term neotectonic deformation of the VMFS, in the inter-seismic phase, the faults of this fault system have strike-slip behavior. Therefore, the second case that was considered was strike-slip sinistral kinematics, which is consistent with some of the geomorphological data (Castro & Brignardello, 1997) and dip and strike of the damage zone (Thorson, 1999; Muñoz, 2013;).

To obtain comparable Newmark displacements (D_N), all the scenarios were considered with the same magnitude. To get the maximum values of D_N, the extreme scenarios were considered, where the complete segment would be displaced. The maximum magnitude of a dip-slip or strike-slip on Marga-Marga or on Aconcagua fault is $Mo = 4.027 \cdot 10^{+19} Nm$, equivalent a Mw 7.0, according to the source parametrizations of

Leonard (2010). The input parameters for the computation of the ground motion includes strike, dip, rake, length width of the fault, and location of the hypocenter (Table 2).

Table 2: Values of input parameters for compute broadband synthetic ground motion

VARIABLES	MARGAMARGA fault		ACONCAGUA fault	
	Dip – Slip (Normal)	Strike Slip (Sinistral)	Dip – Slip (Normal)	Strike Slip (Sinistral)
Length (km)	65.9	65.9	53.4	53.4
Width (km) W	20.0	20.0	20.0	20.0
Area (km²)	1318.5	1318.5	1067.8	1067.8
Strike (°) φ	130.0	130.0	290.0	290.0
Dip (°) θ	Random (60,80)	90	Random (60,80)	90
Rake (°)	-90.0	0.0	-90.0	0.0
Distance in strike direction (km)	20	20	35	35
Distance in down-dip direction (km) d_d	Random (0.0, W)			
Depth of top of co-seismic rupture area Z_{TOR} (km)	Random (1.0,20.0)			
Hypocenter depth	$Z_{TOR} + d_d sin(\theta)$	$Z_{TOR} + d_d$	$Z_{TOR} + d_d sin(\theta)$	$Z_{TOR} + d_d$

Epicenter coordinates	Y UTM E (m)	$Y = y_1 + d_d cos(\theta) sin(\psi)$ $\psi = 360° - \varphi y_1 = 264794$	264794	$Y = y_1 + d_d cos(\theta) sin(\psi)$ $\psi = 360° - \varphi y_1 = 269222$	269222
	X UTM N (m)	$X = x_1 + d_d cos(\theta) cos(\psi) \psi = 360° - \varphi x_1 = 6341400$	6341400	$X = x_1 + d_d cos(\theta) cos(\psi) \psi = 360° - \varphi y_1 = 6354190$	6354190

To synthesize seismic signals of the strong motion, the two possible fault kinematics were considered. Thus, the source parameters of fault geometry, corner frequency, and focal mechanism were parametrized according to Leonard (2010). Due to the stochastic behavior of the rupture of the fault plane used in the method of Crempien and Archuleta (2015), around 50 simulations were performed for each sub-case. Broadband synthetic seismograms were simulated between 0 and 20 Hz (Crempien and Archuleta, 2015). For simplicity, the model does not consider site conditions or topographic amplification; site conditions were not taken in account due to the small sedimentary thickness on the slopes. The limitations of this model are the ground motion are simulated at stations further than 1km from the fault trace; so, the model cannot offer a good estimation of the co-seismic displacements next to the fault trace. The computed D_N do not consider the topographic effects that could be important in some steep slopes. The model considers only the maximum intensity of earthquakes, Mw7.0 for all scenarios.

5.2. GIS-based spatial analysis of the geo-location of synthetic seismograms and landslide assessment

First, multiple ring buffers equally spaced every 100m were created. On each ring, equally spaced points every 100 were created. Points with slope steeper than 15°, different lithology and slope orientation were selected. Second, the areas were chosen according to the hazard susceptibility analysis and to the localization of these selected. Because most of the large landslides triggered by crustal earthquakes commonly occur in the surrounding area of the fault trace, at distances less than 15km (Sepúlveda et al., 2010; Shinoda and Miyata, 2017; Roback et al., 2018). Nevertheless, some co-seismic landslides can occur at greater distances, where there would be a much lower landslide density.

After the hazard categorization according to the slope angle, lithology, and competence of the material (Fig. 3), 14 areas of 1 km x 1 km were selected to develop the qualitative approach for each earthquake scenario at a local scale (Fig. 6) based on the computed broadband synthetic seismograms and Newmark sliding block analysis. The areas were selected by considering the location of slopes categorized as having medium-to-high landslide hazard, which are mostly associated with sedimentary soft rock and intrusive rocks with medium-to-low competence (Fig. 3). These areas are all located further than 1 km from the fault trace, where the model of Crempien and Archuleta (2015) can be applied. Additionally, the areas were selected considering the location with respect to the fault plane: at the footwall or hanging-wall block in dip-slip earthquake scenarios, or at the left-wall or right-wall block in strike-slip earthquake scenarios related to each fault. In each area, around six representative points were selected on slopes which were categorized as having medium-to-very high landslide hazard.

Points were selected with different rock or soil cover and different slope orientations, with distances of between 100 and 500 meters between each point. The dip angle and dip direction were calculated based on the 5-m resolution DEM. Using the dip angle and

the superficial geological information, the FS and a_c were calculated according to the range of values of γ, c', and ϕ' in Table 3. The thickness t is 1m for all cases on metamorphic, igneous, or sedimentary rock, and is 0.1 to 0.5 m for unconsolidated sedimentary deposits. For each scenario and selected point, to compute the displacements under the most unfavorable conditions, the minimum value of FS was used.

For all cases, according to the selection criteria for the 1 km x 1 km areas, seven of these areas were chosen in the southern block of the Aconcagua fault and in the northern block of the Marga–Marga fault, in the cities of Viña del Mar and Concón (shown as blue squares in Figure 6). These areas are in the footwall of each fault in the dip-slip scenarios. For the Marga–Marga fault scenarios, six areas were situated in Valparaíso in the SW block of the Marga–Marga fault (shown as red squares in Figure 6), which is the hanging wall in the corresponding dip-slip earthquake scenario. For the Aconcagua fault scenarios, six areas were located in the north of the cities of Concón, Quintero, and Puchuncaví in the NE block of the Aconcagua fault, which is also the hanging wall in the dip-slip earthquake scenario (shown as green squares in Figure 6). In each area, between four and 16 points were chosen representing critical slopes whose hazard was categorized as moderate-to-very high (see Fig. 3). The criteria that were used to choose the points for analysis were as follows: (a) the points must be between 100 and 500 m from each other; and (b) the points must have different lithologies, slope dips (although the dips must be larger than 15◦), and slope orientations. The same points were used to perform the analysis for dip-slip and strike-slip scenarios; however, different points were used for the Aconcagua fault and Marga–Marga fault scenarios. Figure 6 shows an example of a 1 km x 1 km area with the location of the simulated stations for each case together with the geological map, whose color legend coincides with that of the simplified geological map in Figure 1.

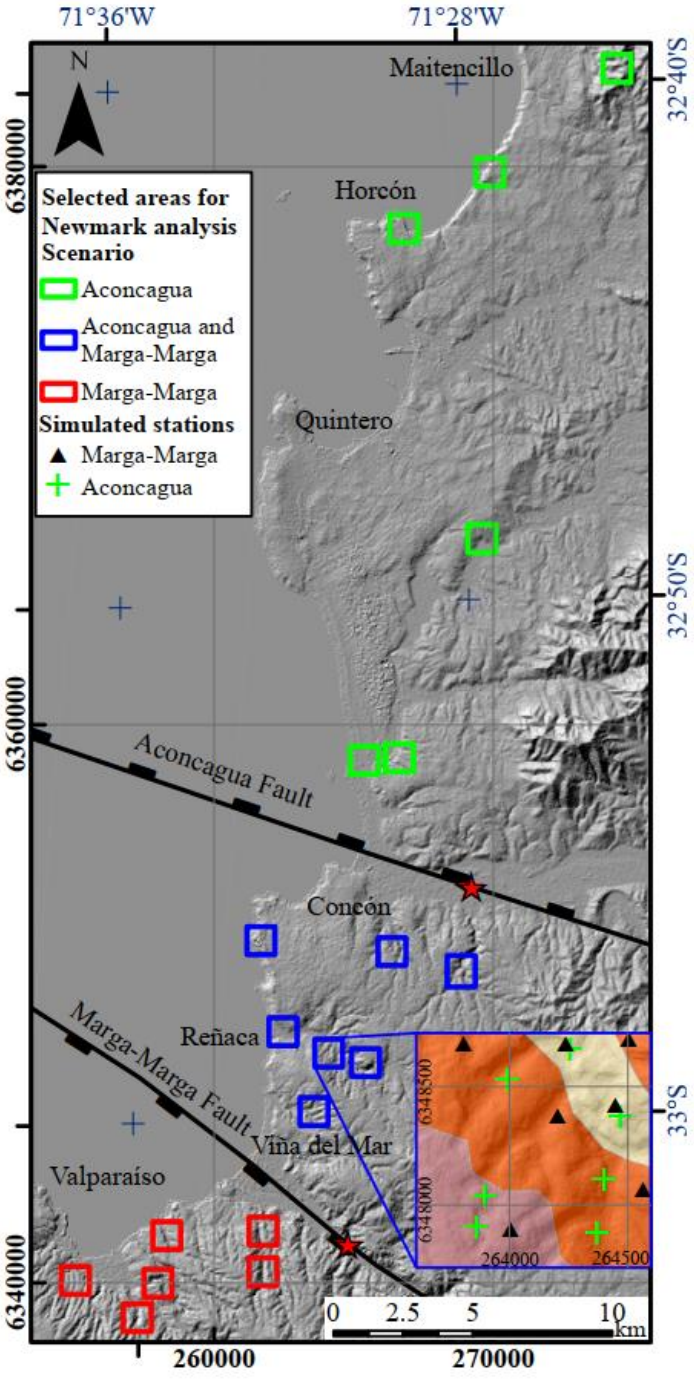

Figure 6: Map showing the locations of areas chosen to generate synthetic seismograms and apply Newmark analysis. The example magnified area shows the location of simulated stations for each case; these stations are located on slopes with different angles and different rock or soil units. The colors of the rock units are as in the simplified geological map in Figure 1.

Table 3: Range of values for shear strengths for each geological unit

Geological Unit	c’ MPa	γ kN/m^3	ϕ Deg
Paleozoic and Mesozoic intrusive rocks	35 – 55	25 – 30	26 – 45
Neogene continental sedimentary rocks with low cohesion	0 – 20	18 – 21	30 – 46
Neogene marine sedimentary rocks with low cohesion	0 – 20	17 – 21	25 – 40
Quaternary eolian deposits	0 – 1	14 – 19	18 – 34
Quaternary alluvial and fluvial deposits	0 – 1	17 – 19	30 – 45

Range of values of effective cohesion (c’), unit weight (γ), friction angle (ϕ) based on (Peck et al., 1974; Koloski, 1989; Carter & Bentley, 1991; Dysli, 2000; Jibson et al., 2000; Jang et al., 2018)

5.Broadband synthetic seismograms and Newmark displacements

A total of around 50 simulations were performed for each of the four potential scenarios, giving a total of 185 simulations, namely an Aconcagua fault dip-slip normal earthquake, an Aconcagua fault strike-slip sinistral earthquake, a Marga–Marga fault dip-slip normal earthquake, and a Marga–Marga fault strike-slip sinistral earthquake. Some examples of synthetic seismograms for the vertical (Z), E-W (E), and N-S (N) components are shown

in Figure 7, which are plotted according to the distance to the fault plane. The stations with negative distances are in the footwall in the dip-slip cases, in the SW block in the Aconcagua fault strike-slip case, and in the NE block in the Marga–Marga fault strike-slip case.

The ranges of effective cohesion (c'), bulk density (γ), and effective friction angle (ϕ') based on Jang et al. (2018), Jibson et al. (2000), Dysli (2000), Carter and Bentley (1991), Koloski (1989), and Peck et al. (1974) (Table 3).

As shown in Figure 7, in dip-slip cases, the largest average PGA and IA reached 10.5 m/s^2 and 6.0 m/s, respectively. In those cases, the highest values of the intensity measures were recorded in the footwall and on the horizontal component. In strike-slip cases, the ground motion was symmetrically distributed on both sides of faults, with lower values of the intensity measures.

For each case, the Newmark Displacement was calculated in dry and saturated conditions; these represent the extreme cases of a drought scenario (where $m = 0$) and a scenario with water-saturated conditions (where $m = 1$). In the strike-slip scenarios, there are large values of DN on both sides of the fault trace, mostly associated with a symmetrical rupture on a vertical fault plane. In the dip-slip scenarios, most of the large values of DN are in the hanging wall; however, there are some extreme cases where the maximum value of DN occurs in the footwall (Figure 10). This distribution is closely related to the high directivity of the rupture. The spatial distribution of DN is similar to the distribution of the intensity measures in both blocks of the faults (Figures 8 and 9).

As shown in Figure 10, in general, in the dry cases, all of Newmark displacements are from negligible to 100 m, whereas in the saturated cases, the Newmark displacements are from millimeters to more than 100 m. Under saturated conditions, the maximum values of DN are up to 86 m in the Marga–Marga fault normal scenario, 21 m in the Marga–Marga fault sinistral scenario, 19.38 m in the Aconcagua fault normal scenario, and 13.93 m in the Aconcagua fault sinistral scenario. Under dry conditions, the

maximum DN for the same four scenarios are 1.29, 0.65, 1.59, and 1.06 m, respectively. The results show the groundwater conditions and the depth of the water table in the analyzed sliding blocks are very important to the computed D_N values. Displacements greater than a few meters should be interpreted as slope failure. These displacements are related to Quaternary alluvial deposits in the Marga–Marga fault cases and eolian recent deposits of loose sand and alluvial deposits in the Aconcagua fault cases.

A comparison between the slopes of the analyzed points with Quaternary alluvial or eolian deposits and the potential co-seismic displacements shows that a larger number of landslides are associated with strike-slip earthquakes on the Marga–Marga fault due to a symmetrical distribution of PGA, PGV, and IA on both sides of the fault trace.

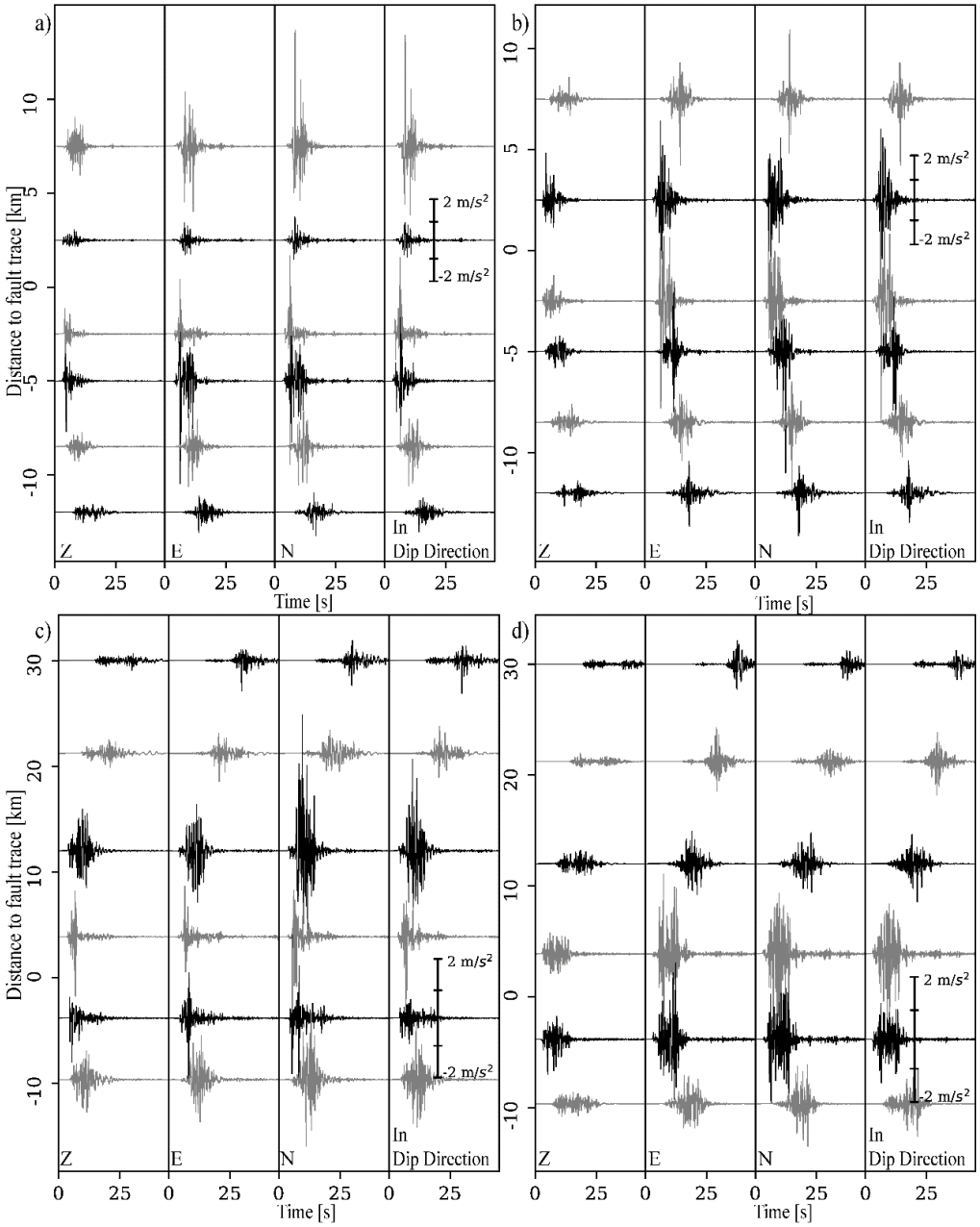

Figure 7: Examples of synthetic acceleration–time histories for all computed scenarios. (a) Marga–Marga fault dip-slip Mw 7.0 earthquake. (b) Marga–Marga fault strike-slip Mw 7.0 earthquake. (c) Aconcagua fault dip-slip Mw 7.0 earthquake. (d) Aconcagua fault strike-slip Mw 7.0 earthquake. The offset of the signals corresponds to the distance to the fault trace. The locations of seismograms in the hanging-wall block for dip-slip normal cases and in the left block for strike-slip sinistral cases are shown as negative values.

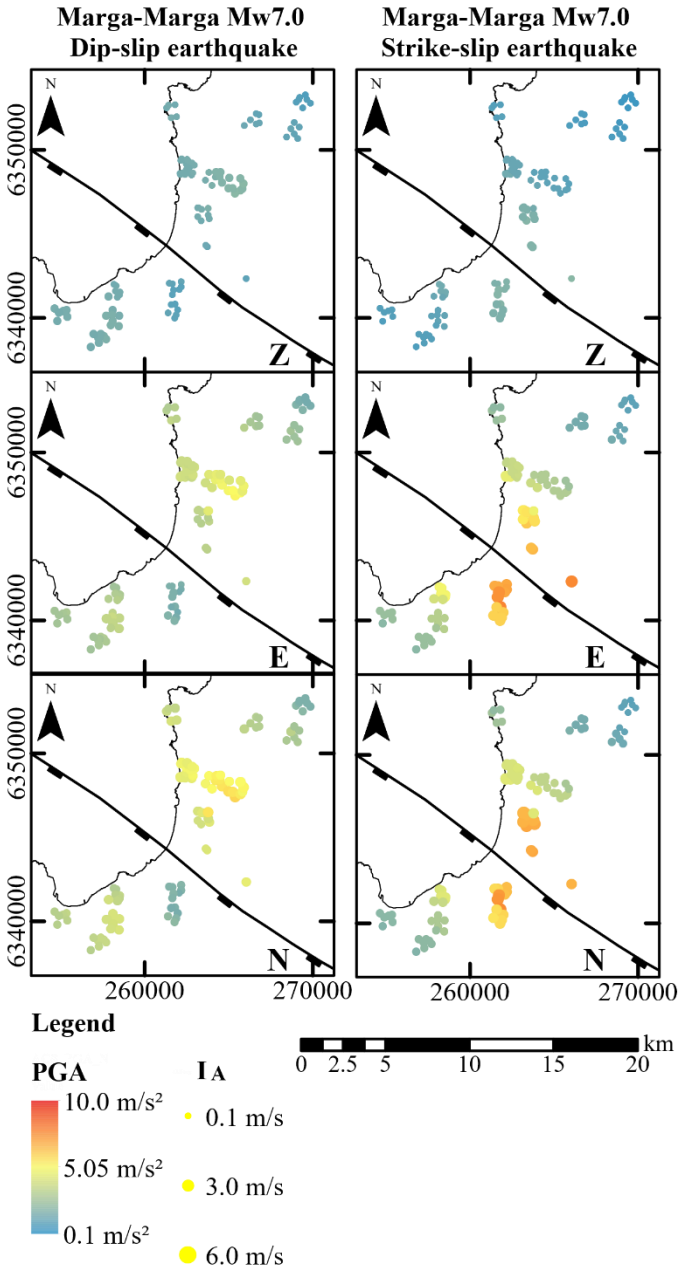

Figure 8: Map of the locations of synthetic stations and their average PGA and IA for the vertical, E-W, and N-S components of computed ground motions for Marga–Marga fault strike-slip and dip-slip earthquake scenarios

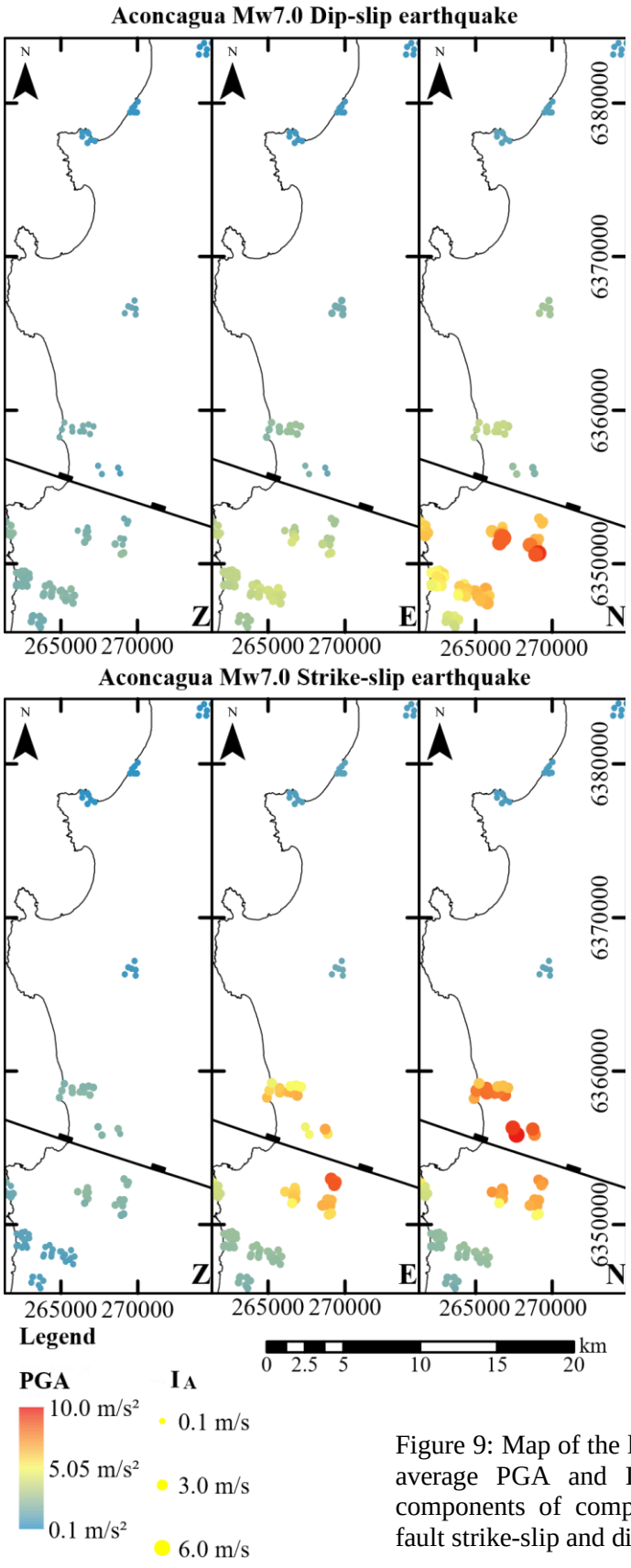

Figure 9: Map of the locations of synthetic stations and their average PGA and IA for the vertical, E-W, and N-S components of computed ground motions for Aconcagua fault strike-slip and dip-slip earthquake scenarios.

6.1. **Spatial distribution of landslides**

Using the computed Newmark displacements and the location of each synthetic station, each station and its calculated values of intensity measures and DN values were geo-referenced. Figure 10 shows some magnified areas for the Marga–Marga fault earthquake scenarios and Figure 11 shows some for the Aconcagua fault earthquake scenarios. The potential displacements are plotted as arrows, whose size is related to the magnitude and whose direction is the dip direction of each analyzed slope. In both figures, the potential displacements under saturated conditions are shown in the left column and the potential displacements under dry conditions are shown in the right column. In Figure 11, areas A and B are in the N-block of the Marga–Marga fault (hanging wall in dip-slip scenarios), where there are larger displacements in dip-slip and strike-slip displacements than the displacements in areas C and D, which in the S-block. In Figure 12, Area F is in the N-block of the Aconcagua fault (hanging wall in the dip-slip scenario), while areas A, B, and E are in the S block of the Aconcagua fault.

In the Marga–Marga fault scenarios, some slopes in areas A, B, and D have significant displacements for the dip-slip earthquake scenario, and the other areas have larger displacements under this scenario. In Area C (the closest area to the Marga–Marga fault trace), seven out of eight slopes only produce a landslide in strike-slip scenarios. Part of the potential landslides coalesce in the same creek, such as in areas C and D.

In the Aconcagua fault scenarios, in general, the displacements are larger in the dip-slip case than in the strike-slip case. Some slopes in areas A, B, and E have significant displacements only in the dip-slip earthquake scenario. Under saturated conditions, all areas have larger displacements in the strike-slip cases than in the dip-slip cases. In Area F, four out of six points have the largest displacements in the strike-slip case under saturated conditions. Those points correspond to high-angle slopes on Quaternary unconsolidated sedimentary fill.

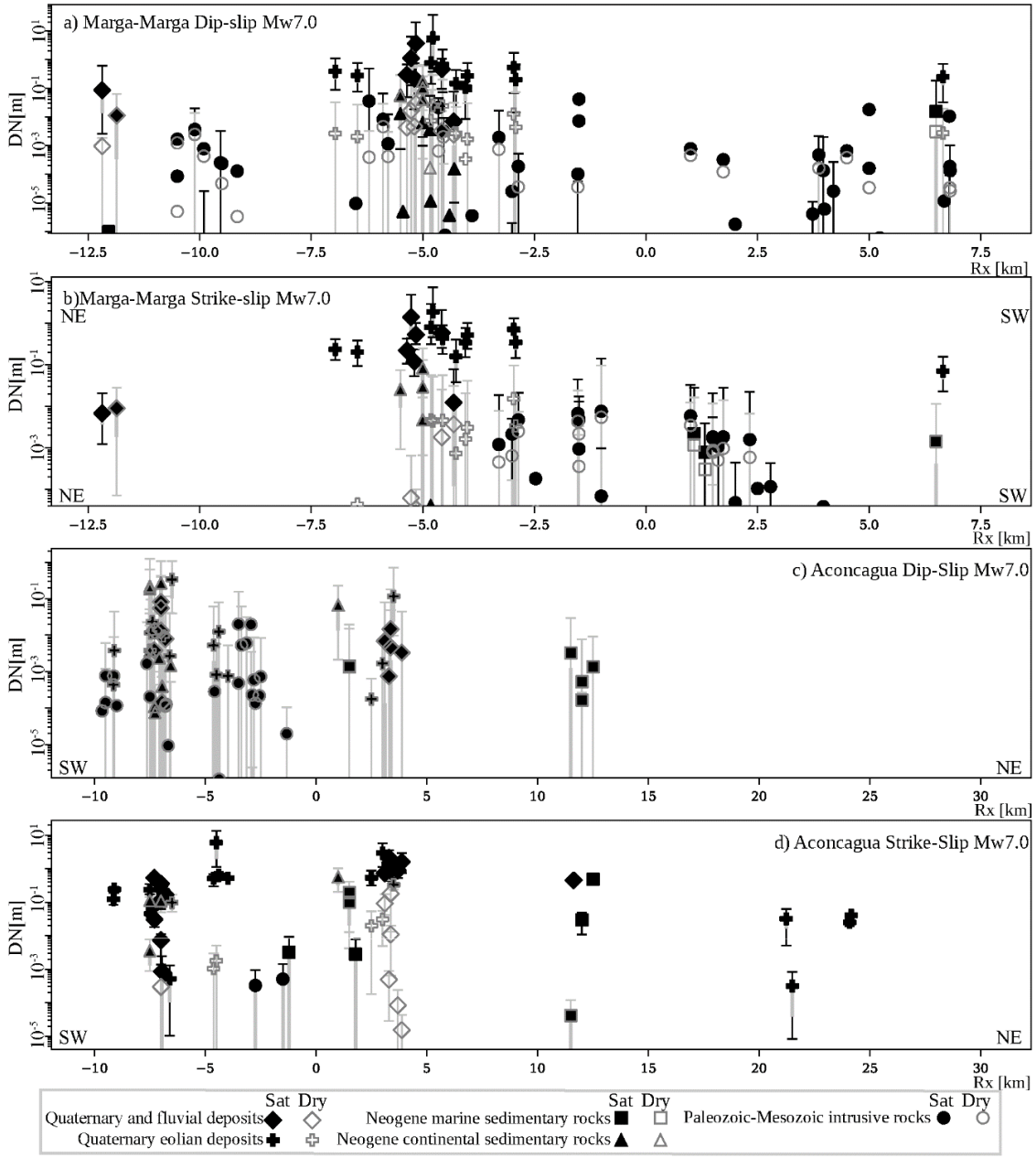

Figure 10: Newmark displacements (log (DN [m])) vs distance to fault trace (Rx, in km) for all considered earthquake scenarios. (a) Marga–Marga fault dip-slip Mw 7.0 earthquake. (b) Marga–Marga fault strike-slip Mw 7.0 earthquake. (c) Aconcagua fault dip-slip Mw 7.0 earthquake. (d) Aconcagua fault strike-slip Mw 7.0 earthquake. Computed displacements are shown according to lithology and soil water conditions (saturated or dry).

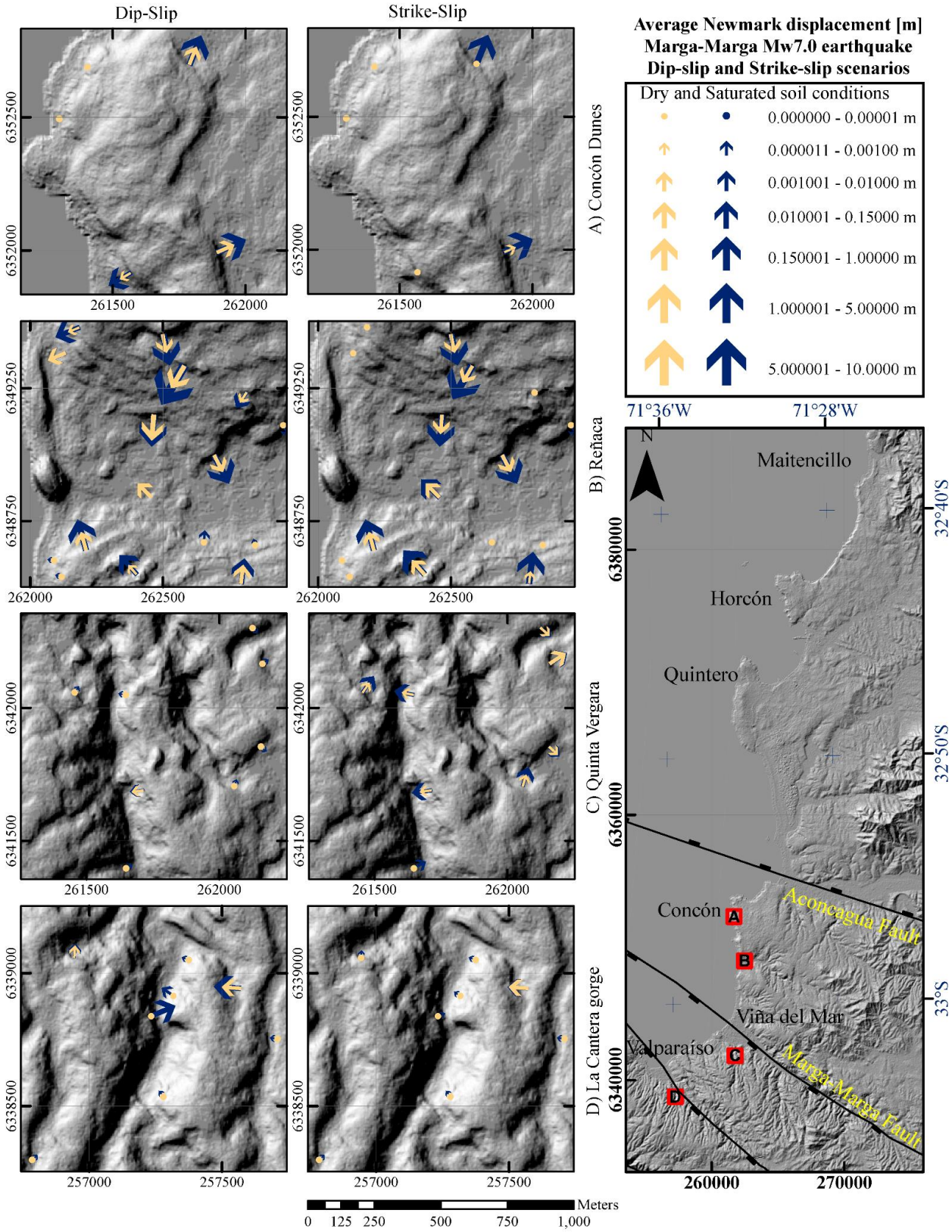

Figure 11: Maps of co-seismic displacements for Marga–Marga fault dip-slip and strike-slip scenarios under dry and saturated conditions

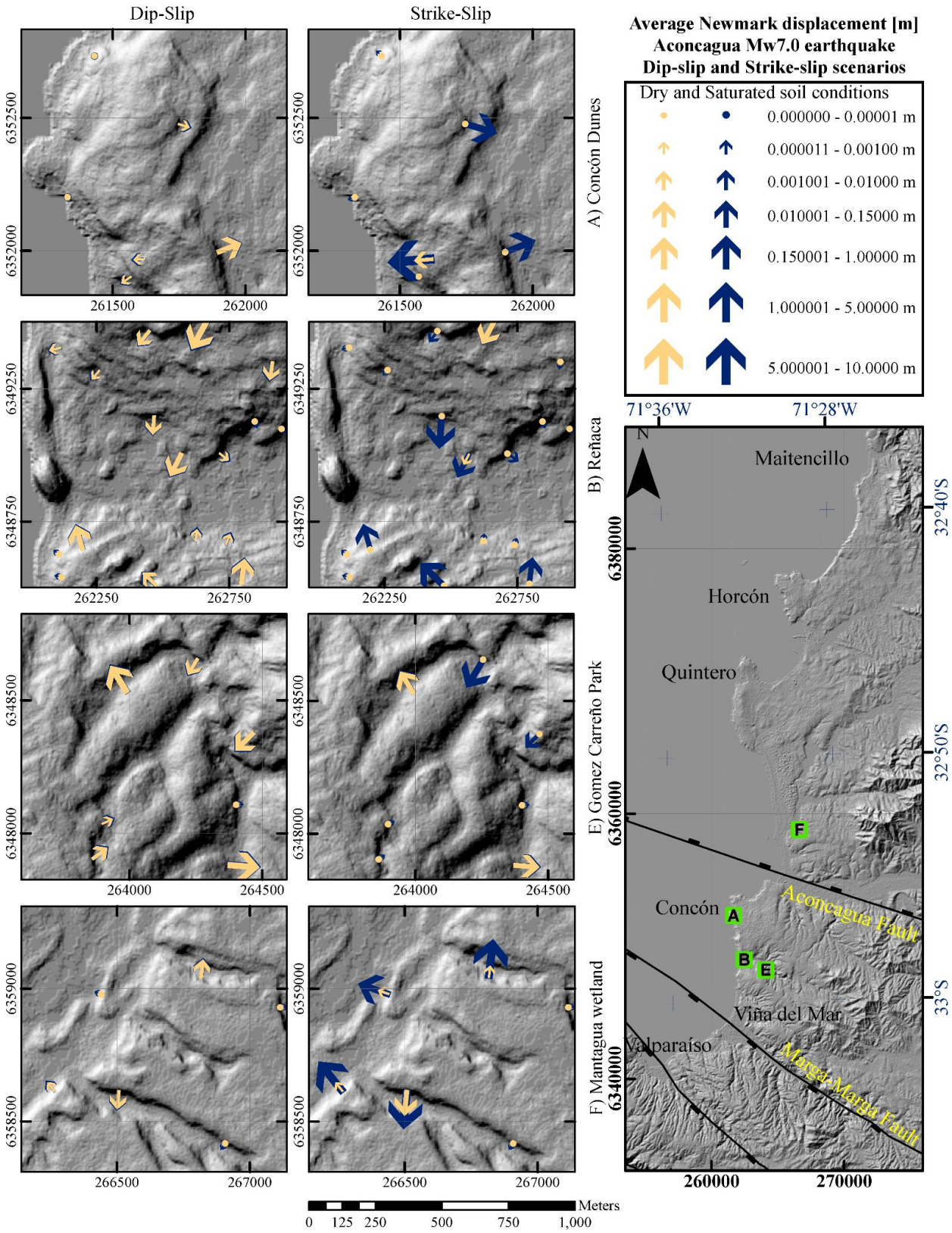

Figure 12: Maps of co-seismic displacements for Aconcagua fault dip-slip and strike-slip scenarios under dry and saturated conditions.

7. Discussion

The locations of the magnified areas and their points that were selected for local Newmark analysis on the slopes were chosen considering the initial analysis of conditioning factors. On the one hand, the magnitude and spatial distribution of potential displacements are due to the geological characteristics of the slopes, as well as their lithology, geotechnical properties (e.g., cohesion, friction angle, density, humidity, etc.), hydrological conditions (e.g., phreatic level), and other slope characteristics (e.g., dip and orientation). Additionally, it is relevant to consider the geomorphological conditioning factors (Chigira et al., 2003; Chigira and Yagi, 2006; Higaki and Abe, 2013; Sugimoto et al., 2013; Kargel et al., 2016), such as whether the slopes correspond to pediments, dunes, gorges, or cliffs, or whether they are anthropic. On the other hand, the characteristics of the earthquake scenarios exert a control on the magnitude and spatial distribution of the displacements (Sepúlveda et al., 2005; Sepúlveda et al., 2008; Sepúlveda et al., 2010; Gorum and Carranza, 2015; Roback et al., 2018).

The computed displacements are a first approximation of the range of magnitudes of the potential real landslides that might occur during a certain earthquake scenario. The predicted displacements offer an index to correlate with landslides in the field (Jibson et al., 2000; Jibson, 2011). Pseudo-static methods can lead to the underestimation of the intensity measures and DN (Crespellani et al., 1998; Romeo, 2000; Rathje and Saygili, 2008; Chousianitis et al., 2014; Sharifi-Mood et al., 2017). However, physics-based permanent-displacement analysis allows a rigorous analysis which takes into account the rupture process and parameters, and slope characteristics such as lithology, cohesion, dip, and hydrological conditions (Miles and Ho, 1999; Allstadt et al., 2013; Huang et al., 2020). Even though numerous assumptions are required, the computed displacements on critical slopes offer an approach to predict the potential behavior for other slopes with the same characteristics in the study area. To obtain a complete landslide assessment, an escalation of the spectral response and the amplitude of the

synthetic signals is needed, since otherwise it is not possible to interpolate the computed DN.

We have analyzed the displacements of dip-slip and strike-slip scenarios for two different faults in the forearc of the Coastal Range of Central Chile. The probabilistic assessment of the seismic scenarios used in this work is the subject of new studies. It is necessary to study the slip rates, recurrence rate, fault geometry, neotectonic activity of the Marga-Marga and Aconcagua faults based on geomorphology and geophysical data.

7.1. Controlling factors for landslide distribution and displacement magnitude

Concerning the spatial distribution of slopes where displacement occurs at least once in the simulations, the control of fault kinematics seems to be stronger than that of lithology; however, the magnitude of the computed displacements are strongly controlled by lithology and the critical acceleration of the slopes. Valagussa et al. (2019) found that the strong ground motion controls the size of landslides and modulates the distribution of cohesion, lithology, and slope because of cohesion reduction and the distribution of accelerations.

The computed data show a slight correlation between the Newmark displacement and the ground-motion intensity measures. Since the rupture process controls the seismic wave propagation, in the dip-slip earthquake scenarios, the largest displacements are in the footwall, whose peak accelerations are local maxima (Abrahamson and Somerville, 1996; Song et al., 2018).

In most of the analyzed points, this model based on the simulation of ground motion and the classical approach of Newmark analysis underestimates the co-seismic displacements (Jibson, 2011). This is since, on the one hand, this approach does not consider topographic amplification, site effects, or the effects of dynamic pore pressure increase. On the other hand, in this method, critical acceleration is taken as a constant and the sliding material is considered to be a rigid block without deformation. However,

at particular points situated on Quaternary loose deposits, the computed values of DN for saturated conditions are much larger—for example, 86.5 m in the Marga–Marga fault normal earthquake case, 20.9 m in the Marga–Marga fault sinistral case, 19.4 m in the Aconcagua fault normal case, and 13.9 m in the Aconcagua fault sinistral case. Then, for any of the evaluated scenarios, the slope fails for practical purposes. These outliers are related to FS (very close to FS=1) and very low critical accelerations. The assessment obtained from the models presented here offers a first approximation of the co-seismic landslides that can potentially be caused by crustal earthquakes in the Andean forearc.

It is well known that the magnitude and spatial distribution of landslides depends on the fault mechanism and the directivity of the rupture propagation (Roback et al., 2018). The landslide density directly depends on the fault kinematics: dip-slip earthquakes are associated with a larger landslide density in the hanging wall block than strike-slip earthquakes (Tatard and Grasso, 2013; Gorum and Carranza, 2015). In this study, it was found that, in most cases, the displacements are larger for dip-slip earthquakes than strike-slip earthquakes; the computed displacements in dip-slip cases can be up to four times larger than in strike-slip cases, which can correspond to differences in displacement of up to 20 m.

7.2. Field interpretation of computed landslides

Landslides occur over large time scales and are part of the geomorphological cycle and the landscape evolution, as proposed by Fan et al. (2019). Even if most of the landslide displacements that occur on intrusive rocks or regolith are submillimetric to millimetric, they increase the landslide hazard by causing destabilization of blocks and slope weakening. Therefore, after further rainfall, fracture propagation and slope failure might occur in such locations.

At the local scale, there are areas with Quaternary deposits in urban areas, such as in the cities of Concón and Viña del Mar, where the landslide displacements occur on slopes which face one another. In those cases, the potential mass movement would affect

populated gullies and small valleys due to the coalescence of several landslides, thus increasing the hazard in the down-slope areas and triggering debris flows and slope weakening. From figures 11 and 12, it can be seen that displacements can potentially occur for any slope orientation. For example, in the Gomez Carreño Park area and Reñaca area (areas E) and B) respectively in figures 11, 12 and in the figures of the supplementary material), for all considered scenarios, the displacements are constrained to gullies and scarps on both sides of the gorges in the N-S, W-E, SE-NW, NE-SW, and SW-NE directions. In the same manner, in all considered scenarios, landslides on Quaternary dunes in Concón can occur on both sides of the dunes and in E-W or W-E directions.

Several authors have proposed categorizations of the co-seismic landslide hazard and some interpretations of the calculated DN. Wieczorek et al. (1985) considered that modeled permanent displacements larger than 0.05 m imply macroscopic ground cracking and failure. Meanwhile, Keefer and Wilson (1989) concluded that the displacement threshold for coherent landslides is 0.1 m. Romeo (2000) used a minimum value of DN of 10−5 m and considered that all displacements above this value were not significant. Blake et al. (2002) recommended considering D_N thresholds of 0.05 m and 0.15 m for slopes with large rigid human constructions (e.g., buildings and pools) and for ductile soils without engineered improvements (e.g., gardens and community equipment areas), respectively. The following criteria for deep landslides are used by the California Geological Survey and California State Mining and Geology Board (2008): DN values of 0.0 to 0.15 m imply that serious landslides are unlikely; values of 0.15 to 1.0 m indicate serious displacements with strength loss and slope failure; and values of more than 1.0 m indicate significant landslides. Jibson and Michael (2009) found that, for shallow landslide hazard, if DN is less than 0.01 m, the hazard is low; if it is between 0.01 and 0.05 m, the hazard is moderate; if it is between 0.05 and 0.15 m, the hazard is high; and if it is more than 0.15 m, the hazard is very high.

Based on these interpretations, the average computed displacements are classified according to Jibson and Michael (2009) criteria. In Figure 13 the area B) of Reñaca is taken as example to show the analysis of the slope hazard based on the average D_N values. Each computed displacement using synthetic seismograms is interpreted as a larger slope with same geological, geotechnical and geomorphological characteristics.

It is possible to offer an interpretation of the potential landslide location and the magnitude of the displacement according to Jibson and Michael (2009) criteria. Each analyzed point in this work is part of a larger slope, with the same geotechnical, geological, and geomorphological properties and with the same soil or rock coverage and similar slope angles. It is possible to assume that all slopes might have the same potential displacement behavior under each seismic scenario. For instance, taking Area B) Reñaca from figures 11 and 12, we show the interpretation of the potential co-seismic slope displacements for all considered cases in Figure 13. Only for the Marga–Marga fault dip-slip scenario, under saturated conditions, there is a slope with Very High hazard and a computed D_N of order of 10^1m. In general, in this area, the potential displacements due to an earthquake on the Aconcagua fault are smaller than for the equivalent scenario on the Marga–Marga fault. This can be explained by the fact that this area is in the footwall of the Aconcagua fault and in the hanging wall of the Marga–Marga fault in the dip-slip earthquake scenarios, and it is closer to the Marga-Marga fault trace than to the Aconcagua fault trace.

The computed displacement that are larger than 1.0m there is slope failure. These areas might be affected by landslide reactivations in the future. The slope stability problem might change to a dynamic problem of a flow failure on the slope, where there is slope failure. The internal deformation of the block must be taken in account in further analysis, considering the post-earthquake slope profiles (Leshchinsky, 2018)and a discretization of the medium to study the internal deformation (Soga et al., 2018)

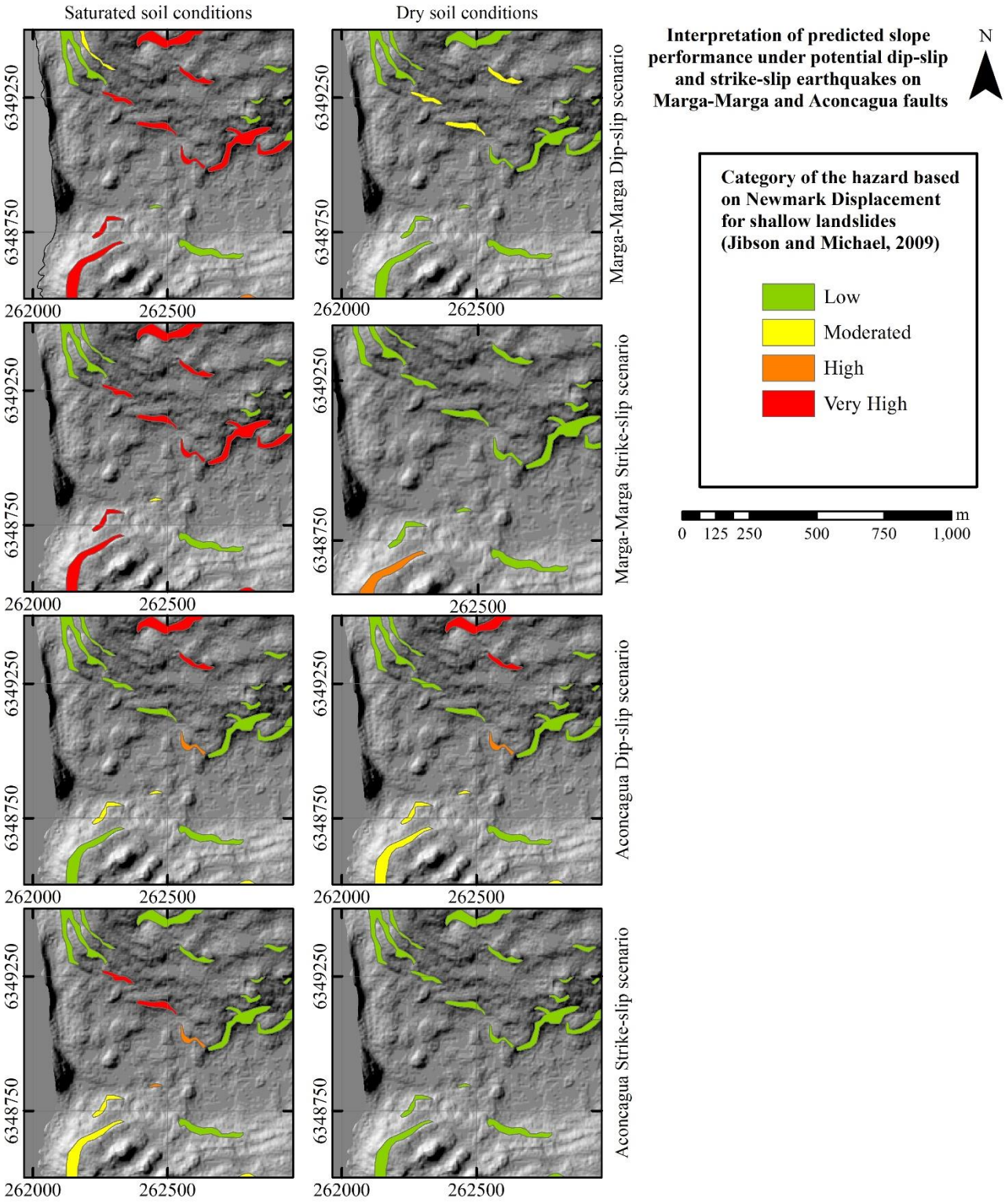

Figure 13: Interpretation of computed displacements for all scenarios for area B) of Figures 11 and 12

8. Concluding remarks

Crustal seismicity is associated with many geological hazards, the most immediate of which are co-seismic landslides, which are studied here. Co-seismic landslides can affect landscape evolution, sedimentary processes, and the changes in the hazard of future landslides or the reactivation of these and old landslides. In the analyzed earthquake scenarios for the Marga–Marga and Aconcagua faults in the Coastal Range of Central Chile, the lithology and geotechnical properties of slopes exert a stronger control on the magnitude of the displacements than the ground motion and its parameters (e.g., focal mechanism, kinematics, location at one or another side of the fault trace, the distance to the rupture plane, the distance to the fault trace). Secondarily, the locations of large displacements are controlled by the directivity of the seismic rupture.

The results show that the potential displacements under dry and saturated conditions differ by at least one order of magnitude, so the hydrological conditions of the soil must be taken into account in more detail in the assessment of potential future co-seismic landslides. The largest computed displacements are located on Quaternary eolian, fluvial, and alluvial deposits with loose sand and silt.

The computed displacements in all earthquake scenarios are comparable to each other because all scenarios have a magnitude Mw7.0. The largest simulated displacements are in the dip-slip scenarios at some points in the footwall and at the points on loose sedimentary deposits, which is due to lithological and rupture propagation controls. The largest simulated local displacements are observed on some slopes between the Aconcagua and Marga–Marga faults, which might be due to a strong lithological control.

In future works, site effects, the topographic amplification of seismic waves, the internal deformation of the slope material, and hydrological conditions should be taken in account in order to improve the model.

Acknowledgements

The authors offer thanks to Felipe del Valle for providing the fault geometry, to the FONDEF project D10E1027 Mas Andes 2.0 for their partial funding, and to CIGIDEN, FONDAP Project 15110017, for providing access to their cluster to compute the synthetic seismograms.

References

Abrahamson, N. A., and Somerville, P. G. (1996). Effects of the hanging wall and footwall on ground motions recorded during the Northridge earthquake. Bulletin of the Seismological Society of America, 86, 93-99.

Aki, K. (1984). Asperities, Barriers, Characteristic Earthquakes and Strong Motion Prediction. Journal of Geophysical Research, 89, 5867-5872.

Alfaro, A. (2011). Peligro sísmico en el segmento norte de la región del Maule, Chile. Ph.D. thesis Universidad de Chile.

Allmendinger, R. W., and González, G. (2010). Invited review paper: Neogene to Quaternary tectonics of the coastal Cordillera, northern Chile. Tectono-physics, 495, 93-110. doi:10.1016/j.tecto.2009.04.019.

Allmendinger, R. W., González, G., Yu, J., Hoke, G., and Isacks, B. (2005). Trench-parallel shortening in the Northern Chilean Forearc: Tectonic and climatic implications. Bulletin of the Geological Society of America, 117,660 89-104. doi:10.1130/B25505.1.

Allstadt, K., Vidale, J. E., and Frankel, A. D. (2013). A Scenario Study of Seismically Induced Landsliding in Seattle Using Broadband Synthetic Seismograms. Bulletin of the Seismological Society of America, 103, 2971-2992. doi:10.1785/0120130051.

Alvarado, P., Barrientos, S., Saez, M., Astroza, M., and Beck, S. (2009). Source study and tectonic implications of the historic 1958 Las Melosas crustal earthquake, Chile, compared to earthquake damage. Physics of the Earth and Planetary Interiors, 175, 26-36. doi:10.1016/j.pepi.2008.03.015.

Ammirati, J. B., Vargas, G., Rebolledo, S., Abrahami, R., Potin, B., Leyton, F., and Ruiz, S. (2019). The crustal seismicity of the western Andean thrust (Central Chile, 33◦-34◦ s): Implications for regional tectonics and seismic hazard in the Santiago area. Bulletin of the Seismological Society of America, 109, 1985-1999. doi:10.1785/0120190082.

Arias, A. (1970). Measure of earthquake intensity. In R. Hansen (Ed.), Seismic design for nuclear power plants Seismic design for nuclear power plants (p. pp. 438-483). Massachusetts institute of technology press, Cambrige, MA.

Aron, F., Allmendinger, R. W., Cembrano, J., González, G., and Yáñez, G. (2013). Permanent fore-arc extension and seismic segmentation: Insights from the 2010 Maule earthquake, Chile. Journal of Geophysical Research: Solid Earth, 118, 724-739. doi:10.1029/2012JB009339.

Arriagada, C., Arancibia, G., Cembrano, J., Martínez, F., Carrizo, D., Van Sint Jan, M., Sáez, E., González, G., Rebolledo, S., Sepúlveda, S. A.,

Contreras-Reyes, E., Jensen, E., and Yáñez, G. (2011). Nature and tectonic significance of co-seismic structures associated with the Mw 8.8 Maule earthquake, central-southern Chile forearc. Journal of Structural Geology, 33, 891-897.doi:10.1016/j.jsg.2011.03.004.29

Barrientos, S., Vera, E., Alvarado, P., and Monfret, T. (2004). Crustal seismicity in central Chile. Journal of South American Earth Sciences, 16, 759-768. doi:10.1016/j.jsames.2003.12.001.

Beck, S., Barrientos, S., Kausel, E., and Reyes, M. (1998). Source characteristics of historic earthquakes along the central Chile subduction zone. Journal of South American Earth Sciences, 11, 115-129. doi:10.1016/S0895-9811(98)00005-4.

Binnie, A., Dunai, T. J., Binnie, S. A., Victor, P., González, G., and Bolten, A. (2016). Accelerated late quaternary uplift revealed by 10Be exposure dating of marine terraces, Mejillones Peninsula, northern Chile. Quaternary Geochronology, 36, 12-27. doi:10.1016/j.quageo.2016.06.005.

Blake, T., Hollingsworth, R., Stewart, J., D'Antonio, R., Earnest, J., Gharib, F., Hollingsworth, R., Horsman, L., Hsu, D., Kupferman, S., Masuda, R., Pradel, D., Real, C., Reeder, W., Sathialingam, N., Simantob, E., and Stewart, J. (2002). Guidelines for analyzing and mitigating landslide hazards in California. Recommend Procedures for Implementation of DMG Special Publication, 117, 1-132.

Bloch, W., Kummerow, J., Salazar, P., Wigger, P., & Shapiro, S. A. (2014). High-resolution image of the North Chilean subduction zone: Seismicity, reflectivity and fluids. Geophysical Journal International, 197(3), 1744–1749. https://doi.org/10.1093/gji/ggu084

Bommer, J. J., and Rodriguez, C. E. (2002). Earthquake-induced landslides in Central America. Engineering Geology, 63, 189-220. URL: http: //linkinghub.elsevier.com/retrieve/pii/S0013795201000813. doi:10.710 1016/S0013-7952(01)00081-3.

Boyce, D., Charrier, R., and Farías, M. (2020). The First Andean Compressive Tectonic Phase: Sedimentologic and Structural Analysis of Mid-Cretaceous Deposits in the Coastal Cordillera, Central Chile (32◦50S). Tectonics, 39, 0-2. doi:10.1029/2019TC005825.

Bray, J. D. (2007). Simplified Seismic Slope Displacement Procedures. In Earthquake Geotechnical Engineering 1979 (pp. 327- 353). doi:10.1007/978-1-4020-5893-6_14.

Bray, J. D., and Travasarou, T. (2007). Simplified Procedure for Estimating Earthquake-Induced Deviatoric Slope Displacements. Journal of Geotechnical and Geoenvironmental Engineering, 133, 381-392. doi:10.1061/(ASCE)1090-0241(2007)133:4(381).

Briggs, R. (2016). Earthquakes: Megathrusts and mountain building. Nature Geoscience, 9, 346-348.

Brune, J. N. (1970). Tectonic stress and the spectra of seismic shear waves from earthquakes. Journal of Geophysical Research, 75, 4997-5009. URL: http://doi.wiley.com/10.1029/JB075i026p04997. doi:10.1029/JB075i026p04997.

Brune, J. N. (1971). Seismic sources, fault plane studies and tectonics. Eos, Transactions American Geophysical Union, 52, IUGG 178. URL: http://doi.wiley.com/10.1029/EO052i005pIU178. doi:10. 1029/EO052i005pIU178.

Caccavale, M., Matano, F., and Sacchi, M. (2017). An integrated approach to earthquake-induced landslide hazard zoning based on probabilistic seismic scenario for Phlegrean Islands (Ischia, Procida and Vivara), Italy. Geomorphology, 295, 235-259. URL: http://dx.doi.org/10.1016/j.geomorph.2017.07.010. doi:10.1016/j.geomorph.2017.07.010.

California Geological Survey, and California State Mining and Geology Board (2008). Guidelines for evaluating and mitigating seismic hazards in California volume 117. California Department of Conservation, California Geological Survey.

Carrillo-Briceño, J. D. (2013). Condrictios fósiles del Plioceno Superior de la Formación Horcon, Region de Valparaíso, Chile central. Revista Chilena de Historia Natural, 86, 191-206. Carter, M., and Bentley, S. P. (1991). Correlations of soil properties. Pentech Press Publishers. Castro, C., and Brignardello, L. (1997). Geomorfología aplicada a la ordenación territorial de la franja costera entre Concón y Quintay (32◦ 55'S y 33◦ 15' S). Revista Norte Grande, 24, 113-125.

Carter, M., & Bentley, S. P. (1991). Correlations of soil properties. In Correlations of soil properties. Pentech Press Publishers.

Castro, C., & Brignardello, L. (1997). Geomorfología aplicada a la ordenación territorial de la franja costera entre Concón y Quintay (32° 55'S y 33° 15' S). Revista Norte Grande, 24, 113–125.

Cembrano, J., González, G., Arancibia, G., Ahumada, I., Olivares, V., and Herrera, V. (2005). Fault zone development and strain partitioning in an extensional strike-slip duplex: A case study from the Mesozoic Atacama fault system, Northern Chile. Tectonophysics, 400, 105-125. doi: 10.1016/j.tecto.755 2005.02.012.

Charrier, R., Ramos, V. A., Tapia, F., and Sagripanti, L. (2014). Tectonostratigraphic evolution of the Andean Orogen between 31 and 37 ◦ S (Chile and Western Argentina). In S. A. Sepúlveda, L. B. Giambiagi, S. M. Moreiras, L. Pinto, M. Tunik, G. Hoke, and M. Farías (Eds.), Geodynamic Processes in the Andes of Central Chile and Argentina. Geological Society, London, Special Publications, 399 (pp. 13-61). volume 399. doi:10.1144/SP399.20.

Chen, M., Tang, C., Xiong, J., Shi, Q. Y., Li, N., Gong, L. F., Wang, X. D., and Tie, Y. (2020). The long-term evolution of landslide activity near the epicentral area of the 2008 Wenchuan earthquake in China. Geomorphology, 367. doi:10.1016/j.geomorph.2020.107317.

Chigira, M., Wang, W. N., Furuya, T., and Kamai, T. (2003). Geological causes and geomorphological precursors of the Tsaoling landslide triggered by the 1999 Chi-Chi earthquake, Taiwan. Engineering Geology, 68 , 259-273. doi:10.1016/S0013-7952(02)00232-6.

Chigira, M., and Yagi, H. (2006). Geological and geomorphological characteristics of landslides triggered by the 2004 Mid Niigta prefecture earthquake in Japan. Engineering Geology, 82 , 202-221. doi:10.1016/j.enggeo.2005.10.006.

Chousianitis, K., Del Gaudio, V., Kalogeras, I., and Ganas, A. (2014). Predictive model of Arias intensity and Newmark displacement for regional scale evaluation of earthquake-induced landslide hazard in Greece. Soil Dynamics and Earthquake Engineering, 65 , 11-29. URL: http://dx.doi.org/10.1016/j.soildyn.2014.05.009. doi:10.1016/j.soildyn.2014.05.009.

Cortés, J. (2012). Activité des failles de la plaque supérieure dans l'avantarc côtier du nord du Chili (~23◦30'S): Paléosismologie, implications néotectoniques et relation avec le cycle de subduction. Ph.D. thesis 'Université Toulouse III - Paul Sabatier.

Creixell, C., Parada, M. , Roperch, P., Morata, D., Arriagada, C., and de Arce, C. P. (2006). Syntectonic emplacement of the Middle Jurassic Concón Mafic Dike Swarm, Coastal Range, central Chile (33◦ S). Tectonophysics, 425 , 101-122. doi:10.1016/j.tecto.2006.07.005.

Crempien, J. G. F., and Archuleta, R. J. (2015). UCSB Method for Simulation of Broadband Ground Motion from Kinematic Earthquake Sources. Seismological Research Letters, 86, 61-67. doi:10.1785/0220140103.

Crespellani, T., Madiai, C., and Vannucchi, G. (1998). Discussion: Earthquake destructiveness potential factor and slope stability. G´eotechnique, 48 , 411- 419. doi:10.1680/geot.2001.51.3.281.

De Blasio, F. V. (2011). Friction, Cohesion, and Slope Stability. In Introduction to the Physics of Landslides (pp. 23-52). Dordrecht: Springer Netherlands. doi:10.1007/800 978-94-007-1122-8-2.

De Los Arcos, S., Partarrieu, D., Carrillo-Briceño, J., and Amson, E. (2017). The Southernmost Occurrence of the Aquatic Sloth Thalassocnus (Mammalia, Tardigrada) in Two New Pliocene Localities in Chile. Ameghiniana, 54, 351-369. doi:10.5710/AMGH.29.12.2016.3004.

Del Gaudio, V., and Wasowski, J. (2011). Advances and problems in understanding the seismic response of potentially unstable slopes. Engineering Geology, 122, 73-83. doi:10.1016/j.enggeo.2010.09.007.

Du, W. (2018). Effects of directionality and vertical component of ground motions on seismic slope displacements in Newmark sliding-block analysis. Engineering Geology, 239, 13-21.doi:10.1016/j.enggeo.2018.03.012.

Du, W., and Wang, G. (2016). A one-step Newmark displacement model for probabilistic seismic slope displacement hazard analysis. Engineering Geology, 205, 12-23. URL: http://linkinghub.elsevier.com/retrieve/pii/S0013795216300436. doi:10.1016/j.enggeo.2016.02.011.

Dysli, M. (2000). Swiss Standard SN 670 010b, Characteristic Coefficients of soils. Strasse und Verkehr, 86, 93-94.

Ekström, G., Nettles, M., and Dziewonski, A. (2012). The global CMT project 2004-2010: Centroid-moment tensors for 13,017 earthquakes. Physics of the Earth and Planetary Interiors, 200-201, 1-9. URL: https://linkinghub.elsevier.com/retrieve/pii/S0031920112000696. doi:10.1016/j.pepi.2012.04.002.

Encinas, A., Finger, K. L., Nielsen, S. N., Lavenu, A., Buatois, L. A., Peterson, D. E., and Le Roux, J. P. (2008). Rapid and major coastal subsidence during the late Miocene in south-central Chile. Journal of South American Earth Sciences, 25, 157-175. URL: http://linkinghub.elsevier.com/retrieve/pii/S0895981107000879. doi:10.1016/j.jsames.2007.07.001.

Encinas, A., Hervé, F., Villa-Martínez, R., Nielsen, S. N., Finger, K. L., and Peterson, D. E. (2006). Finding of a Holocene marine layer in Algarrobo (33◦22'S), central Chile. Implications for coastal uplift. Revista geológica de Chile, 33, 339-345.

Fan, X., Scaringi, G., Korup, O., West, A. J., Westen, C. J., Tanyas, H., Hovius, N., Hales, T. C., Jibson, R. W., Allstadt, K. E., Zhang, L., Evans, S. G., Xu, C., Li, G., Pei, X., Xu, Q., and Huang, R. (2019). Earthquake-Induced Chains of Geologic Hazards: Patterns, Mechanisms, and Impacts. Reviews of Geophysics, 57, 421-503. URL: https://onlinelibrary.wiley.com/doi/abs/10.1029/2018RG000626. doi:10.1029/2018RG000626.

Farías, M., Charrier, R., Carretier, S., Martinod, J., Fock, A., Campbell, D., Cáceres, J., and Comte, D. (2008). Late Miocene high and rapid surface uplift and its erosional response in the Andes of central Chile (33◦ - 35◦S). Tectonics, 27. doi:10.1029/2006TC002046.

Farías, M., Comte, D., Charrier, R., Martinod, J., David, C., Tassara, A.,Tapia, F., and Fock, A. (2010). Crustal-scale structural architecture in central Chile based on seismicity and surface geology: Implications for Andean mountain building. Tectonics, 29, 57-78. doi:10.1029/2009TC002480.

Farías, M., Comte, D., Roecker, S., Carrizo, D., and Pardo, M. (2011). Crustal extensional faulting triggered by the 2010 Chilean earthquake: The Pichilemu Seismic Sequence. Tectonics, 30. doi:10.1029/2011TC002888.

Farías, V. (2012). Análisis geomorfológico de megadeslizamientos entre las Quebradas Camarones y Tiliviche, Región de Tarapacá. Ph.D. thesis Universidad de Chile.

Frisch, W., Meschede, M., and Blakey, R. (2011). Plate motions and earthquake zones. doi:10.1007/978-3-540-76504-2.

Fuenzalida, F. (2015). Susceptibilidad de remociones en masa en Cuenca de Las Zorras, afectada por catástrofe Incendiaria, Comuna de Valparaíso, Abril 2014. Ph.D. thesis Universidad de Chile.

Gana, P., and Tosdal, R. M. (1996). Geocronología U-Pb y K-Ar en intrusivos del Paleozoico y Mesozoico de la Cordillera de la Costa, Región de Valparaíso, Chile.

Gana, P., Wall, R., Gutiérrez, A., and SERNAGEOMIN (1996). Mapa geológico del area de Valparaíso-Curacaví, regiones de Valparaíso y Metropolitana, Escala 1:100.000.

Giambiagi, L., Tassara, A., Mescua, J., Tunik, M., Alvarez, P. P., Godoy, E., Hoke, G., Pinto, L., Spagnotto, S., Porras, H., Tapia, F., Jara, P., Bechis, F., García, V. H., Suriano, J., Moreiras, S. M., and Pagano, S. D. (2015). Evolution of shallow and deep structures along the Maipo-Tunuyán transect (33◦40'S): 880 From the Pacific coast to the Andean foreland. Geological Society Special Publication, 399, 63-82. doi:10.1144/SP399.14.

González, A. (2008). Análisis estructural entre los valles del Río Tinguiririca y Teno, Cordillera Principal de Chile Central: Microsismicidad y Geología Superficial. Ph.D. thesis Universidad de Chile. URL: http://repositorio.uchile.cl/handle/2250/103153.

González, G., Salazar, P., Loveless, J. P., Allmendinger, R. W., Aron, F., & Shrivastava, M. (2015). Upper plate reverse fault reactivation and the unclamping of the megathrust during the 2014 northern Chile earthquake sequence. Geology, 43(8), 671–674. https://doi.org/10.1130/G36703.1

Gonzalez, P. (2010). Geología y geomorfología del complejo de Remoción en Masa La Engorda, Chile Central. Ph.D. thesis Universidad de Chile.

Gorum, T., and Carranza, E. J. M. (2015). Control of style of faulting on spatial pattern of earthquake-triggered landslides. International Journal of Environmental Science and Technology, 12, 3189-3212. URL: http://link.springer.com/10.1007/s13762-015-0752-y. doi:10.1007/s13762-015-0752-y.

Gorum, T., Fan, X., van Westen, C. J., Huang, R. Q., Xu, Q., Tang, C., and Wang, G. (2011). Distribution pattern of earthquake-induced landslides triggered by the 12 May 2008 Wenchuan earthquake. Geomorphology, 133, 152-167. URL: http://dx.doi.org/10.1016/j.geomorph.2010.12.030. doi:10.1016/j.geomorph.2010.12.030.

Griffiths, D. V., and Lane, P. A. (1999). Slope stability analysis by finite elements. Geotechnique, 49, 387-403. doi:10.1680/geot.1999.49.3.387.

Guerrero, B. (2020). Segmentación del alzamiento tectónico cuaternario en la
Cordillera de la Costa Occidental de Chile Central (33◦-34◦S) a partir de Terrazas Marinas. Ph.D. thesis University of Chile.

Han, L., Ma, Q., Zhang, F., Zhang, Y., Zhang, J., Bao, Y., and Zhao, J. (2019). Risk Assessment of An Earthquake-Collapse-Landslide Disaster Chain by Bayesian Network and Newmark Models. International Journal of Environmental Research and Public Health, 16, 3330. URL: https://www.mdpi.com/1660-4601/16/18/3330. doi:10.3390/ijerph16183330.

Harp, E. L., Hartzell, S. H., Jibson, R. W., Ramirez-Guzman, L., and Schmitt, R. G. (2014). Relation of landslides triggered by the Kiholo Bay Earthquake to modeled ground motion. Bulletin of the Seismological Society of America, 104, 2529-2540. doi:10.1785/0120140047.

Harp, E. L., Keefer, D. K., Sato, H. P., and Yagi, H. (2011). Landslide inventories: The essential part of seismic landslide hazard analyses. Engineering Geology, 915. doi:10.1016/j.enggeo.2010.06.013.

Hayes, G. P., Bergman, E., Johnson, K. L., Benz, H. M., Brown, L., and Meltzer, A. S. (2013). Seismotectonic framework of the 2010 February 27Mw 8.8 Maule, Chile earthquake sequence. Geophysical Journal International, 195, 1034-1051. doi:10.1093/gji/ggt238.

Heinze, B. (2003). Active Intraplate Faulting in the Forearc of North Central Chile (30◦-31◦ S). Implications from Neotectonic Field Studies, GPS Data, and Elastic Dislocation Modeling. Technical Report.

Higaki, D., and Abe, S. (2013). Classification of the Geomorphology, Geology and Movement Types of Earthquake Landslides. In Earthquake-Induced Landslides (pp. 37-44). Berlin, Heidelberg: Springer Berlin Heidelberg. doi:10.1007/978-3-642-32238-9_5.

Hoffmann-Rothe, A., Kukowski, N., Dresen, G., Echtler, H., Oncken, O., Klotz, J., Scheuber, E., and Kellner, A. (2006). Oblique Convergence along the Chilean Margin: Partitioning, Margin-Parallel Faulting and Force Interaction at the Plate Interface. In O. Oncken, G. Chong, G. Franz, P. Gies, E.-J. G¨otze, V. A. Ramos, M. R. Strecke, and R. Wigger (Eds.), The Andes chapter Chapter 6. (pp. 125-146). Springer Berlin Heidelberg.doi:10.1007/978-3-540-48684-8-_}6.

Huang, D., Wang, G., Du, C., Jin, F., Feng, K., and Chen, Z. (2020). An integrated SEM-Newmark model for physics-based regional co-seismic landslide assessment. Soil Dynamics and Earthquake Engineering, 132, 106066. doi:10.1016/j.soildyn.2020.106066.

Huang, R. (2013). Slope Motion Response and Failure Under Strong 945 Earthquakes: Recording, Monitoring and Modeling. In K. Ugai (Ed.), Earthquake-Induced Landslides chapter 7. (pp. 59-73). Berlin, Heidelberg: Springer Berlin Heidelberg. URL: http://link.springer.com/10.1007/978-3-642-32238-9_7. doi:10.1007/978-3-642-32238-9-_}7.

Idini, B., Rojas, F., Ruiz, S., and Pastén, C. (2017). Ground motion prediction equations for the Chilean subduction zone. Bulletin of Earthquake Engineering, 15, 1853-1880. doi:10.1007/s10518-016-0050-1.

Isacks, B. L. (1988). Uplift of the central Andean Plateau and bending of the Bolivian Orocline. Journal of Geophysical Research, 93(B4), 3211–3231. https://doi.org/10.1029/JB093iB04p03211

Jafarian, Y., Lashgari, A., and Haddad, A. (2019). Predictive model and probabilistic assessment of sliding displacement for regional scale seismic landslide hazard estimation in Iran. Bulletin of the Seismological Society of America, 960 109, 1581-1593. doi:10.1785/0120190004.

Jang, H. S., Zhang, Q. Z., Kang, S. S., and Jang, B. A. (2018). Determination of the Basic Friction Angle of Rock Surfaces by Tilt Tests. Rock Mechanics and Rock Engineering, 51, 989-1004. doi:10.1007/s00603-017-1388-7.

Jara-Muñoz J., and Melnick, D. (2015). Unraveling sea-level variations and tectonic uplift in wave-built marine terraces, Santa María Island, Chile. Quaternary Research (United States), 83, 216-228. doi:10.1016/j.yqres.2014.10.002.

Jibson, R. W. (1993). Predicting Earthquake-Induced Landslide Displacements Using Newmark's Sliding Block Analysis. Transportation Research Record, (pp. 9-17).

Jibson, R. W. (2007). Regression models for estimating co-seismic landslide displacement. Engineering Geology, 91, 209-218. doi:10.1016/j.enggeo. 2007.01.013.

Jibson, R. W. (2011). Methods for assessing the stability of slopes during earthquakes-A retrospective. Engineering Geology, 122, 43-50. doi:10.1016/980 j.enggeo.2010.09.017.

Jibson, R. W., Harp, E. L., and Michael, J. A. (2000). A method for producing digital probabilistic seismic landslide hazard maps. Engineering Geology, 58, 271-289. doi:10.1016/S0013-7952(00)00039-9.

Jibson, R. W., and Keefer, D. K. (1993). Analysis of the seismic origin of landslides: examples from the New Madrid seismic zone. Geological Society of America Bulletin, 105, 521-536. doi:10.1130/0016-7606(1993)105<0521

Jibson, R. W., and Michael, J. A. (2009). Maps Showing Seismic Landslide Hazards in Anchorage, Alaska.

Kan, M. E., Taiebat, H. A., and Taiebat, M. (2017). Framework to assess Newmark-type simplified methods for evaluation of earthquake-induced deformation of embankments. Canadian Geotechnical Journal, 54, 392-404. doi:10.1139/cgj-2016-0069.

Kargel, J. S., Leonard, G. J., Shugar, D. H., Haritashya, U. K., Bevington, A., Fielding, E. J., Fujita, K., Geertsema, M., Miles, E. S., Steiner, J., Anderson, E., Bajracharya, S., Bawden, G. W., Breashears, D. F., Byers, A., Collins, B., Dhital, M. R., Donnellan, A., Evans, T. L., Geai, M. L., Glasscoe, M. T., Green, D., Gurung, D. R., Heijenk, R., Hilborn, A., Hudnut, K., Huyck, C., Immerzeel, W. W., Liming, J., Jibson, R., Kaab, A., Khanal, N. R., Kirschbaum, D., Kraaijenbrink, P. D. A., Lamsal, D., Shiyin, L., Mingyang, L., McKinney, D., Nahirnick, N. K., Zhuotong, N., Ojha, S., Olsenholler, J., Painter, T. H., Pleasants, M., Pratima, K. C., Yuan, Q. I., Raup, B. H., Regmi, D., Rounce, D. R., Sakai, A., Donghui, S., Shea, J. M., Shrestha, A. B., Shukla, A., Stumm, D., van der Kooij, M., Voss, K., Xin, W., Weihs, B., Wolfe, D., Lizong, W., Xiaojun, Y., Yoder, M. R., and Young, N. (2016). Geomorphic and geologic controls of geohazards induced by Nepals 2015 Gorkha earthquake. Sciencexpress, 351, 1-18. URL: http://www.sciencemag.org/cgi/doi/10.1126/science.aac8353. doi:10.1126/science.aac8353.

Keefer, D., and Wilson, R. (1989). Predicting earthquake-induced landslides, with emphasis on arid and semi-arid environments. Landslides in a semi-arid environment, 2, 118-149.

Keefer, D. K. (1984a). Landslides caused by earthquakes. Geological Society of America Bulletin, 95, 406-421. doi:10.1130/0016-7606(1984)95<406:1015 LCBE>2.0.CO;2.

Keefer, D. K. (1994). The importance of earthquake-induced landslides to longterm slope erosion and slope-failure hazards in seismically active regions. Geomorphology, . doi:10.1016/0169-555X(94)90021-3.

Keefer, D. K. (2000). Statistical analysis of an earthquake-induced landslide distribution | the 1989 Loma Prieta , California event. Engineering Geology, 58, 231-249.

Keefer, D. K. (2012). Earthquake-induced landslides and their effects on alluvial fans. Journal of Sedimentary Research, . doi:10.2110/jsr.69.84.

Koloski, J. W. , S. S. D. , & T. D. W. (1989). Geotechnical properties of geologic materials. Engineering Geology in Washington, 1, 19–24.Lara, M. (2007). Metodología para la evaluación y zonificación de Peligro de Remociones en Masa con Aplicación en Quebrada San Ram´on, Santiago Oriente, Región Metropolitana. Ph.D. thesis.

Lara, M., Sepúlveda, S. A., Celis, C., Rebolledo, S., and Ceballos, P. (2018). Landslide susceptibility maps of Santiago city Andean foothills, Chile. Andean Geology, 45, 433. doi:10.5027/andgeoV45n3-3151.

Laursen, J., Scholl, D. W., and von Huene, R. (2002). Neotectonic deformation of the central Chile margin: Deepwater forearc basin formation in response to hot spot ridge and seamount subduction. Tectonics, 21, 2-1. doi:10.1029/2001TC901023.

Lavenu, A., and Encinas, A. (2005). Deformacinó frágil de los depósitos neógenos de la cuenca de Navidad (Cordillera de la Costa, 34◦S, Chile central). Revista geológica de Chile, 32, 229-248. doi:10.4067/S0716-02082005000200004.

Lay, T., Kanamori, H., Ammon, C. J., Koper, K. D., Hutko, A. R., Ye, L., Yue, H., and Rushing, T. M. (2012). Depth-varying rupture properties of subduction zone megathrust faults. Journal of Geophysical Research: Solid Earth, 117. doi:10.1029/2011JB009133.

Legrand, D., Barrientos, S., Bataille, K., Cembrano, J., and Pavez, A. (2011). The fluid-driven tectonic swarm of Aysen Fjord, Chile (2007) associated with two earthquakes (Mw=6.1 and Mw=6.2) within the Liquiñe-Ofqui Fault Zone. Continental Shelf Research, 31,154-161. doi:10.1016/j.csr.2010.05.008.

Lenti, L., and Martino, S. (2012). The interaction of seismic waves with step-like
slopes and its influence on landslide movements. Engineering Geology, 126, 19-36.doi: 10.1016/j.enggeo.2011.12.002.

Leonard, M. (2010). Earthquake Fault Scaling: Self-Consistent Relating of Rupture Length, Width, Average Displacement, and Moment Release. Bulletin of the Seismological Society of America, 100, 1971-1988. URL: https://pubs.geoscienceworld.org/bssa/article/100/5A/1971-1988/325106. doi:10.1785/0120090189.

Leshchinsky, B. A. (2018). Nested Newmark model to calculate the 1065 post-earthquake profile of slopes. Engineering Geology, 233, 139-145. URL: https://doi.org/10.1016/j.enggeo.2017.12.006. doi:10.1016/j.enggeo.2017.12.006.

Leyton, F., Ruiz, S., and Sepulveda, S. A. (2009). Reevaluacion del peligro sismico probabilistico en Chile central. URL: http://www.scielo.1070 cl/scielo.php?script=sci_arttextandpid=S0718-71062010000200011. doi:10.5027/andgeoV37n2-a11.

Liu, J. G., Mason, P. J., Yu, E., Wu, M. C., Tang, C., Huang, R., and Liu, H. 1075 (2012). GIS modelling of earthquake damage zones using satellite remote sensing and DEM data. Geomorphology, 139-140, 518-535. doi:10.1016/j.geomorph.2011.12.002.

Liu, Y., Li, H., Xiao, K., Li, J., Xia, X., and Liu, B. (2014). Seismic stability analysis of a layered rock slope. Computers and Geotechnics, 1080 55, 474-481. doi:10.1016/j.compgeo.2013.10.002.

Loveless, J. P., Allmendinger, R. W., Pritchard, M. E., and González, G. (2010). Normal and reverse faulting driven by the subduction zone earthquake cycle in the northern Chilean fore arc. Tectonics, 29, 1-16. doi:10.1029/1085 2009TC002465.

Madariaga, R. (1976). Dynamics of an expanding circular fault. Bulletin of the Seismological Society of America, 66, 639-666.

Malamud, B. D., Turcotte, D. L., Guzzetti, F., and Reichenbach, P. (2004). Landslide inventories and their statistical properties. Earth Surface Processes and Landforms, . doi:10.1002/esp.1064.

Marc, O., Hovius, N., Meunier, P., Gorum, T., & Uchida, T. (2016). A seismologically consistent expression for the total area and volume of earthquake-triggered landsliding. Journal of Geophysical Research: Earth Surface, 121(4), 640–663. https://doi.org/10.1002/2015JF003732

Marc, O., Meunier, P., and Hovius, N. (2017). Prediction of the area affected by earthquake-induced landsliding based on seismological parameters. Natural Hazards and Earth System Sciences, 17, 1159-1175. doi:10.5194/nhess-17-1159-2017.

Marquardt, C., Lavenu, A., Ortlieb, L., Godoy, E., and Comte, D. (2004). Coastal neotectonics in Southern Central Andes: Uplift and deformation of marine terraces in Northern Chile (27◦S). Tectonophysics, 394, 193-219. doi:10.1016/j.tecto.2004.07.059.

Martinod, J., Regard, V., Riquelme, R., Aguilar, G., Guillaume, B., Carretier, S., Cort´es-Aranda, J., Leanni, L., and H´erail, G. (2016). Pleistocene uplift, climate and morphological segmentation of the Northern Chile coasts (24◦S-32◦S): Insights from cosmogenic 10Be dating of paleoshorelines. Geomorphology, 274, 78-91. doi:10.1016/j.geomorph.2016.09.010.

Melnick, D. (2016a). Rise of the central Andean coast by earthquakes straddling the Moho. Nature Geoscience, 9, 1-8. doi:10.1038/ngeo2683.

Melnick, D. (2016b). Rise of the central Andean coast by earthquakes straddling the Moho. Nature Geoscience, 9, 401-407. doi:10.1038/ngeo2683.

Melnick, D., Bookhagen, B., Strecker, M. R., and Echtler, H. P. (2009). Segmentation of megathrust rupture zones from fore-arc deformation patterns over hundreds to millions of years, Arauco peninsula, Chile. Journal of Geophysical Research: Solid Earth, 114, 1-23. doi:10.1029/2008JB005788.

Melnick, D., Hillemann, C., Jara-Mu~noz, J., Garrett, E., Cortés-Aranda, J., Molina, D., Tassara, A., and Strecker, M. R. (2019). Hidden Holocene Slip Along the Coastal El Yolki Fault in Central Chile and Its Possible Link With Megathrust Earthquakes. Journal of Geophysical Research: Solid Earth, 124, 7280-7302. doi:10.1029/2018JB017188.

Meunier, P., Hovius, N., and Haines, A. J. (2007). Regional patterns of earthquake-triggered landslides and their relation to ground motion. Geophysical Research Letters, 34, 1-5. doi:10.1029/2007GL031337.

Meunier, P., Hovius, N., & Haines, J. A. (2008). Topographic site effects and the location of earthquake induced landslides. Earth and Planetary Science Letters, 275(3–4), 221–232. https://doi.org/10.1016/j.epsl.2008.07.020

Miles, S. B., and Ho, C. L. (1999). Rigorous landslide hazard zonation using Newmark's method and stochastic ground motion simulation. Soil Dynamics and Earthquake Engineering, 18, 305-323. doi:10.1016/S0267-7261(98)1130 00048-7.

Mordojovic, C. (1981). Sedimentary Basins of Chilean Pacific Offshore. In Energy Resources of the Pacific Region (pp. 63-82). doi:10.1306/St12420C7.

Mpodozis, C., & Cornejo, P. (2012). Cenozoic tectonics and porphyry copper system of the Chilean Andes. Economic Geology. Special Publication, 16, 329–360.

Muñoz, E. (2013). Susceptibilidad de remociones en masa y de respuesta sísmica asociada a fallas mayores en zonas urbanas, estudio de caso en Viña del Mar, V Región. MSc Thesis University of Chile.

National Academies of Sciences (2003). Preventing Earthquake Disasters: The Grand Challenge in Earthquake Engineering: A Research Agenda for the Network for Earthquake Engineering Simulation. Washington, D.C. doi:10.17226/10799.

National Academies of Sciences. (2018). Thriving on Our Changing Planet: A Decadal Strategy for Earth Observation from Space. National Academies Press. https://doi.org/10.17226/24938

Newmark, N. M. (1965). Effects of Earthquakes on Dams and Embankments. Geotechnique, 15, 139-160. doi:10.1680/geot.1965.15.2.139.

Niemeyer, H., González, G., and Martínez-De Los R´ıos, E. (1996). Cenozoic tectonic evolution of the active continental margin of Northern Antofagasta, Chile [Evolución tectónica cenozoica del margen continental activo de Antofagasta, norte de Chile Hans Niemeyer]. Revista Geológica de Chile, 23, 165-186.

Niño, M., Jaimes, M. A., Reinoso, E., Ni~no, M., Jaimes, M. A., Reinoso, E., Reinoso, E., and Robles, V. A. (2014). Seismic-event-based methodology to obtain earthquake-induced translational landslide regional hazard maps. 73, 1697-1713. doi:10.1007/s11069-014-1163-y.

Nowicki, M. A., Wald, D. J., Hamburger, M. W., Hearne, M., and Thompson, E. M. (2014). Development of a globally applicable model for near real-time prediction of seismically induced landslides. Engineering Geology, 173, 54-65. URL: http://dx.doi.org/10.1016/j.enggeo.2014.02.002. doi:10.1016/j.enggeo.2014.02.002.

Parada, M. A., Feraud, G., Fuentes, F., Aguirre, L., Morata, D., and Larrondo, P. (2005). Ages and cooling history of the Early Cretaceous Caleu pluton: Testimony of a switch from a rifted to a compressional continental margin in central Chile. Journal of the Geological Society, 162, 273-287. doi:10.1144/0016-764903-173.

Parker, R. N., Rosser, N. J., and Hales, T. C. (2017). Spatial prediction of earthquake-induced landslide probability. Natural Hazards and Earth System Sciences Discussions, (pp. 1-29). doi:10.5194/nhess-2017-193.

Peck, R., Hanson, W., and Thornburn, T. (1974). Foundation engineering volume 10. New York: Wiley. URL: http://library.dmr.go.th/Document/TextBooks/3044.pdf.

Pellicani, R., Argentiero, I., and Spilotro, G. (2017). GIS-based predictive models

for regional-scale landslide susceptibility assessment and risk mapping along road corridors. Geomatics, Natural Hazards and Risk, 8, 1012- 1033. doi:10.1080/19475705.2017.1292411.

Podolskiy, E. A., Chambon, G., Naaim, M., and Gaume, J. (2015). Evaluating snow weak-layer failure parameters through inverse finite element modelling of shaking-platform experiments. Natural Hazards and Earth System Sciences, 15, 119-134. URL: https://www.nat-hazards-earth-syst-sci.net/15/119/2015/. doi:10.5194/nhess-15-119-2015.

Rathje, E. M., and Antonakos, G. (2011). A unified model for predicting earthquake-induced sliding displacements of rigid and flexible slopes. Engineering Geology, 122, 51-60. doi:10.1016/j.enggeo.2010.12.004.

Rathje, E. M., and Saygili, G. (2008). Probabilistic Seismic Hazard Analysis for the Sliding Displacement of Slopes: Scalar and Vector Approaches. Journal of Geotechnical and Geoenvironmental Engineering, 134, 804-814. doi:10.1061/(ASCE)1090-0241(2008)134:6(804).

Rivano, S., and Sepulveda, P. (1991). Carta Geológica de Chile n.69, escala 1:250000: Hoja Illapel, Región de Coquimbo.

Rivano, S., Sepúlveda, P., Boric, R., and Espiñeira, D. (1993). Hojas Quillota y Portillo, V Región, Escala 1: 250.000.

Roback, K., Clark, M. K., West, A. J., Zekkos, D., Li, G., Gallen, S. F., Chamlagain, D., and Godt, J. W. (2018). The size, distribution, and mobility of

landslides caused by the 2015 Mw7.8 Gorkha earthquake, Nepal. Geomorphology, . doi:10.1016/j.geomorph.2017.01.030.

Rodrigo, C. (2011). Bathymetric interpretation of the valparaiso area: Comments on the paper by HP vergara and R Astudillo, 'offshore structural highs of the valparaiso region, central Chile'. Revista de Biologia Marina y Oceanografia, 46, 249-255. URL: http://www.jpl.nasa.gov/srtm.

1200 doi:10.4067/s0718-19572011000200014.

Rodríguez, C. E., Bommer, J. J., and Chandler, R. J. (1999). Earthquake-induced landslides: 1980-1997. Soil Dynamics and Earthquake Engineering, 18, 325-346. doi:10.1016/S0267-7261(99)00012-3.

Rodríguez, M. P. (2008). Evolución de la erosión y del relieve del antearco de Chile central (33-34◦) durante el Ne´ogeno mediante el an´alisis de minerales pesados detríticos y la geomorfología. Ph.D. thesis.

Rodríguez, M. P., Carretier, S., Charrier, R., Saillard, M., Regard, V., Herail, G., Hall, S., Farber, D., and Audin, L. (2013). Geochronology of pediments and marine terraces in north-central Chile and their implications for Quaternary uplift in the Western Andes. Geomorphology, 180-181, 33-46. doi:10.1016/j.geomorph.2012.09.003.

Romeo, R. (2000). Seismically induced landslide displacements: A predictive model. Engineering Geology, 58, 337-351. doi:10.1016/S0013-7952(00)00042-9.

Ruiz, J. A., Hayes, G. P., Carrizo, D., Kanamori, H., Socquet, A., and Comte, D. (2014). Seismological analyses of the 2010 March 11, Pichilemu, Chile MW 7.0 and MW 6.9 coastal intraplate earthquakes. Geophysical Journal International, 197, 414-434. doi:10.1093/gji/ggt513.

Ruiz, S., and Madariaga, R. (2018). Historical and recent large megathrust earthquakes in Chile. Tectonophysics, 733, 37-56. doi:10.1016/j.tecto.2018.01.015.

Sabaj, R. (2008). Identificación y caracterización de estructuras potencialmente activas en la cordillera de la costa, entre los 33◦ y 33◦45' Sur, . (p. 92).

Sáez, E., Marquardt, C., Yáñez, G., Montalva, G., Valdivia, D., and del Valle, F. (2018). Mapa de Amenaza Sísmica en Bloque San Antonio - Los Vilos. Technical Report Proyecto FONDEF D10E1027.

Saillard, M., Hall, S., Audin, L., Farber, D., Herail, G., Martinod, J., Regard,V., Finkel, R., and Bondoux, F. (2009). Non-steady long-term uplift rates and Pleistocene marine terrace development along the Andean margin of Chile (31◦S) inferred from 10Be dating. Earth and Planetary Science Letters, 277, 50-63. doi:10.1016/j.epsl.2008.09.039.

Santibáñez, I., Cembrano, J., García-Pérez, T., Costa, C., Yáñez, G., Marquardt, C., Arancibia, G., and González, G. (2019). Crustal faults in the chilean Andes: Geological constraints and seismic potential. Andean Geology,1240 46, 32-65. doi:10.5027/andgeov46n1-3067.

Satake, K., Heidarzadeh, M., Quiroz, M., and Cienfuegos, R. (2020). History and features of trans-oceanic tsunamis and implications for paleotsunami studies. Earth-Science Reviews, 202, 103112. doi:10.1016/J.EARSCIREV.2020.103112.

Satake, K., and Tanioka, Y. (1999). Sources of tsunami and tsunamigenic earthquakes in subduction zones. Pure and Applied Geophysics. doi:10.1007/

s000240050240.

Sepulveda, S. A., Astroza, M., Kausel, E., Campos, J., Casas, E. A., Rebolledo, S., and Verdugo, R. (2008). New findings on the 1958 Las Melosas earthquake sequence, central Chile: Implications for seismic hazard related to shallow crustal earthquakes in subduction zones. Journal of Earthquake Engineering, 12, 432-455. doi:10.1080/13632460701512951.

Sepúlveda, S. A., Giambiagi, L. B., Moreiras, S. M., Pinto, L., Tunik, M., Hoke, 1255 G. D., and Farías, M. (2015). Geodynamic processes in the andes of central Chile and Argentina: An introduction. Geological Society Special Publication, 399, 1-12. doi:10.1144/SP399.21.

Sepúlveda, S. A., Murphy, W., Jibson, R. W., and Petley, D. N. (2005). Seismically induced rock slope failures resulting from topographic amplification of strong ground motions: The case of Pacoima Canyon, California. Engineering Geology, 80, 336-348. doi:10.1016/j.enggeo.2005.07.004.

Sepúlveda, S. A., and Serey, A. (2009). Tsunamigenic, earthquake-triggered rock slope failures during the April 21, 2007 Aysén earthquake, southern Chile (45.5°S). Andean Geology, 36, 131-136. doi: 10.4067/1265 S0718-71062009000100010.

Sepúlveda, S. A., Serey, A., Lara, M., Pavez, A., and Rebolledo, S. S. (2010). Landslides induced by the April 2007 Ays´en Fjord earthquake , Chilean Patagonia. Landslides, 7, 483-492. doi:10.1007/s10346-010-0203-2.

Serey, A., Piñero-Feliciangeli, L., Sepúlveda, S. A., Poblete, F., Petley, D. N., and Murphy, W. (2019). Landslides induced by the 2010 Chile megathrust earthquake: a comprehensive inventory and correlations with geological and seismic factors. Landslides. doi:10.1007/s10346-019-01150-6.

SERNAGEOMIN (2003). Mapa Geol´ogico de Chile: versión digital. Servicio Nacional de Geología y Minería, Publicación Geolóogica Digital, No. 4 (CD-ROM, version1.0, 2003). Santiago.

Shafique, M. (2020). Spatial and temporal evolution of co-seismic landslides after the 2005 Kashmir earthquake. Geomorphology, 362. doi:10.1016/j.geomorph.2020.107228.

Shanmugam, G., and Wang, Y. (2015). The landslide problem. doi:10.3724/SP.1280 J.1261.2015.00071.

Shao, X., Ma, S., Xu, C., and Zhou, Q. (2020). Effects of sampling intensity and non-slide/slide sample ratio on the occurrence probability of co-seismic landslides. Geomorphology, 363, 107222. doi:10.1016/j.geomorph.2020.107222.

Sharifi-Mood, M., Olsen, M. J., Gillins, D. T., and Mahalingam, R. (2017).

Performance-based, seismically-induced landslide hazard mapping of Western Oregon. Soil Dynamics and Earthquake Engineering, 103, 38-54.1290 doi:10.1016/j.soildyn.2017.09.012.

Shearer, P. M. (1975). Introduction to Seismology volume 40. doi:10.1111/j.1365-246X.1975.tb01612.x.

Schulz, W. H., Galloway, S. L., & Higgins, J. D. (2012). Evidence for earthquake triggering of large landslides in coastal Oregon, USA. Geomorphology, 141–142, 88–98. https://doi.org/10.1016/j.geomorph.2011.12.026

Sielfeld, G., Ruz, J., Brogi, A., Cembrano, J., Stanton-Yonge, A., PérezFlores, P., and Iturrieta, P. (2019). Oblique-slip tectonics in an active volcanic chain: A case study from the Southern Andes. Tectonophysics, 770,228221. URL: https://doi.org/10.1016/j.tecto.2019.228221. doi:10.1016/j.tecto.2019.228221.

Soga, K., Alonso, E., Yerro, A., Kumar, K., Bandara, S., Kwan, J. S. H., Koo, R. C. H., Law, R. P. H., Yiu, J., Sze, E. H. Y., & Ho, K. K. S. (2018). Trends in large-deformation analysis of landslide mass movements with particular emphasis on the material point method. Geotechnique, 68(5), 457–458. https://doi.org/10.1680/jgeot.16.D.004

Song, J., Gao, Y., and Feng, T. (2018). Probabilistic assessment of earthquakeinduced landslide hazard including the effects of ground motion directionality. Soil Dynamics and Earthquake Engineering, 105, 83-102. URL: https://doi.org/10.1016/j.soildyn.2017.11.027. doi:10.1016/j.soildyn.2017.11.027.

Stavrou, A., Lawrence, J. A., Mortimore, R. N., and Murphy, W. (2011). A geotechnical and GIS based method for evaluating risk exposition along coastal cliff environments: A case study of the chalk cliffs of southern England. Natural Hazards and Earth System Science, 11, 2997-3011. doi:10.5194/nhess-11-2997-2011.

Sugimoto, H., Takeshi, T., Uto, T., and Honma, H. (2013). Geomorphologic and Geologic Features of Landslides Induced by the 2011 Off the Pacific Coast of Tohoku Earthquake, in Shirakawa Hills, Fukushima Prefecture. In K. Ugai, H. Yagi, and A. Wakai (Eds.), Earthquake-Induced Landslides (pp. 189-201). Berlin, Heidelberg: Springer Berlin Heidelberg. doi:10.1007/1315-978-3-642-32238-9-_20.

Tanya¸s, H., van Westen, C. J., Allstadt, K. E., Anna Nowicki Jessee, M., Gorum, T., Jibson, R. W., Godt, J. W., Sato, H. P., Schmitt, R. G., Marc, O., and Hovius, N. (2017). Presentation and Analysis of a Worldwide Database of Earthquake-Induced Landslide Inventories. Journal of Geophysical Research: 1320 Earth Surface, 122, 1991-2015. doi:10.1002/2017JF004236.

Tatard, L., and Grasso, J. R. (2013). Controls of earthquake faulting style on near field landslide triggering: The role of co-seismic slip. Journal of Geophysical Research: Solid Earth, 118, 2953-2964. URL: http://doi.wiley.com/10.1002/jgrb.50215. doi:10.1002/jgrb.50215.

Thomas, H. (1958). Geología de la cordillera de la costa entre el valle de la Ligua y la cuesta de barriga. Inst. Invest. Geol. (Chile), 2. URL: http://bibliotecadigital.ciren.cl//handle/123456789/25099.

Thorson, R. (1999). La Falla Marga-Marga. Technical Report Departamento de Obras Civiles, Universidad Técnica Federico Santa María.

Towhata, I. (2008). Geotechnical Earthquake Engineering. Springer Series in Geomechanics and Geoengineering. Berlin, Heidelberg: Springer Berlin Heidelberg. doi:10.1007/978-3-540-35783-4.

Urzúa, A., Christian, J. T., Silva, R., and Bonani, A. (2014). Rational selection of critical acceleration factors for sliding stability. Engineering Geology, 183, 241-246. doi:10.1016/j.enggeo.2014.08.011.

Vahedifard, F., and Meehan, C. L. (2011). A Multi-Parameter Correlation for Predicting the Seismic Displacement of an Earth Dam or Embankment. Geotechnical and Geological Engineering, 29, 1023-1034. doi:10.1007/s10706-011-9434-9.

Valagussa, A., Marc, O., Frattini, P., and Crosta, G. B. (2019). Seismic and geological controls on earthquake-induced landslide size. Earth and Planetary Science Letters, 506, 268-281. URL: https://doi.org/10.1016/j.epsl.1345 2018.11.005. doi:10.1016/j.epsl.2018.11.005.

Valdenegro, P., Muñoz, M., Yáñez, G., Parada, M. A., and Morata, D. (2019). A model for thermal gradient and heat flow in central Chile: The role of thermal properties. Journal of South American Earth Sciences, 91, 88-101. URL: https://doi.org/10.1016/j.jsames.2019.01.011. doi:10.1016/j.1350 jsames.2019.01.011.

Valdivia, D., Elgueta, S., del Valle, F., Marquardt, C., Yáñez, G., and Hodgkin, A. (2018). Variaci´on del nivel del mar durante el Neógeno en Chile Central: Eustatismo vs Tectonismo. In Congreso Geológico Chileno. Concepción.

Veylon, G., Luu, L. H., Merckl´e, S., Bard, P. Y., Delvallee, A., Carvajal, C., and Frigo, B. (2017). A simplified method for estimating Newmark displacements of mountain reservoirs. Soil Dynamics and Earthquake Engineering, 100, 518-528. URL: http://dx.doi.org/10.1016/j.soildyn.2017.07.003. doi:10.1016/j.soildyn.2017.07.003.

Vigny, C., Socquet, A., Peyrat, S., Ruegg, J.-C., M´etois, M., Madariaga, R., Morvan, S., Lancieri, M., Lacassin, R., Campos, J., Carrizo, D., BejarPizarro, M., Barrientos, S., Armijo, R., Aranda, C., Valderas-Bermejo, M.-C., Ortega, I., Bondoux, F., Baize, S., Lyon-Caen, H., Pavez, A., Vilotte,J. P., Bevis, M., Brooks, B., Smalley, R., Parra, H., Baez, J.-C., Blanco, M.,Cimbaro, S., and Kendrick, E. (2011). The 2010 Mw 8.8 Maule megathrust earthquake of Central Chile, monitored by GPS. Science (New York, N.Y.),332, 1417-1421. doi:10.1126/science.1204132.

Von Huene, R., Corvalán, J., Flueh, E. R., Hinz, K., Korstgard, J., Ranero, C. R., and Weinrebe, W. (1997). Tectonic control of the subducting Juan Fernández Ridge on the Andean margin near Valparaiso, Chile. Tectonics, 16, 474-488. doi:10.1029/96TC03703.

Wall, R., Gana, P., Gutiérrez, A., and SERNAGEOMIN (1996). Mapa geológico del area de San Antonio-Melipilla: regiones de Valparaíso, Metropolitana y del Libertador General Bernardo O'Higgins, Escala 1:100.000. Wartman, J., Dunham, L., Tiwari, B., and Pradel, D. (2013). Landslides in Eastern Honshu Induced by the 2011 Tohoku Earthquake. Bulletin of the Seismological Society of America, 103, 1503-1521. URL: https://pubs.geoscienceworld.org/bssa/article/103/2B/1503-1521/331673. doi:10.1785/0120120128.

Wasowski, J., Jibson, R. W., Huang, R., and van Asch, T. (2014). Special Issue "The long-term geologic hazards in areas struck by large-magnitude earthquakes". Engineering Geology, 182, 109-110. URL: http://dx.doi.org/10.1016/j.enggeo.2014.11.003. doi:10.1016/j.enggeo.2014.11.003.

Wasowski, J., Keefer, D. K., and Lee, C. T. (2011). Toward the next generation of research on earthquake-induced landslides: Current issues and future challenges. Engineering Geology, 122, 1-8. URL: http://dx.doi.org/10.1016/j.enggeo.2011.06.001. doi:10.1016/j.enggeo.2011.06.001.

Wieczorek, G., Wilson, R., and Harp, E. (1985). Map showing slope stability during earthquakes in San Mateo County, California. Technical Report. URL: http://pubs.er.usgs.gov/publication/i1257E. doi:10.3133/i1257E.

Worni, R., Huggel, C., Dorren, L. K., and Jaboyedoff, M. (2013). Numerical Modeling of Flows and Falls volume 7. Elsevier Ltd. doi:10.1016/B978-0-12-374739-6.00177-9.

1390 Xu, C. (2015). Preparation of earthquake-triggered landslide inventory maps using remote sensing and GIS technologies: Principles and case studies. Geoscience Frontiers, 6, 825-836. doi:10.1016/j.gsf.2014.03.004.

Yáñez, G. A., Gana, P., and Fernandez, R. (1998). Origin and geological significance of the Melipilla Anomaly, Central Chile. Revista Geologica De Chile, 25, 175-198.

Yáñez, G. a., Ranero, C. R., von Huene, R., and Díaz, J. (2001). Magnetic anomaly interpretation across the southern central Andes (32◦-34◦S): The role of the Juan Fernández Ridge in the late Tertiary evolution of the margin. Journal of Geophysical Research, 106, 6325. doi:10.1029/2000JB900337.

Yáñez, G., & Rivera, O. (2019). Crustal dense blocks in the fore-arc and arc region of Chilean ranges and their role in the magma ascent and composition: Breaking paradigms in the Andean metallogeny. Journal of South American Earth Sciences, 93(April), 51–66. https://doi.org/10.1016/j.jsames.2019.04.006

Yuan, R., Deng, Q., Cunningham, D., Han, Z., Zhang, D., and Zhang, B. (2017). Erratum to: Newmark displacement model for landslides induced by the 2013 Ms 7.0 Lushan earthquake, China (Frontiers of Earth Science, (2016), 10, 4, (740-750), 10.1007/s11707-015-0547-y). Frontiers of Earth Science, 11, 202. doi:10.1007/s11707-017-0635-2.

Zhang, Y., Yang, Z., Guo, C., Wang, T., Wang, D., and Du, G. (2017). Predicting landslide scenes under potential earthquake scenarios in the Xianshuihe fault zone, Southwest China. Journal of Mountain Science, 14, 1262-1278. doi:10.1007/s11629-017-4363-6

5 DISCUSSION

Fan et al. (2018) argues that co-seismic landslides form the firsts events of a chain of geologic hazards caused by earthquakes. This chain of hazards goes up to decades or centuries where all the wasted material forms part of the source sedimentary material, it interacts with the landscape evolution and it increases the future landslide hazards with reactivation of old landslide deposits or with a slope weakening. So, most of the computed DN on intrusive rocks or regolith are submillimetric to millimetric, it represents crack propagation and an increase of the landslide hazard. So, due an aftershock or a further heavy rainfall, the next slope failure might occur in those points.

In most of the analyzed points the Newmark analysis underestimate the real potential co-seismic displacements (Jibson,2011). The model does not consider topographic amplification, site effects, the dynamic pore pressure is neglected and approximated the problem by a rigid sliding block with constant critical acceleration. Only on Quaternary Eolic deposits the computed DN are maximum up to 86.5 m due a very low critical acceleration.

The displacements and the spatial distribution of earthquake-triggered landslides depends on fault mechanism and directivity on rupture propagation (Roback et al., 2018). Landslides in dip-slip earthquake scenarios have shown larger DN than in the strike-slip earthquake scenarios, whose DN can be up to 4 times larger in dip-slip cases. Due a high directivity on rupture process, there are some points with large PGA, PGV and IA, and consequently large DN on the foot wall in Dip-slip scenarios.

Romeo (2000) poses the minimum Newmark displacement taken in account is 0.00001. All the displacements above this value are considered as not significant. Several authors have proposed categorizations of the hazard based on the calculated Newmark Displacements (California Geological Survey, 2008; Jibson and Michael, 2009) as shown in **Table 4**. A new classification is proposed, based on the computed Newmark displacements, where larger values than 10-3m, smaller than 15cm are considered visible

effects on the slopes, as facture propagation. Displacement larger than 15cm are considered as real landslides.

Table 4: Categorization of the hazard based on Newmark Displacement (Jibson and Michael, 2009)

D_N	Categorization of hazard based on Newmark Displacement
0.0 – 0.01m	Low hazard
0.01 – 0.05 m	Moderated hazard
0.5 – 0.15 m	High
>0.15 m	Very High

Considering the categorization of shallow landslide hazard posed by Jibson and Michael (2009), there are some slopes that have a bigger hazard under normal earthquake scenarios than under sinistral earthquake scenarios. This is consistent with the highest values of I_A and PGA under normal earthquake in the footwall.

In the strike-slip scenarios, the spatial distribution is symmetrical at both sides of their fault traces, similar to the distribution of PGA and I_A. The largest displacements are next to the fault trace, and the computed D_N fades with the distance to the fault. In normal scenarios, the largest displacements are concentrated at the foot wall, due a pulse of directivity in the rupture process (Sommerville e al., 1997). In the same way, under reverse faulting scenarios, due seismic directivity, the co-seismic displacements have a higher density in the hanging wall than in the foot wall (Fan et al., 2019) (Figure 7)

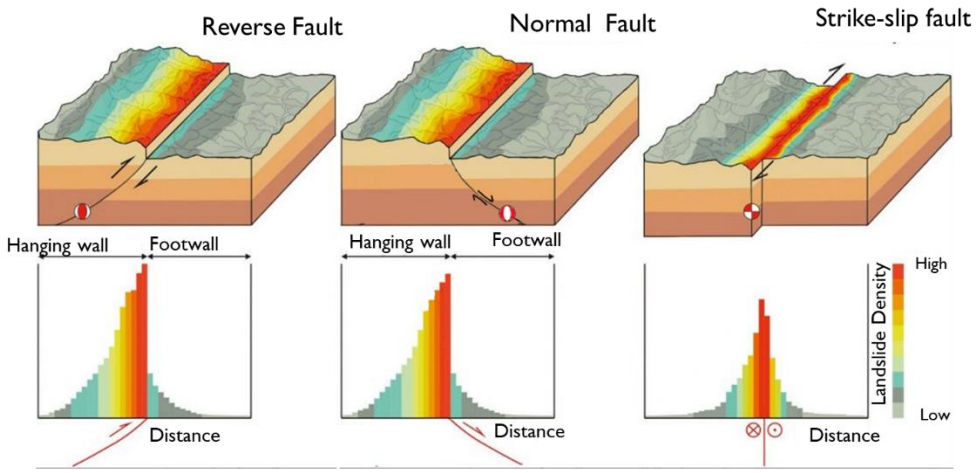

Figure 7: Scheme of spatial distribution of co-seismic landslides under different earthquake kinematic (Modified from Fan et al., 2019)

6 CONCLUSSIONS

Landslide caused by crustal seismicity is part of a larger chain of geologic hazards. They affect the landscape evolution, sedimentary processes, and the changes in the hazard of future landslides or reactivation of old landslides.

1. In the analyzed areas and scenarios, the lithology and their geotechnical properties offers a stronger control than the ground-motion parameters (such as kinematic, localization at one or another block of the fault). Secondarily, the displacements are controlled by the directivity of seismic rupture.

2. The computed displacements under saturated and dry conditions differ at least in 1 order of magnitude.

3. The biggest displacements are located on quaternary aeolian, fluvial or alluvial deposits with loose sand and mud.

4. The displacements in all scenarios are comparable to each other. In the scenarios of dip-slip at some points on the footwall, and on loose sedimentary deposits have the largest displacements, due lithological and rupture propagation controls.

5. Points between Aconcagua and Marga-Marga faults have locally the largest displacements. Probably due a strong lithological control.

6. In future works, the site effects, topographic amplification of seismic waves and internal deformation of the material should be taken in account, to obtain more accurate results.

REFERENCES

Alvarado, P., Barrientos, S., Saez, M., Astroza, M., Beck, S., 2009. Source study and tectonic implications of the historic 1958 Las Melosas crustal earthquake, Chile, compared to earthquake damage. Phys. Earth Planet. Inter. 175, 26–36. https://doi.org/10.1016/j.pepi.2008.03.015

Aron, F., Allmendinger, R.W., Cembrano, J., González, G., Yáñez, G., 2013. Permanent fore-arc extension and seismic segmentation: Insights from the 2010 Maule earthquake, Chile. J. Geophys. Res. Solid Earth 118, 724–739. https://doi.org/10.1029/2012JB009339

Brüggen, J. 1934. Grundzüge der Geologie und Lagerstättenkunde Chiles. Heidelberg Akademie der Wissenschaften, Mathematisch-Naturwissenschaftliche Klasse: 362 p.

Brüggen, J. 1950. Fundamento de la Geología de Chile. Instituto Geográfico Militar: 374 p.

Carrillo-Briceño, J.D., 2013. Condrictios fósiles del Plioceno Superior de la Formación Horcon, Region de Valparaíso, Chile central. Rev. Chil. Hist. Nat. 86, 191–206.

Charrier, R., Pinto, L., & Rodríguez, M. P. (2007). Tectonostratigraphic evolution of the Andean Orogen in Chile. In The geology of Chile (pp. 21-114).

Charrier, R., Ramos, V.A., Tapia, F., Sagripanti, L., 2014. Tectono-stratigraphic evolution of the Andean Orogen between 31 and 37 ° S (Chile and Western Argentina), in: Sepúlveda, S.A., Giambiagi, L.B., Moreiras, S.M., Pinto, L., Tunik, M., Hoke, G.D., Farías, M. (Eds.), Geodynamic Processes in the Andes of Central Chile and Argentina. Geological Society, London, Special Publications, 399. https://doi.org/10.1144/SP399.20

Chigira, M., Wu, X., Inokuchi, T., & Wang, G. (2010). Landslides induced by the 2008 Wenchuan earthquake, Sichuan, China. Geomorphology, 118(3-4), 225-238.

Chen, C. W., Oguchi, T., Hayakawa, Y. S., Saito, H., & Chen, H. (2017). Relationship between landslide size and rainfall conditions in Taiwan. Landslides, 14(3), 1235-1240.

Chen, M., Tang, C., Xiong, J., Shi, Q.Y., Li, N., Gong, L.F., Wang, X.D., Tie, Y., 2020. The long-term evolution of landslide activity near the epicentral area of the 2008 Wenchuan earthquake in China. Geomorphology 367. https://doi.org/10.1016/j.geomorph.2020.107317

Covacevich, V.; Frassinetti, D. 1986. El género Cancellaria en el Mioceno de Chile, con descripción de cuatro especies nuevas (Gastropoda: Cancellariidae). Revista Geológica de Chile 28-29: 33-67.

Covacevich, V.; Frassinetti, D. 1990. La Fauna de Lo Abarca: Hito biocronoestratigráfico y paleoclimático en el Terciario Superior marino de Chile Central. In Segundo Simposio sobre el Terciario de Chile: 51-71. Concepción.

Creixell, C., Parada, M.Á., Roperch, P., Morata, D., Arriagada, C., de Arce, C.P., 2006. Syntectonic emplacement of the Middle Jurassic Concón Mafic Dike Swarm, Coastal Range, central Chile (33° S). Tectonophysics 425, 101–122. https://doi.org/10.1016/j.tecto.2006.07.005

Crempien, J.G.F., Archuleta, R.J., 2015. UCSB Method for Simulation of Broadband Ground Motion from Kinematic Earthquake Sources. Seismol. Res. Lett. 86, 61–67. https://doi.org/10.1785/0220140103

Cruden, D.M., Varnes, D.J., 1996. Landslides: investigation and mitigation. Chapter 3-Landslide types and processes. Transp. Res. board Spec. Rep. 247.

Darwin, C. 1846. Geological observations on South America. Smith, Elder and Co.: 279 p. London.

De Los Arcos, S., Partarrieu, D., Carrillo-Briceño, J., Amson, E., 2017. The Southernmost Occurrence of the Aquatic Sloth Thalassocnus (Mammalia, Tardigrada) in Two New Pliocene Localities in Chile. Ameghiniana 54, 351–369. https://doi.org/10.5710/AMGH.29.12.2016.3004

Du, W. (2018). Effects of directionality and vertical component of ground motions on seismic slope displacements in Newmark sliding-block analysis. Engineering Geology, 239, 13-21.doi:10.1016/j.enggeo.2018.03.012.

Ekström, G., Nettles, M., Dziewoński, A.M., 2012. The global CMT project 2004–2010:

Centroid-moment tensors for 13,017 earthquakes. Phys. Earth Planet. Inter. 200–201, 1–9. https://doi.org/10.1016/j.pepi.2012.04.002

Encinas, A., Le Roux, J. P., Buatois, L. A., Nielsen, S. N., Finger, K. L., Fourtanier, E., & Lavenu, A. (2006). Nuevo esquema estratigráfico para los depósitos marinos mio-pliocenos del área de Navidad (33º00'-34º30'S), Chile central. Revista geológica de Chile, 33(2), 221-246.

Encinas, A., Finger, K. L., Nielsen, S. N., Lavenu, A., Buatois, L. A., Peterson, D. E., & Le Roux, J. P. (2008). Rapid and major coastal subsidence during the late Miocene in south-central Chile. Journal of South American Earth Sciences, 25(2), 157-175.

Fan, X., Scaringi, G., Korup, O., West, A. J., Westen, C. J., Tanyas, H., Hovius, N., Hales, T. C., Jibson, R. W., Allstadt, K. E., Zhang, L., Evans, S. G., Xu, C., Li, G., Pei, X., Xu, Q., and Huang, R. (2019). Earthquake-Induced Chains of Geologic Hazards: Patterns, Mechanisms, and Impacts. Reviews of Geophysics, 57, 421-503. URL: https://onlinelibrary.wiley.com/doi/abs/10.1029/2018RG000626. doi:10.1029/2018RG000626.

Farías, M., Charrier, R., Carretier, S., Martinod, J., Fock, A., Campbell, D., ... & Comte, D. (2008). Late Miocene high and rapid surface uplift and its erosional response in the Andes of central Chile (33–35 S). Tectonics, 27(1).

Farías, M., Comte, D., Roecker, S., Carrizo, D., Pardo, M., 2011. Crustal extensional faulting triggered by the 2010 Chilean earthquake: The Pichilemu Seismic Sequence. Tectonics 30, n/a-n/a. https://doi.org/10.1029/2011TC002888

Gana, P.; Yáñez, G.; Wall, R1994. Evolución geotectónica de la Cordillera de la Costa de Chile Central (33°-34°S): control geológico y geofísico. In Congreso Geológico Chileno, No. 7, Actas, Vol. 1, p. 38-42, Concepción

Gana, P., Tosdal, R.M., 1996. Geocronología U-Pb y K-Ar en intrusivos del Paleozoico y Mesozoico de la Cordillera de la Costa, Región de Valparaíso, Chile. Rev. Geol. Chile.

Gana, P., Wall, R., Gutiérrez, A., 1996a. Mapa Geológico del Area de Valparaiso - Curacavi: Leyenda Ampliada y Listado de Yacimientos.

Gana, P., Wall, R., Gutiérrez, A., SERNAGEOMIN, 1996b. Mapa geológico del area de Valparaíso-Curacaví, regiones de Valparaíso y Metropolitana, Escala 1:100.000.

Giambiagi, L., Tassara, A., Mescua, J., Tunik, M., Alvarez, P. P., Godoy, E., Hoke, G., Pinto, L., Spagnotto, S., Porras, H., Tapia, F., Jara, P., Bechis, F., García, V. H., Suriano, J., Moreiras, S. M., and Pagano, S. D. (2015). Evolution of shallow and deep structures along the Maipo-Tunuyán transect (33◦40'S): 880 From the Pacific coast to the Andean foreland. Geological Society Special Publication, 399, 63-82. doi:10.1144/SP399.14.

González, A. 2008. Análisis estructural entre los valles del río Tinguiririca y Teno, Cordillera Principal de Chile Central: Microsismicidad y Geología Superficial. Memoria de Título (Inédito), Universidad de Chile: 90 p

González, G., Salazar, P., Loveless, J. P., Allmendinger, R. W., Aron, F., & Shrivastava, M. (2015). Upper plate reverse fault reactivation and the unclamping of the megathrust during the 2014 northern Chile earthquake sequence. Geology, 43(8), 671-674.

Hayes, G. P., Bergman, E., Johnson, K. L., Benz, H. M., Brown, L., and Meltzer, A. S. (2013). Seismotectonic framework of the 2010 February 27Mw 8.8 Maule, Chile earthquake sequence. Geophysical Journal International, 195, 1034-1051. doi:10.1093/gji/ggt238.

Hovius, N., Meunier, P., Lin, C. W., Chen, H., Chen, Y. G., Dadson, S., ... & Lines, M. (2011). Prolonged seismically induced erosion and the mass balance of a large earthquake. Earth and Planetary Science Letters, 304(3-4), 347-355.

Hungr, O., Leroueil, S., Picarelli, L., 2014. The Varnes classification of landslide types, an update. Landslides 11, 167–194. https://doi.org/10.1007/s10346-013-0436-y

Isacks, B. L. (1988). Uplift of the central Andean plateau and bending of the Bolivian orocline. Journal of Geophysical Research: Solid Earth, 93(B4), 3211-3231.

Jibson, R.W., 1993. Predicting Earthquake-Induced Landslide Displacements Using Newmark's Sliding Block Analysis. Transp. Res. Rec. 9–17.

Jibson, R. W., & Keefer, D. K. (1993). Analysis of the seismic origin of landslides: Examples from the New Madrid seismic zone. Geological Society of America Bulletin, 105(4), 521-536.

Jibson, R.W., 2011. Methods for assessing the stability of slopes during earthquakes-A retrospective. Eng. Geol. 122, 43–50. https://doi.org/10.1016/j.enggeo.2010.09.017

Keefer, D.K., 1994. The importance of earthquake-induced landslides to long-term slope erosion and slope-failure hazards in seismically active regions. Geomorphology. https://doi.org/10.1016/0169-555X(94)90021-3

Korup, O., Densmore, A. L., & Schlunegger, F. (2010). The role of landslides in mountain range evolution. Geomorphology, 120(1-2), 77-90.

Lara, M., 2007. Metodología para la evaluación y zonificación de Peligro de Remociones en Masa con Aplicación en Quebrada San Ramón, Santiago Oriente, Región Metropolitana. Mem. para Optar al Título Geólogo. https://doi.org/10.1017/CBO9781107415324.004

Laursen, J., Scholl, D.W., von Huene, R., 2002. Neotectonic deformation of the central Chile margin: Deepwater forearc basin formation in response to hot spot ridge and seamount subduction. Tectonics 21, 2-1-2–27. https://doi.org/10.1029/2001TC901023

Lay, T., Kanamori, H., Ammon, C.J., Koper, K.D., Hutko, A.R., Ye, L., Yue, H., Rushing, T.M., 2012. Depth-varying rupture properties of subduction zone megathrust faults. J. Geophys. Res. Solid Earth 117. https://doi.org/10.1029/2011JB009133

Le Roux, J.P., Olivares, D.M., Nielsen, S.N., Smith, N.D., Middleton, H., Fenner, J., Ishman, S.E., 2006. Bay sedimentation as controlled by regional crustal behaviour, local tectonics and eustatic sea-level changes: Coquimbo Formation (Miocene-Pliocene), Bay of Tongoy, central Chile. Sediment. Geol. 184, 133–153. https://doi.org/10.1016/j.sedgeo.2005.09.023

Legrand, D., Barrientos, S., Bataille, K., Cembrano, J., and Pavez, A. (2011). The fluid-driven tectonic swarm of Aysen Fjord, Chile (2007) associated with two earthquakes (Mw=6.1 and Mw=6.2) within the Liquiñe-Ofqui Fault Zone. Continental Shelf Research, 31,154-161. doi:10.1016/j.csr.2010.05.008.

Leonard, M., 2010. Earthquake Fault Scaling: Self-Consistent Relating of Rupture Length, Width, Average Displacement, and Moment Release. Bull. Seismol. Soc. Am. 100, 1971–1988. https://doi.org/10.1785/0120090189

Leyton, F., Ruiz, S., & Sepulveda, S. (2010). Re-evaluation of probabilistic seismic hazard in central Chile. Andean Geology, 37(2), 455-472.F.

Marc, O., Hovius, N., Meunier, P., Gorum, T., & Uchida, T. (2016). A seismologically consistent expression for the total area and volume of earthquake-triggered landsliding. Journal

Meunier, P., Uchida, T., & Hovius, N. (2013). Landslide patterns reveal the sources of large earthquakes. Earth and Planetary Science Letters, 363, 27-33.

Mordojovic, C., 1981. Sedimentary Basins of Chilean Pacific Offshore, in: Energy Resources of the Pacific Region. pp. 63–82. https://doi.org/10.1306/St12420C7

Murphy, B. (2015). Coseismic landslides. In Landslide Hazards, Risks and Disasters (pp. 91-129). Academic Press.

Nakamura, S., Wakai, A., Umemura, J., Sugimoto, H., Takeshi, T., 2014. Earthquake-induced landslides: Distribution, motion and mechanisms. Soils Found. 54, 544–559. https://doi.org/10.1016/j.sandf.2014.06.001

Newmark, N.M., 1965. Effects of Earthquakes on Dams and Embankments. Géotechnique 15, 139–160. https://doi.org/10.1680/geot.1965.15.2.139

Okamoto, T., Sakurai, M., Tsuchiya, S., Yoshimatsu, H., Ogawa, K., Wang, G., 2013. Secondary Hazards Associated with Co-seismic Landslide, in: Earthquake-Induced Landslides. Springer Berlin Heidelberg, Berlin, Heidelberg, pp. 77–82. https://doi.org/10.1007/978-3-642-32238-9_8

Parada, M. A., Nyström, J. O., & Levi, B. E. A. T. R. I. Z. (1999). Multiple sources for the Coastal Batholith of central Chile (31–34 S): geochemical and Sr–Nd isotopic evidence and tectonic implications. Lithos, 46(3), 505-521.

Peralta-Prato, J., Solórzano, A., 2019. How many species of the aquatic sloth thalassocnus (Xenarthra: Megatheriidae) were in Chile ?: New evidences from the bahía inglesa formation, with a reappraisal of their biochronological affinities. Andean Geol. 46, 693–702. https://doi.org/10.5027/andgeov46n3-3221

Perez-Estay, N.P.; Yáñez, G.; Carretier, S.; Lira, E.; Maringue, J. 2016. Seismic hazard in low slip rate crustal faults, estimating the characteristic event and the most hazardous zone: study case San Ramón fault, in central Andes. Natural Hazards Earth System Sciences 16: 2511-2528.

Ramos, V. A. (2009). Anatomy and global context of the Andes: Main geologic features and the Andean orogenic cycle. Backbone of the Americas: Shallow subduction, plateau uplift, and ridge and terrane collision, 204, 31-65.

Rivano, S., and Sepúlveda, P. 1986. Hoja Illapel, Región de Coquimbo, Chile. Servicio Nacional de Geologia y Mineria, Carta Geológica de Chile 69

Rivano, S., Sepúlveda, P., Boric, R., Espiñeira, D., 1993. Hojas Quillota y Portillo, V Región, Escala 1: 250.000.

Roback, K., Clark, M. K., West, A. J., Zekkos, D., Li, G., Gallen, S. F., ... & Godt, J. W. (2018). The size, distribution, and mobility of landslides caused by the 2015 Mw7. 8 Gorkha earthquake, Nepal. Geomorphology, 301, 121-138.

Ruiz, S., Madariaga, R., 2018. Historical and recent large megathrust earthquakes in Chile. Tectonophysics 733, 37–56. https://doi.org/10.1016/j.tecto.2018.01.015

Sabaj, R., 2008. Identificación y caracterización de estructuras potencialmente activas en la cordillera de la costa, entre los 33° y 33°45' Sur 92.

Santibáñez, I., Cembrano, J., García-Pérez, T., Costa, C., Yáñez, G., Marquardt, C., Arancibia, G., González, G., 2019. Crustal faults in the chilean Andes: Geological constraints and seismic potential. Andean Geol. 46, 32–65. https://doi.org/10.5027/andgeov46n1-3067

Sepúlveda, S.A., Astroza, M., Kausel, E., Campos, J., Casas, E.A., Rebolledo, S., Verdugo, R., 2008. New findings on the 1958 Las Melosas earthquake sequence, central Chile: Implications for seismic hazard related to shallow crustal earthquakes in subduction zones. J. Earthq. Eng. 12, 432–455. https://doi.org/10.1080/13632460701512951

Sepúlveda, S. A., Serey, A., Lara, M., Pavez, A., & Rebolledo, S. (2010). Landslides induced by the April 2007 Aysén fjord earthquake, Chilean Patagonia. Landslides, 7(4), 483-492.

Shinoda, M., & Miyata, Y. (2017). Regional landslide susceptibility following the Mid NIIGATA prefecture earthquake in 2004 with NEWMARK'S sliding block analysis. Landslides, 14(6), 1887-1899.

Somerville, P. G., Smith, N. F., Graves, R. W., & Abrahamson, N. A. (1997). Modification of empirical strong ground motion attenuation relations to include the amplitude and duration effects of rupture directivity. Seismological research letters, 68(1), 199-222.

Tavera, J., 1960. El Plioceno de la Bahía Horcon en la Provincia de Valparaiso. An. la Fac. Ciencias Físicas y Matemáticas 17, 348–368.

Tavera, J. 1968. Estudio de la formación Navidad en el Provincia de Santiago con referencia especial a las localidades tipos de Navidad, Matanza, Boca Rapel y Topocalma. Sociedad Geológica de Chile, Resúmenes: 59-60.

Tavera, J. 1979. Estratigrafía y paleontología de la Formación Navidad, Provincia de Colchagua, Chile (Lat. 30°50'-34°S). Boletín del Museo Nacional de Historia Natural, 36: 176 p. Chile.

Thomas, H. 1958. Geología de la Cordillera de la Costa entre el valle de La Ligua y la cuesta Barriga. Instituto de Investigaciones Geológicas, Boletín, No. 2, 86 p. Santiago.

Thorson RM. 1999. La Falla ‘Marga-Marga’ Viña del Mar. University of Santa Maria

Towhata I (2008) Geotechnical Earthquake Engineering.

Springer, Berlin, Germany

Valdenegro, P., Muñoz, M., Yáñez, G., Parada, M.A., Morata, D., 2019. A model for thermal gradient and heat flow in central Chile: The role of thermal properties. J. South Am. Earth Sci. 91, 88–101. https://doi.org/10.1016/j.jsames.2019.01.011

Valdivia, D., Elgueta, S., del Valle, F., Marquardt, C., Yáñez, G., and Hodgkin, A. (2018). Variación del nivel del mar durante el Neógeno en Chile Central: Eustatismo vs Tectonismo. In Congreso Geológico Chileno. Concepción.

Varnes, D.J., 1978. Slope Movement Types and Processes. Spec. Rep. 176, 11–33.

Varnes, D.J., 1984. Landslide hazard zonation: a review of principles and practice. United Nations Education, Scientific and Cultural Organization, Paris, France.

Vergara, M., Levi, B., Nyström, J. O., & Cancino, A. (1995). Jurassic and Early Cretaceous island arc volcanism, extension, and subsidence in the Coast Range of central Chile. Geological Society of America Bulletin, 107(12), 1427-1440.

Vigny, C., Socquet, A., Peyrat, S., Ruegg, J.-C., Métois, M., Madariaga, R., Morvan, S., Lancieri, M., Lacassin, R., Campos, J., Carrizo, D., Bejar-Pizarro, M., Barrientos, S., Armijo, R., Aranda, C., Valderas-Bermejo, M.-C., Ortega, I., Bondoux, F., Baize, S., Lyon-Caen, H., Pavez, A., Vilotte, J.P., Bevis, M., Brooks, B., Smalley, R., Parra, H., Baez, J.-C., Blanco, M., Cimbaro, S., Kendrick, E., 2011. The 2010 Mw 8.8 Maule megathrust earthquake of Central Chile, monitored by GPS. Science 332, 1417–1421. https://doi.org/10.1126/science.1204132

Wall, R., Gana, P., Gutiérrez, A., SERNAGEOMIN, 1996. Mapa geológico del area de San Antonio-Melipilla: regiones de Valparaíso, Metropolitana y del Libertador General Bernardo O'Higgins, Escala 1:100.000.

Wall, R., Lara, L.E., 2001. Lavas las Pataguas - volcanismo alcalino en el antearco andino del Mioceno Inferior Chile Central. Rev. geológica Chile 28, 243–258.

Webb, L.E., Klepeis, K.A., 2019. 40Ar/39Ar constraints on the tectonic evolution of the late Paleozoic and early Mesozoic accretionary complex of coastal central Chile, Andean Tectonics. Elsevier Inc. https://doi.org/10.1016/b978-0-12-816009-1.00020-4

Yañez, G.A., Gana, P., Fernandez, R., 1998. Origin and geological significance of the Melipilla Anomaly, Central Chile. Rev. Geol. Chile 25, 175–198

Yáñez, G. a., Ranero, C.R., von Huene, R., Díaz, J., 2001. Magnetic anomaly interpretation across the southern central Andes (32°–34°S): The role of the Juan Fernández Ridge in the late Tertiary evolution of the margin. J. Geophys. Res. 106, 6325. https://doi.org/10.1029/2000JB900337

Yáñez, G., & Rivera, O. (2019). Crustal dense blocks in the fore-arc and arc region of Chilean ranges and their role in the magma ascent and composition: Breaking paradigms in the Andean metallogeny. Journal of South American Earth Sciences, 93(April), 51–66. https://doi.org/10.1016/j.jsames.2019.04.006

ANNEX

A1_Aconcagua_MargaMarga_Data.xlsx

A2_AN_STATS_D.csv

A3_AN_STATS_S.csv

A4_AS_STATS_D.csv

A5_AS_STATS_S.csv

A6_MN_STATS_D.csv

A7_MN_STATS_S.csv

A8_MS_STATS_D.csv

A9_MS_STATS_S.csv

Readme_Annexs.txt